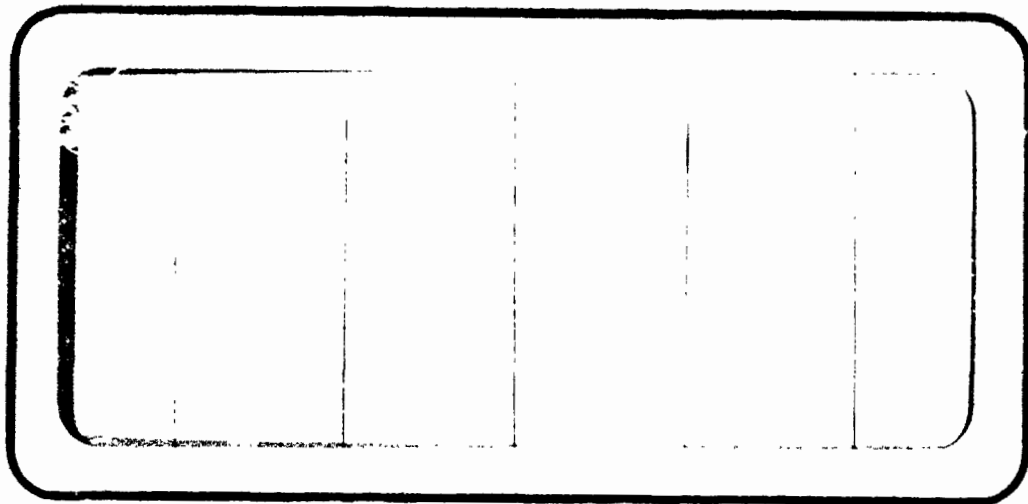


11-20-74

NASA-CR-112 253



(NASA-CR-112253) STUDY OF MODAL COUPLING
PROCEDURES FOR THE SHUTTLE: A MATRIX
METHOD FOR DAMPING SYNTHESIS Final
Report (TRW Systems Group) 120 p HC
\$5.25

N75-10982

Unclas
02226

CSSL 22B G3/18

TRW
SYSTEMS GROUP

ONE SPACE PARK • REDONDO BEACH, CALIFORNIA





FINAL REPORT

STUDY OF MODAL COUPLING PROCEDURES FOR THE SHUTTLE:
A MATRIX METHOD FOR DAMPING SYNTHESIS

Contract Number 0-16232-C
Task 8-3C
(Under Prime Contract NAS1-10635)

Prepared by T. K. Hasselman

Approved: R. Gluck
R. Gluck, Head
Analytical Dynamics

Approved: D. H. Mitchell
D. H. Mitchell, Manager
Dynamics Department

December, 1972
TRW No. 18058-6001-RU-00

MEL-72-D-44

Prepared for
Grumman Aerospace Corporation
Bethpage, New York 11714

TRW Systems Group
One Space Park
Redondo Beach, California 90278

STUDY OF MODAL COUPLING PROCEDURES FOR THE SHUTTLE:
A MATRIX METHOD FOR DAMPING SYNTHESIS

Timothy K. Hasselman

Distribution of this report is provided in the interest of
information exchange. Responsibility for the contents re-
sides in the authors or organization that prepared it.

Issued by Originator as Report No. MEL 72-D-44

(18058-6001-RU-00)

Prepared By

TRW Systems Group
One Space Park
Redondo Beach, California 90278

Under Subcontract 0-16232C LM to
Grumman Aerospace Corporation
As Part of Contract NAS 1-10635 to
Langley Research Center
NATIONAL AERONAUTICS AND SPACE ADMINISTRATION

TABLE OF CONTENTS

	<u>Page</u>
PART A. FORMULATION	1
1. Introduction and Summary	2
2. Background	3
3. Objectives and Scope	5
4. Modal Synthesis	7
5. Forms of the Substructure Modal Damping Matrix	10
6. Use of Damped Modes to Compute the Modal Damping Matrix	14
7. Use of Resonant Response to Identify Damped Modes	18
PART B. VERIFICATION	23
8. Analytical Verification	24
8.1 Numerical Comparison of Coupling Procedures	25
8.2 Approximation of the Modal Damping Matrix	34
8.3 Identification of Damped Modes	38
8.4 Conclusions	46
9. Experimental Verification	47
9.1 Description of Tests	47
9.2 Summary of Test Results	58
9.3 Orbiter Damping Matrix	58
9.4 Booster Damping Matrix	74
9.5 Damping Synthesis	82
9.6 Conclusions	85
PART C. APPLICATION AND REFINEMENT OF PROCEDURES	86
10. Current Applicability	87
11. Data Acquisition	90
12. Comparison with Energy Method	92
13. Final Conclusions	93
14. Recommendations for Future Work	96
Acknowledgements	96
References	97
Appendix: Convergence of the Modal Separation Procedure	A-1

LIST OF FIGURES

	<u>Page</u>
1. Schematic Models of Space Shuttle Orbiter and Tank Substructures	26
2. Schematic Model of Coupled Space Shuttle Orbiter/Tank Assembly	27
3. Nonproportional Damping Model for Orbiter and Tank	29
4. Four-Degree of Freedom Lumped Parameter Model	35
5. Acceleration Response of the 4-d.o.f. Model	39
6. 1/15-Scale Dynamic Model of Orbiter and Booster Substructures	48
7. Ball Damper Test Configuration	
a. Vertical Motion	51
b. Horizontal Motion	52
8. Ball Damper Characteristics Determined from Measurements of Damping Force and Velocity	54
9. Ball Damper Installation for Orbiter Test	
a. Nose Damper	55
b. Midspan Damper	56
c. Tail Damper	57
10. Ball Damper Installation for Coupled Orbiter/Booster Test	
a. Orbiter Nose Damper	59
b. Orbiter Midspan Damper	60
c. Orbiter Tail Damper	61
11. Orbiter Acceleration Response at First Resonant Frequency	66
a. Coincident and Quadrature Response	
b. Coincident Response (Expanded Scale)	
12. Orbiter Acceleration Response at Second Resonant Frequency	67
a. Coincident and Quadrature Response	
b. Coincident Response (Expanded Scale)	
13. Orbiter Acceleration Response at Third Resonant Frequency	68
a. Coincident and Quadrature Response	
b. Coincident Response (Expanded Scale)	

List of Figures (Cont'd)

	<u>Page</u>
14. Comparison of Ball Damper Characteristics Obtained by Different Methods	72
15. Imaginary Parts of Damped Orbiter Bending Modes	73
16. Booster Acceleration Response at First Resonant Frequency	77
a. Quadrature response	
b. Coincident Response (Expanded Scale)	
17. Booster Acceleration Response at Second Resonant Frequency	78
a. Quadrature Response	
b. Coincident Response (Expanded Scale)	
18. First Damped Bending Mode of the Booster	79
a. Real Part	
b. Imaginary Part	
19. Second Damped Bending Mode of the Booster	80
a. Real Part	
c. Imaginary Part	

LIST OF TABLES

	<u>Page</u>
1. Damping Constants C_{jj} By Modal Synthesis for Case 1	30
a. No Mass Loading in Free-Free Modes	
b. Mass-Loaded Junction Points in Free-Free Modes	
2. Damping Constants C_{jj} By Modal Synthesis for Case 2	30
a. No Mass Loading in Free-Free Modes	
b. Mass-Loaded Junction Points in Free-Free Modes	
3. Damping Constants C_{jj} By Modal Synthesis for Case 3	31
4. Damping Constants C_{jj} By Modal Synthesis for Case 4	31
5. Effect of Neglecting ρ^{BB} in Modal Damping Computations, Case 2b	33
6. Effect of Neglecting Off-Diagonal Terms of the Modal Damping Matrix in Synthesis Computations, Case 1b	33
7. Effect of Adding Longitudinal Dampers to Orbiter and Tank, 30-d.o.f. Case 1b	33
8. Eigenvalues and Eigenvectors for a 4-d.o.f. System	36
9. Comparison of Modal Damping Matrices	37
10. Complex Resonant Acceleration Response	41
11. Normalized Resonant Acceleration Response	41
12. Initial Modal Mass Matrix	42
13. Normalized Change in Modal Vector Length	42
14. Improved Modal Vectors	43
15. Final Modal Mass Matrix	43
16. Comparison of Modal Damping Matrices	45
17. Effect of Truncation on Computation of the Modal Damping Matrix	45
18. Mass Distribution for the 1/15-Scale Dynamic Model of a Shuttle Vehicle	49
19. Ball Damper Characteristics	53
20. Experimental Modal Frequencies and Damping Values	62

List of Tables (Cont'd)

	<u>Page</u>
21. Comparison of Orbiter Modal Damping Matrices	71
22. Improvement of Orthogonality Among Booster Mode	74
23. Convergence Indicators for Booster Damping Matrix Calculations	75
24. A Comparison of Predicted and Measured System Damping	84

PART A: FORMULATION

1.0 Introduction and Summary

Reliable evaluation of the dynamic characteristics of large structural systems such as the Space Shuttle vehicle will require combined analytical and experimental efforts. Because of its size and physical configuration, full-scale vibration testing of the entire vehicle may be impractical. Testing would then be limited to isolated substructures of the system such as the Orbiter, Tank and Booster. Analytical means are being sought to utilize data from sub-structure tests to predict characteristics of the connected assembly. Modal coupling or synthesis has been used in the past to predict undamped dynamic characteristics including vibration modes and frequencies. While the Shuttle will require special consideration in the application of modal synthesis because of its unusual configuration, existing methods have been developed to a point where the capability is within the state of the art.

This is not true in the case of damping, however. A generally applicable method for predicting the damping in a structural system on the basis of substructure damping has not yet been demonstrated. Yet, a reasonably accurate assessment of structural damping will be necessary in order to properly evaluate conditions of resonant response to either sinusoidal or random excitation. If reliable predictions are to be made without recourse to testing the entire vehicle, this capability will be essential.

Reported herein is the development of a method for damping synthesis. The method has been applied successfully to real structures as well as analytical models. It depends on the ability to determine an appropriate modal damping matrix for each substructure. Previous attempts at using this approach have failed because of invalid restrictions placed on the nature of substructure damping. In the past, modal damping matrices have been assumed diagonal for lack of being able to determine the coupling terms which are significant in the general case of nonproportional damping. This problem has been overcome by formulating the damped equations of motion as a linear perturbation of the undamped equations for light structural damping. Damped modes are defined as complex vectors derived from the complex frequency response vectors of each substructure and are obtained directly from sinusoidal vibration tests. The damped modes are used to compute first order approximations to the modal damping matrices. The perturbation approach avoids ever having to solve a complex eigenvalue problem. This is a useful fact which a number of investigators have failed to recognize.

2. Background

A variety of dissipative mechanisms contribute to the overall damping properties of a complex structure. They may include material damping caused by microscopic slip between particles within the material, thermal loss due to molecular abrasion and, in most cases, structural hysteresis. At the macroscopic level, losses may arise from relative slip in mechanical joints, from acoustic radiation, and from viscous losses due to liquid sloshing or vibration of viscoelastic materials. Detailed investigations of damping in simple structures have revealed various nonlinear damping laws [1,2]*. Some lead to linear equations of motion, while others do not. However, specific nonlinear phenomena are likely to be obscured when appearing together in a complex structure. One may find it difficult to define a particular nonlinear damping law for general application. Although Chang [3] has concluded that a simple nonlinear damping law may be appropriate for some complex structures, based on his interpretation of test data from Saturn-type vehicles and their scale models, other interpretations of the same data indicate linear damping with respect to amplitude for many of the modes considered individually. Chang's interpretation ignores differences in damping among the various modes, with no clear physical justification.

Since modal synthesis presupposes linearity, it is consistent to treat damping in the same manner. In view of the computational advantages offered by linearization and the lack of much strong physical evidence supporting the selection of a particular nonlinear model, the tentative assumption of equivalent linear damping appears to be justified.

Recent attempts have been made to predict the modal damping properties of structural systems based on the modal damping of their respective substructures when damping is known to be linear. Collins, Hart, Hurty, and Kennedy [4] showed that the uncoupled modal damping properties of substructures do not constitute sufficient information to enable one to predict damping in the system modes using the standard matrix transformation approach. Kana and Huzar [5] confirmed this finding and went on to develop a completely different approach based on total energy dissipation rather than energy dissipation associated with any particular mode. They adopted a representation of structural damping similar to Chang's,

* Numbers in square brackets designate references at end of text.

plotting dissipative energy per cycle versus kinetic energy. These quantities, obtained experimentally at each of the structure's resonant frequencies within a certain range, define points through which smooth curves are drawn. The curves are used to define the overall dissipative properties of the structure through a continuous frequency spectrum. After determining the coupled system modes, the kinetic energy of each component is determined. Going back to the energy plots, one may pick off appropriate levels of dissipative energy for each component and sum them to get the total dissipative energy of the system. From this, damping is found for each of the system modes. While the authors demonstrate successful application of the method for the structural models employed, certain pitfalls are noted. A significant one has to do with how the points fall on the energy plots. If they do not align themselves reasonably well along some smooth curve, obvious difficulties arise. This could very well be the case when the amount of damping varies greatly from mode to mode, particularly if the variability is irregular. In this case, the authors suggest the possible grouping of points into different classes of modes in the hope that smooth curves may still be drawn. The chance for ambiguity here is not difficult to imagine, and further study will be required before the method is acceptable for general use.

On the other hand, the matrix approach is not affected by nonuniform in the distribution of damping. In addition, it lends itself to a form common used by analysts. It is clear (at least in the case of linear viscous damping) that failure to predict damping in the system modes on the basis of component modal damping is attributable to the fact that the off-diagonal elements of the modal damping matrix are neglected. Hasselman [6] showed that the diagonal elements of the modal damping matrix correspond to the modal damping constants for each mode. Furthermore, it is shown that, in general, the off-diagonal elements will be of the same order of magnitude as the diagonal elements. They may therefore not be neglected in transformations involving the component modal damping matrices. The problem is to somehow determine these elements.

3. Objectives and Scope

This investigation is part of a broader study directed toward the development of modal coupling procedures for the Space Shuttle vehicle. The principal objectives have been to formulate analytical procedures and then verify them using experimental data. TRW and the Grumman Aerospace Corporation (GAC) have been jointly responsible for the formulation of procedures. Experimental verification has been made by TRW and GAC on the basis of test data furnished by the NASA Langley Research Center (LaRC). GAC has performed that part of the study which involves synthesis of system modes and frequencies, while TRW has developed and implemented a damping synthesis technique, which is discussed in this report.

The scope of the present work fits within the framework of conventional modal synthesis methods. Modal damping matrices derived at the substructure level are operated on by the same transformations used to couple and diagonalize the undamped equations of motion at the system level. The main focus is placed on obtaining the appropriate modal damping matrices.

Some basic assumptions are made: that the damping forces in the structure are small compared to either the elastic forces or inertial forces, and that they vary linearly with respect to the amplitude of the motion. It has furthermore been assumed in the present development that the damping in the structure may be represented by constant viscous damping. The Voigt model is used (as opposed to the Maxwell model, for example). This is clearly an appropriate first step to take in the investigation of a linearized matrix approach.

To relate this study to other recent work done in the same area, it is recalled that both [4] and [5] reported attempts to use the standard matrix coupling transformations as a means of predicting modal damping at the system level based on measurements of uncoupled modal damping at the substructure level. That is, diagonal modal damping matrices were assumed. Reference [4] concluded that, in general, more information is required to enable the prediction of damping in this way. Reference [5] concluded somewhat to the contrary that a different method should be sought, and proceeded to develop an energy approach instead. The present work begins with the conclusions of Reference [4] and moves in the direction of identifying and obtaining the additional information required by the matrix method. The basic problem can be formulated so that within the scope of the linearized approach, information is provided by the off-diagonal terms of the substructure modal damping matrices and a description of any damping which may take place between substructural interfaces.

Corresponding to the major objectives of the effort, this report is organized into three parts: A, B, and C. Part A includes the formulation of methods. Part B includes the presentation and discussion of results obtained by applying the theory to both ideal and practical problems. Application of the theory to ideal problems which satisfy the inherent assumptions serves to verify the theoretical development and provide additional insight into practical application. As such, it is an essential link between the theoretical work which tends to become involved, and the results of practical application which embody a number of uncertainties associated with data acquisition and reduction.

While every attempt has been made to minimize the influence of these uncertainties, a systematic treatment of their influence on the final results was not within the scope of this study. Vibration tests were conducted with standard equipment, and data were recorded on analog tape. Analog data reduction procedures were also used. Manual transfer of the analog data to digital form on punched cards was employed. Although the analog data were visually displayed in digital form, some real-time variation did occur so that the person recording the data was required, in some cases, to mentally average the results before writing them down.

The need for a final evaluation of the study, including a discussion of the current applicability of methods, suggested the addition of Part C. Some general comments pertaining to the matrix method and a comparison with the energy method of Kana and Huzar are made. Conclusions and recommendations are contained therein.

4. Basic Equations for Modal Synthesis

There are various coupling procedures available for modal synthesis depending on the type of substructure modes used. From the standpoint of damping synthesis, the basic equations are the same. Without going into detail, the general procedure may be outlined rather simply.

It is convenient to begin writing equations for each substructure in terms of a discrete coordinate system in which the displacement vector will be denoted as x^i . These coordinates may be thought of as resulting from some finite element discretization of the substructure, although it is recognized that the equations in this form need not be defined when basing an analysis on vibration test data. However, a mass matrix corresponding to such a coordinate system will be required so that conceptually this step is necessary. The equations may be written

$$\mu \ddot{x}^i + \rho \dot{x}^i + \kappa x^i = f^i \quad (1)$$

The force vector f^i corresponds to displacements x^i , while μ^i , ρ^i , and κ^i are square matrices containing, respectively, the mass, damping, and stiffness coefficients of the equations. In the case of free vibration, f^i will represent only the interaction forces between adjacent components. Similar sets of equations may be written for each of N components and arrayed in a diagonal pattern such that a complete set of equations representing the complete structure becomes

$$\mu \ddot{x} + \rho \dot{x} + \kappa x = f \quad (2)$$

where

$$x = \begin{Bmatrix} x^1 \\ x^2 \\ \vdots \\ x^N \end{Bmatrix} \quad \text{and} \quad \mu = \begin{bmatrix} \mu^1 & & & \\ & \mu^2 & & \\ & & \ddots & \\ & & & \mu^N \end{bmatrix}$$

The matrices ρ and κ are of the same form as μ .

There are three transformations involved in going from (2) to a reduced set of equations in system modal coordinates. The first transformation, denoted by ϕ_R , involves the hypothetical undamped substructure modes. The subscript R is used to signify that these modes are real. The transformation may be written

$$x = \phi_R p \quad (3)$$

where

$$\phi_R = \begin{bmatrix} \phi_R^1 & & & & \\ & \phi_R^2 & & & \\ & & \dots & & \\ & & & \phi_R^N & \end{bmatrix}$$

and ϕ_R^1 is a rectangular matrix whose columns define the characteristic deformation shapes of the substructure. They may include static as well as dynamic shapes.

The second transformation is a rectangular matrix denoted by β , and is used to introduce compatibility constraints at substructural interfaces. The final transformation, ϕ_R , involves the hypothetical undamped modes of the system where each column of ϕ_R is a system eigenvector in the coupled component mode coordinates. These two transformations relate the p coordinate vector to a new coordinate vector η , whose elements correspond to the system eigenvectors ϕ_R . Thus

$$p = \beta \phi_R \eta = T \eta. \quad (4)$$

It is convenient both conceptually and notationally to combine β and ϕ_R into the single transformation matrix T . Transformation of (2) to the η coordinate system gives equations of the form

$$I \ddot{\eta} + C \dot{\eta} + \Lambda \eta = 0 \quad (5)$$

when ϕ_R is normalized to give unit modal mass. In other words,

$$T^T \phi_R^T \mu \phi_R T = I \quad (6a)$$

$$T^T \phi_R^T \rho \phi_R T = C \quad (6b)$$

$$T^T \phi_R^T k \phi_R T = \Lambda \quad (6c)$$

where I is an identity matrix, Λ is a diagonal matrix of system eigenvalues (frequencies squared), and C is, in general, a fully populated modal damping matrix at the system level.

The nonhomogeneous form of Equation (5) is used to solve the forced response problem. The off-diagonal elements of C are usually neglected while the diagonal elements, according to [6] are given by

$$C_{jj} = 2\zeta_j \Lambda_j^{1/2}, \quad (7)$$

ζ_j being the critical damping ratio for the jth mode. Without full-scale testing of the composite structure, ζ_j cannot be obtained directly. The problem then is to find some other means of determining C_{jj} .

In Equation (6b), it is convenient to let $\phi_R^T \rho \phi_R = c$ where

$$c = \begin{bmatrix} c^1 & & & \\ & c^2 & & \\ & & \ddots & \\ & & & c^N \end{bmatrix}$$

and $c^i = \phi_R^{iT} \rho^i \phi_R^i$. The scalar C_{jj} may then be expressed in the form

$$C_{jj} = \sum_i T_j^{iT} c^i T_j^i \quad (8)$$

where T_j denotes the jth column of T and

$$T = \begin{bmatrix} T^1 \\ T^2 \\ \vdots \\ T^N \end{bmatrix}$$

corresponding to the partitioning of c. The matrices T^i are given by synthesis of the undamped equations. It remains then to evaluate c^i .

5. Forms of the Substructure Modal Damping Matrix

Identification of substructure damping properties will depend on the type of substructure modes used in the synthesis. The mode types are governed by the boundary conditions imposed. Interface boundaries may be free, fixed, or reflect some intermediate degree of fixity by (by application of mass loading, for example). The case involving free-interface boundary conditions is the simplest, both conceptually and from an experimental viewpoint. In this case, the modal matrix ϕ_R^i will contain rigid body and elastic modes. For free vibration modes, ϕ_R^i may be partitioned to distinguish between the rigid body and elastic (normal) modes.

$$\phi_R^i = \begin{bmatrix} iR & | & iN \\ \phi_R & | & \phi_R \end{bmatrix} \quad (9)$$

Relative to the modal coordinates p^i , c^i may be partitioned as

$$c^i = \begin{bmatrix} iR^T & | & \\ -\phi_R & | & \\ iN^T & | & \\ \phi_R & | & \end{bmatrix} [\rho^i] \begin{bmatrix} iR & | & \\ \phi_R & | & \\ iN & | & \\ \phi_R & | & \end{bmatrix} = \begin{bmatrix} c^{iRR} & | & c^{iRN} \\ -c^{iNR} & | & c^{iNN} \end{bmatrix} \quad (10)$$

In the absence of external damping,

$$c^i = \begin{bmatrix} 0 & | & 0 \\ - & | & \\ 0 & | & c^{iNN} \end{bmatrix}$$

The submatrix c^{iNN} may be determined by the method discussed in [6]. After obtaining all the c^i matrices, $i = 1$ to N , modal damping for the coupled system can be determined by Equation (8). For mass-loaded interface modes, the form of c^i is also given by (10).

When fixed-interface substructure modes are used, the determination of c^i will be more difficult. In this case, ϕ_R^i may include three different types of modes--rigid body, constraint, and normal modes. The constraint modes appear only for redundantly interconnected substructures and are introduced so that the motion of interface boundary points is completely defined. These are usually

chosen to be static deformation shapes which are obtained by displacing each boundary coordinate sequentially while holding all others fixed and applying no loading whatsoever at points other than attachment points. Under these conditions, ϕ_R^i may be partitioned in the manner

$$\phi_R^i = \begin{bmatrix} \phi_R^{iRB} & I & 0 \\ \phi_R^{iRI} & \phi_R^{iC} & \phi_R^{iN} \end{bmatrix} \quad (11)$$

where ϕ_R^{iRB} is the portion of rigid body modes corresponding to boundary points, ϕ_R^{iRI} is the complementary part corresponding to internal points, I is an identity matrix, ϕ_R^{iC} defines the static deformation shapes of the substructure internal to its interface boundary, and ϕ_R^{iN} represents the fixed boundary normal modes. In evaluating the matrix product

$$c^i = \phi_R^{iT} \rho^i \phi_R^i$$

in this case, ρ^i may be partitioned into submatrices corresponding to boundary and internal coordinates

$$\rho^i = \begin{bmatrix} \rho^{iBB} & \rho^{iBI} \\ \rho^{iIB} & \rho^{iII} \end{bmatrix}$$

The symmetric matrix c^i is given

$$c^i = \begin{bmatrix} c^{iRR} & c^{iRC} & c^{iRN} \\ c^{iCR} & c^{iCC} & c^{iCN} \\ c^{iNR} & c^{iNC} & c^{iNN} \end{bmatrix} \quad (12)$$

where, temporarily dropping the superscript i and the subscript R for notational convenience,

$$c^{RR} = \phi^{RB^T} \rho^{BB} \phi^{RB} + \phi^{RB^T} \rho^{BI} \phi^{RI} + \phi^{RI^T} \rho^{IB} \phi^{RB} + \phi^{RI^T} \rho^{II} \phi^{RI} \quad (13a)$$

$$c^{RC} = \phi^{RB^T} \rho^{BB} \phi^{RC} + \phi^{RB^T} \rho^{BI} \phi^C + \phi^{RI^T} \rho^{IB} \phi^C + \phi^{RI^T} \rho^{II} \phi^C \quad (13b)$$

$$c^{RN} = \phi^{RB^T} \rho^{BI} \phi^N + \phi^{RI^T} \rho^{II} \phi^N \quad (13c)$$

$$c^{CC} = \rho^{BB} \phi^C + \rho^{BI} \phi^C + \phi^{C^T} \rho^{IB} + \phi^{C^T} \rho^{II} \phi^C \quad (13d)$$

$$c^{CN} = \rho^{BI} \phi^N + \phi^{C^T} \rho^{II} \phi^N \quad (13e)$$

$$c^{NN} = \phi^{N^T} \rho^{II} \phi^N \quad (13f)$$

Only c^{NN} given by (13f) may be obtained directly from fixed boundary vibration tests. In general, c^{RR} , c^{RC} , c^{RN} , c^{CC} , and c^{CN} will not be completely determined.

There are various ways of assigning values to these submatrices. It is first recognized that a representation of ρ^{II} may be derived by the following method. By definition,

$$\phi^{NT} \rho^{II} \phi^N = c^{NN}.$$

Given that

$$\phi^{NT} \mu^{II} \phi^N = I,$$

it follows that

$$\phi^{NT} \rho^{II} \phi^N = \left(\phi^{NT} \mu^{II} \phi^N \right) c^{NN} \left(\phi^{NT} \mu^{II} \phi^N \right). \quad (14)$$

In particular, (14) will be satisfied if

$$\rho^{II} = \hat{\rho}^{II} = \mu^{II} \phi^N c^{NN} \phi^{NT} \mu^{II}. \quad (15)$$

It is to be emphasized that ρ^{II} is not determined uniquely by this method. In fact, $\hat{\rho}^{II}$ may not even resemble ρ^{II} . Nevertheless, $\hat{\rho}^{II}$ will satisfy

$$c^{NN} = \phi^{NT} \hat{\rho}^{II} \phi^N$$

and one may determine values for the submatrices (13a) through (13e) by neglecting all but the last term in each equation and substituting $\rho^{II} = \hat{\rho}^{II}$. This is equivalent to assuming that ρ^{BB} and ρ^{BI} are both null. If this assumption is not acceptable, then additional tests will presumably have to be made.

This line of reasoning was not pursued much further because of practical difficulties associated with obtaining the boundary modes themselves. These are discussed more fully in Reference [7]. From the standpoint of damping, however, it is apparent at the outset that both the free-interface mode method and the fixed-interface mode method suffer from the same basic limitation: the representation of damping near interfacial boundaries will tend to be poor. In the free-interface mode case, the tendency is caused by the fact that convergence of system modes is found to be poor, with more substructure modes required to attain a given degree of accuracy. This is usually explained by the failure of lower

frequency modes to adequately "work" the local structure near interface boundaries. If strain energy in this region is not properly accounted for, it is likely that the dissipative energy may not be either.

In some respects, the problem associated with using fixed interface modes for damping synthesis is similar. Displacements near interface boundaries are usually defined by static displacement shapes for which damping information is not available. So again, the basic problem is an inadequate representation of the structure's dissipative properties near substructural interface boundaries.

On the other hand, the use of mass-loaded interface modes can potentially overcome this problem. Mass loading causes the structure to be "worked" more in these local areas. It is felt that the dissipative properties of the structure can therefore be represented more fully. Selection of the proper mass loading will be important. This topic is also discussed in [7]. Since the damping matrices in this case are of the same form as in the free-interface mode case, their evaluation is straightforward.

6. Use of Damped Modes to Compute the Modal Damping Matrix

In searching for a way to more fully describe the damping properties of a structure, two things become apparent. The first is that most structures tend to be lightly damped, therefore damped modes closely resemble the hypothetical undamped modes except for small differences in phasing. The second is that phase separation techniques presently employed in vibration testing are potentially capable of yielding these small phase differences quantitatively. This phase information can be used to derive a more complete set of structural damping information than simple decay tests provide.

Intuitively, one would expect that if the damping in a structure could be gradually reduced to zero, the damped modes would approach the undamped modes in some continuous fashion. Thus, a damped mode might be representable by a linear perturbation of the corresponding undamped mode. This thinking led to the formulation of the perturbation analysis contained in Reference [6]. The salient features of the derivation are included here using somewhat different notation to provide continuity in the overall formulation.

The basic equations of motion for a substructure are first considered at the discrete coordinate level, as given by (1). Transformation from the discrete coordinates x^i to distributed coordinates p^i using $x^i = \phi_R^i p^i$ results in

$$m_p^{i,i} + c_p^{i,i} + k_p^i = \phi_R^T f^i = f_p^i \quad (16)$$

where

$$m^i = \phi_R^i \mu^i \phi_R^i \quad (17a)$$

$$c^i = \phi_R^i \rho^i \phi_R^i \quad (17b)$$

$$k^i = \phi_R^i \kappa^i \phi_R^i \quad (17c)$$

$$f_p^i = \phi_R^i f^i \quad (17d)$$

The modal damping matrix c^i may assume different forms, as suggested by (10) and (12). The main objective is to determine the submatrix c^{iNN} which appears in both equations. For convenience, (10) and (12) may be put in the same form by writing both (9) and (11) as

$$\phi_R^i = \begin{bmatrix} \phi_{R1}^i & \phi_{R2}^i \\ \phi_{R3}^i & \phi_{R4}^i \end{bmatrix}$$

With this sort of partitioning, (16) becomes

$$\begin{bmatrix} m & 1BB & 1BN \\ m & 1NB & 1NN \end{bmatrix} \begin{Bmatrix} p \\ p \\ p \end{Bmatrix} + \begin{bmatrix} c & 1BB & 1BN \\ c & 1NB & 1NN \end{bmatrix} \begin{Bmatrix} p \\ p \\ p \end{Bmatrix} + \begin{bmatrix} k & 1BB & 1BN \\ k & 1NB & 1NN \end{bmatrix} \begin{Bmatrix} p \\ p \\ p \end{Bmatrix} = \begin{Bmatrix} f \\ p \\ p \end{Bmatrix} \quad (18)$$

Then one may write

$$m \overset{1}{\underset{p}{\text{INN}}} \overset{1}{\text{IN}} + c \overset{1}{\underset{p}{\text{INN}}} \overset{1}{\text{IN}} + k \overset{1}{\underset{p}{\text{INN}}} \overset{1}{\text{IN}} = \bar{f} \overset{1}{\underset{p}{\text{IN}}} \quad (19a)$$

where, in general,

$$\bar{f} \overset{1}{\underset{p}{\text{IN}}} = f \overset{1}{\underset{p}{\text{IN}}} - m \overset{1}{\underset{p}{\text{INB}}} \overset{1}{\text{IB}} - c \overset{1}{\underset{p}{\text{INB}}} \overset{1}{\text{IB}} - k \overset{1}{\underset{p}{\text{INB}}} \overset{1}{\text{IB}} \quad (19b)$$

Now it is recognized that when

$$\phi_R \overset{1}{\underset{R}{\text{IN}}} \overset{1}{\underset{\mu}{\text{I}}} \phi_R \overset{1}{\text{IN}} \equiv I \quad (20)$$

by proper normalization of $\phi_R \overset{1}{\text{IN}}$, that (19a) is of the form

$$I \ddot{q} + \xi \dot{q} + \omega_o^2 q = f_q \quad (21)$$

where ω_o^2 is a diagonal matrix of undamped frequencies squared, and ξ may be viewed as the modal damping matrix.

From this point on, it will simplify the notation considerably to drop the superscript notation used to distinguish different substructures and different classes of modes for a given substructure. It will follow, for example, that $x^1 = x$, $\mu^1 = \mu$, and $\phi_R \overset{1}{\text{IN}} = \phi_R$. With the simplified notation, the homogeneous form of Equation (1) becomes

$$\mu \ddot{x} + \rho \dot{x} + \kappa x = 0 \quad (22)$$

These second order equations may be written in first order form leading to the eigenproblem

$$\left(\begin{bmatrix} -\kappa & 1 & 0 \\ 0 & 1 & -\mu \end{bmatrix} + \lambda_j \begin{bmatrix} -\rho & 1 & -\mu \\ \mu & 1 & 0 \end{bmatrix} \right) \begin{Bmatrix} -\phi_j \\ \lambda_j \end{Bmatrix} = 0 \quad (23)$$

where λ_j is a complex eigenvalue of the form

$$\lambda_j = \sigma_j + i\omega_j \quad (24)$$

and ϕ_j is that part of the complex eigenvector which corresponds to the displacement vector x . The term $-\sigma_j = \zeta_j \omega_{o_j}$ may be interpreted as the decay rate associated with mode j , while $\omega_j = \omega_{o_j} \sqrt{1-\zeta_j^2}$ is the damped natural frequency of that mode. The vector ϕ_j will henceforth be referred to as the j th damped mode. It may be related to the hypothetical undamped mode ϕ_{R_j} by the equation

$$\phi_j = \phi_{R_j} + \delta\phi_{R_j} + i\delta\phi_{I_j} \quad (25)$$

where $\delta\phi_{R_j}$ and $\delta\phi_{I_j}$ are considered to be small compared to ϕ_{R_j} . For lightly damped structures governed by Equation (22), the eigenvectors will occur in conjugate pairs. The resulting matrix of eigenvectors will transform (23) to diagonal form (assuming that μ , ρ , and κ are symmetric) so that, in particular,

$$\begin{bmatrix} -\phi^T & \lambda \phi^T \\ \phi^{*T} & \lambda^* \phi^{*T} \end{bmatrix} \begin{bmatrix} -\rho & -\mu \\ \mu & 0 \end{bmatrix} \begin{bmatrix} -\phi & \phi^* \\ \phi \lambda & \phi^* \lambda^* \end{bmatrix} = \begin{bmatrix} A & 0 \\ 0 & A^* \end{bmatrix} \quad (26)$$

where the asterisk denotes the complex conjugate. Three separate equations may be derived from (26)

$$\phi_j^T \rho \phi_k^* + \phi_j^T \mu \phi_k^* \lambda_k^* + \lambda_j \phi_j^T \mu \phi_k^* = 0 \quad : \quad \text{all } j, k \quad (27a)$$

$$\phi_j^T \rho \phi_k + \phi_j^T \mu \phi_k \lambda_k + \lambda_j \phi_j^T \mu \phi_k = \begin{cases} 0 & : \quad j \neq k \\ A_j & : \quad j = k \end{cases} \quad (27b)$$

$$\phi_j^T \rho \phi_k + \phi_j^T \mu \phi_k \lambda_k + \lambda_j \phi_j^T \mu \phi_k = \begin{cases} 0 & : \quad j \neq k \\ A_j & : \quad j = k \end{cases} \quad (27c)$$

Using Equations (24), (25), and (20), and the perturbation assumptions

$$|\sigma_j| \ll \omega_j$$

$$|\delta\phi_{R_j}|, |\delta\phi_{I_j}| \ll |\phi_{R_j}|$$

$$|\rho\phi_{R_j}| \ll |(\omega_j - \omega_k)\mu\phi_{R_j}|$$

one may derive from (27a) the relationships

$$\epsilon_{jj} = \phi_{R_j}^T \rho \phi_{R_j} = -2\sigma_j = 2\zeta_j \omega_{o_j} \quad (28a)$$

$$\epsilon_{jk} = \phi_{R_j}^T \rho \phi_{R_k} = -(\omega_j - \omega_k) (\phi_{R_j}^T \mu \delta\phi_{I_k} - \delta\phi_{I_j}^T \mu \phi_{R_k}) \quad : \quad j \neq k \quad (28b)$$

From (28b) and (27b), an alternative expression for ξ_{jk} may be found.

$$\xi_{jk} = \omega_j \delta \phi_{I_j}^T \mu \phi_{R_k} + \omega_k \phi_{R_j}^T \mu \delta \phi_{I_k} \quad (29)$$

Finally, from (27c), one may derive

$$A_j = 2\omega_j \left(-2\phi_{R_j}^T \mu \delta \phi_{I_j} + i \right), \quad (30)$$

a relationship which will be needed later.

It will be of interest to examine more closely the structure of Equation (29), and compare it to that of Equation (28a). It has been postulated that ξ_{jk} and ξ_{jj} are of the same order of magnitude (at least when $\omega_j > \omega_k$). This implies that the elements of $\delta \phi_{I_j}$ should be of the same order as δ_j . Since $|\delta \phi_{I_j}| \ll |\phi_{R_j}|$, the phase angles associated with elements of the complex vector ϕ_j will be of the order δ_j . This relationship will govern the accuracy requirements on phase angle data.

The important conclusions to be drawn in this section are that the diagonal elements of the modal damping matrix ξ correspond to the uncoupled modal damping constants for each mode, and that the off-diagonal elements can be determined provided that some way can be found to identify $\delta \phi_{I_j}$.

7. Use of Resonant Response Data to Identify Damped Modes

The method for constructing a nondiagonal damping matrix outlined in Section 6 requires that the damped modes of the structure be known. These modes are complex, having both real and imaginary parts, and occur in conjugate pairs for lightly-damped structures. In a practical sense, it is not likely that these modes will be directly measurable from vibration tests because it is difficult to excite sufficiently "pure" modes. Off-resonant modes may contribute significantly to the total acceleration response, particularly in the coincident component defined to be in phase with the forcing function. The quadrature component leads the force by 90° and is normally used to define the local undamped modes. The fact that off-resonant mode response tends to be relatively small and out-of-phase with that of the resonant mode has provided the basis for phase separation techniques now used to more accurately define the undamped modes; however, contamination of the coincident response by off-resonant mode participation imposes the need for modal separation if the damped modes are to be determined at all. An iterative procedure has been developed and demonstrated. For damping levels on the order of 1%, convergence has been achieved in only one or two iterations although the process may be cycled any number of times should convergence proceed more slowly.

The basic technique to be used for mode separation requires, in addition to resonant response frequencies and damping rates, a knowledge of the force input to the structure. Assuming that the quadrature component of each resonant response is a reasonably accurate representation of the undamped mode associated with that frequency, the extent of off-resonant mode participation can be determined to good approximation and subtracted from the total response, leaving an improved representation of the resonant mode. This procedure was successfully applied by Stahle [8] a decade ago to improve upon the real undamped modes of a structure. The present work extends that method for application to the damped modes which are complex. The generalization is valid provided that the structure is lightly damped. Specific validity criteria which involve quantitative relationships among the distribution of the forcing function, the amount of damping, frequency separation of the modes, and measurement accuracy are derived in the Appendix. In keeping with the simplified notation, the equations which follow may be considered to apply to a substructure even through the superscripts are dropped for notational convenience.

It is assumed that the n equations of motion for a real structure (substructure) may be written in the form

$$\mu \ddot{x} + \rho \dot{x} + \kappa x = f(t) \quad (31)$$

In order to make this development applicable to free-free structures as well as constrained structures, it will be assumed that the displacement vector x defines elastic deformations relative to rigid body motion. In the free-free case, this implies that to utilize total response measurements, rigid body response must first be computed independently and subtracted from the total response. This is discussed further in Section 9.5

Under these conditions, the equations of motion as given by (31) may be transformed according to

$$x = \phi_R q \quad (32)$$

where ϕ_R is a modal matrix containing undamped elastic modes. Then (31) becomes

$$I \ddot{q} + \xi \dot{q} + \omega_o^2 q = \phi_R^T \bar{f}(t) = f_q(t) \quad (21)$$

The force vector $\bar{f}(t)$ will include any forces which couple the elastic modes to other modes, as indicated by (19b). This equation was given earlier as indicated. It is assumed that, in general, a different force vector $\bar{f}(t)$ will be generated to excite a resonant response at each natural frequency Ω_j , and consequently, that

$$\bar{f}(t) = \bar{P}_{x_j} g_j(t) \quad (33)$$

The complex frequency response vector corresponding to Ω_j is then given by

$$H_{q_j} = \left[\left(\omega_o^2 - \Omega_j^2 I \right) + i \Omega_j \xi \right]^{-1} \phi_R^T \bar{P}_{x_j} \quad (34)$$

Initially, it may be assumed (as shown in the Appendix) that

$$\xi_{jk} = -\delta_{jk} (\sigma_j + \sigma_k)$$

where δ_{jk} is the Kronecker delta, and that ϕ_R is equal to the normalized quadrature component of acceleration response. Thus, a vector H_{q_j} may be evaluated for each of the resonant response conditions and transformed back to the x coordinate system by

$$H_{x_j} = \phi_R H_{q_j}$$

Combining these equations in a single matrix equation gives

$$H_x = \phi_R H_q$$

where H_q is assumed to be a nonsingular square matrix. Then

$$\phi_R = H_x H_q^{-1} \quad (35)$$

provides the first estimate of the undamped modes ϕ_R . The vector H_{x_j} is obtained from total acceleration response data as shown in the Appendix. In this way, an improved version of ϕ_R is obtained.

In order to derive an estimate of $\delta\phi_I$, Equation (31) is written in the first order form

$$\begin{bmatrix} -\rho & 1 & -\mu \\ \mu & 1 & 0 \end{bmatrix} \begin{Bmatrix} \dot{x} \\ \ddot{x} \end{Bmatrix} + \begin{bmatrix} -\kappa & 1 & 0 \\ 0 & 1 & -u \end{bmatrix} \begin{Bmatrix} x \\ \dot{x} \end{Bmatrix} = \begin{Bmatrix} -f(t) \\ 0 \end{Bmatrix}$$

Solution of the corresponding first order eigen-problem leads to the transformation

$$\begin{Bmatrix} x \\ \dot{x} \end{Bmatrix} = \begin{bmatrix} -\phi & \phi^* \\ \phi\lambda & \phi^*\lambda^* \end{bmatrix} \begin{Bmatrix} z \end{Bmatrix}$$

The frequency response vector in the z coordinate system is then given by

$$H_{z_j} = \begin{bmatrix} (i\Omega_j I - \lambda) & 0 \\ 0 & (i\Omega_j I - \lambda^*) \end{bmatrix}^{-1} \begin{bmatrix} A & 1 & 0 \\ 0 & 1 & A^* \end{bmatrix}^{-1} \begin{bmatrix} \phi^T \\ \phi^{*T} \end{bmatrix} P_{x_j} \quad (36)$$

where A is a diagonal matrix whose elements are given by (30). If it may be initially assumed that

$$A_j = i2\omega_j$$

and that ϕ is given by the real part of the resonant response matrix, then a vector H_{z_j} may be evaluated for each resonant frequency and transformed back to the x coordinate system by

$$H_{x_j} = [\phi \mid \phi^*] H_{z_j}$$

Combining these equations into a single matrix equation gives

$$H_x = [\phi \mid \phi^*] H_z. \quad (37a)$$

Alternatively, recognizing that ϕ and ϕ^* may be expressed in terms of $\phi_R + \delta\phi_R = \phi_R$ and $\delta\phi_I$, one may write

$$H_x = \phi_R H_R + \delta\phi_I H_I \quad (37b)$$

where H_R and H_I are both complex square matrices. Having already found ϕ_R from (35), $\delta\phi_I$ is given by the equation

$$\delta\phi_I = (H_x - \phi_R H_R) H_I^{-1} \quad (38)$$

With ϕ_R and $\delta\phi_I$ computed, the first iteration is complete. To begin the second iteration, these values are used in (29) and (30) to update the matrices ξ and A , respectively. Then Equations (34) through (38) may be recycled to complete the second iteration. Succeeding iterations follow in the same way.

The entire procedure may be summarized by the following:

Initial values

Define the damped modes initially by the quadrature acceleration response QUAD (H_x). That is,

$$(0) \quad \phi_j = \text{QUAD} (H_{x_j}) / [\text{QUAD} (H_{x_j})^T \mu \text{QUAD} (H_{x_j})]^{1/2}$$

These vectors are defined to be real, and are of the form $\phi_j = \phi_{R_j}$; the imaginary parts $\delta\phi_{I_j} \equiv 0$.

Evaluate matrices ξ and A

$$(1) \quad \xi_{jk} = -\delta_{jk} (\sigma_j + \sigma_k) - (\omega_j - \omega_k) \left(\phi_{R_j}^T \mu \delta\phi_{I_k} - \delta\phi_{I_j}^T \mu \phi_{R_k} \right)$$

$$(2) \quad A_j = -4\omega_j \phi_{R_j}^T \mu \delta\phi_{I_j} + i 2\omega_j$$

where δ_{jk} is the Kronecker delta

$$\delta_{jk} = \begin{cases} 1 & : j = k \\ 0 & : j \neq k \end{cases}$$

Compute the real and imaginary parts of the damped modal matrix ϕ

$$(3)^\dagger H_{q_j} = \left[\begin{pmatrix} \omega_o^2 & & \\ & -\Omega_j^2 & I \\ & & \end{pmatrix} - i\Omega_j \xi \right]^{-1} \bar{P}_{x_j}$$

$$(4) \phi_R = H_x H_q^{-1} ; \quad (\text{in initial step } \phi_{R_j} = \phi_j)$$

$$(5)^\dagger H_{z_j} = \left[\begin{pmatrix} i\Omega_j I - \lambda & & \\ & -0 & \\ & & i\Omega_j I - \lambda^* \end{pmatrix} \right]^{-1} \left[\begin{pmatrix} A & & 0 \\ & I & \\ 0 & & A^* \end{pmatrix} \right]^{-1} \begin{bmatrix} -\phi^T \\ \phi^{*T} \end{bmatrix} P_{x_j}$$

$$(6) H_x = \begin{bmatrix} \phi & \phi^* \end{bmatrix} H_z \approx \phi_R H_R + \delta\phi_R H_I$$

$$(7) \delta\phi_I = \left(H_x - \phi_R H_R \right) H_I^{-1}$$

Steps (1) through (7) may be repeated any number of times. The procedure should converge if the proper conditions are met. These conditions are derived in the Appendix.

[†] Note that \bar{P}_{x_j} is used in Step (3), while P_{x_j} (without the bar) is used in Step (5).

PART B: VERIFICATION

8. Analytical Verification

A variety of examples have been worked in the process of formulating equations and coding them for numerical computation. They were used as check cases to debug computer codes and to facilitate the understanding of unfamiliar concepts. As such, they have been of considerable value in relating the theory to practical application. Some of the examples are included in this section.

The first set of examples to be discussed in Section 8.1 was selected by GAC to demonstrate the relative merits of coupling procedures involving sub-structure modes with different kinds of boundary conditions. The purpose of that investigation was to provide a basis for selecting a coupling procedure best suited for application to the Shuttle. Since the matrix method for damping synthesis relies on the same transformations as the synthesis of undamped equations, it was a simple matter for GAC to punch them on cards and transmit them to TRW. This avoided duplication of effort and provided a consistent set of examples by which to evaluate the convergence of modes and frequencies as well as modal damping in representative Shuttle configurations.

In Section 8.2, a four-degree of freedom lumped parameter model is introduced to demonstrate the computation of a modal damping matrix. In this example, the damped modes are first computed by a complex eigenvalue routine. The modal damping matrix is then computed without using the original damping matrix, using only the mass matrix, the frequencies, and the damped modes. For comparison, the standard computation is made using the known damping matrix. The resulting matrix is nondiagonal in form, confirming that the damping is nonproportional.

The same example is used in Section 8.3 to demonstrate how the damped modes can be deduced from resonant response information. In this case, it is assumed that neither the original damping matrix nor the damped modes are known, only response at each of the system's resonances. The response includes contributions from all the modes in general, but mainly from those which are adjacent in the frequency spectrum. It is shown that the off-resonant mode response can be removed, leaving just the damped modes themselves. Computations involve an iterative procedure which alternately computes the damped modes and the modal damping matrix until both converge.

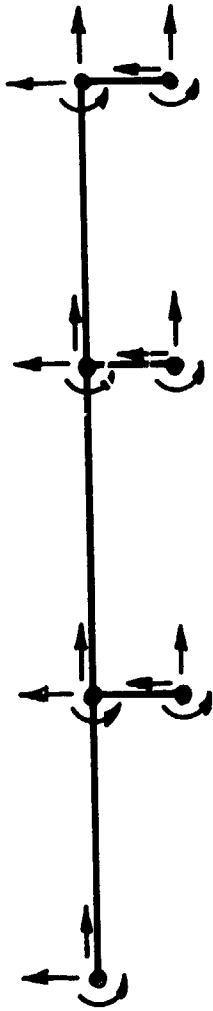
8.1 A Numerical Comparison of Coupling Procedures

A comparative evaluation of the coupling procedures referred to in Section 5 has been made on the basis of math model data furnished by GAC [7]. These data reflect the mass and stiffness properties of realistic Shuttle configurations. Damping parameters for these models have been assumed arbitrarily. The main objective has been to define simple nonproportional damping matrices for each substructure corresponding to its respective discrete coordinate system. Modal damping matrices are then derived from the substructure mode matrices provided by GAC. These are treated in the same way that experimentally derived matrices will be treated in subsequent work.

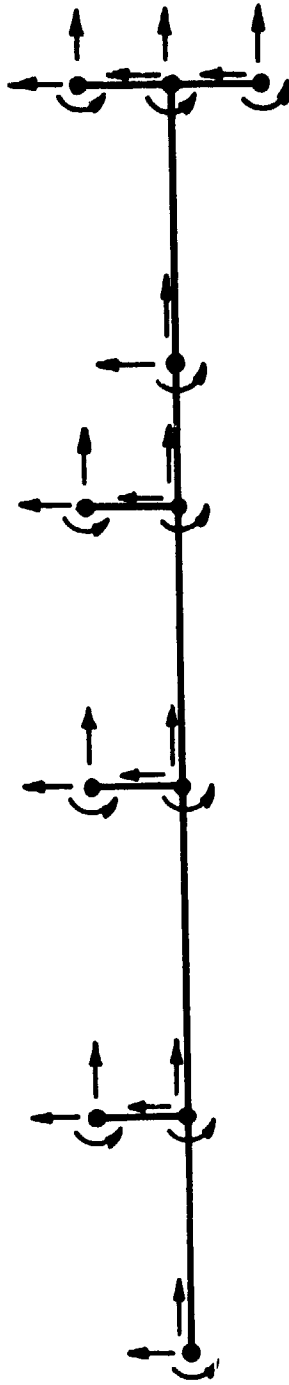
The Shuttle configuration adopted in this study involves two substructures, orbiter and tank, which are connected in a parallel arrangement. Schematic drawings representing each substructure are shown in Figure 1. The coupled configuration is shown in Figure 2. The models are planar, having three coordinates defined for each nodal point: two translations, and one rotation. No mass is associated with any rotational coordinate. Thus, a total of 14 component modes are obtained for the orbiter and 22 for the tank. Pinned connections are assumed at the attachment points. With six constraint equations acting to couple the two vehicles, the total number of degrees of freedom for the coupled vehicle totals 30. Eigenproblem solutions including all 30 degrees of freedom are used for reference. Truncated mode solutions involving 16 and ten degrees of freedom are obtained to evaluate convergence. The former is understood to include 11 uncoupled component modes for each substructure, while the latter includes eight, the lowest in each case.

Numerical computations for four different coupling configurations have been made. These configurations are:

- Case 1. A free-free orbiter coupled to a free-free tank.
- Case 2. An orbiter fixed at its junction points coupled to a free-free tank.
- Case 3. A free-free orbiter coupled to tank fixed at its base whose junction points are free.
- Case 4. An orbiter fixed at its junction points coupled to a tank fixed at its base whose junction points are free.



Orbiter Model



Tank Model

Figure 1. Schematic Models of Space Shuttle Orbiter and Tank Substructures.

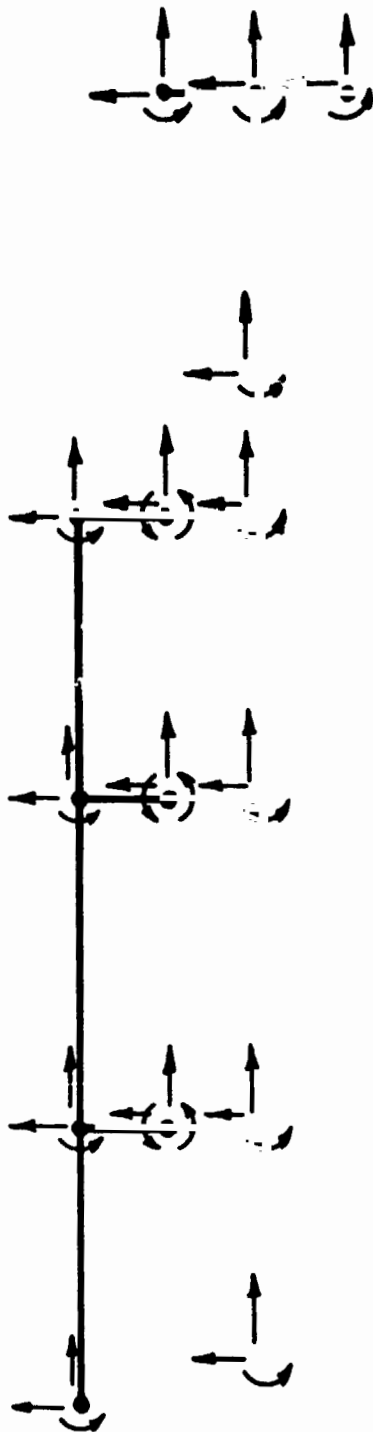


Figure 2. Schematic Model of Coupled Space Shuttle Orbiter/
Tank Assembly

Cases 1 and 2 each include two subcases designated by a and b. Cases 1a and 2a involve the use of free-interface substructure modes when the substructure is considered to be free-free. Cases 1b and 2b correspond to substructure modes reflecting mass loading at the junction points.

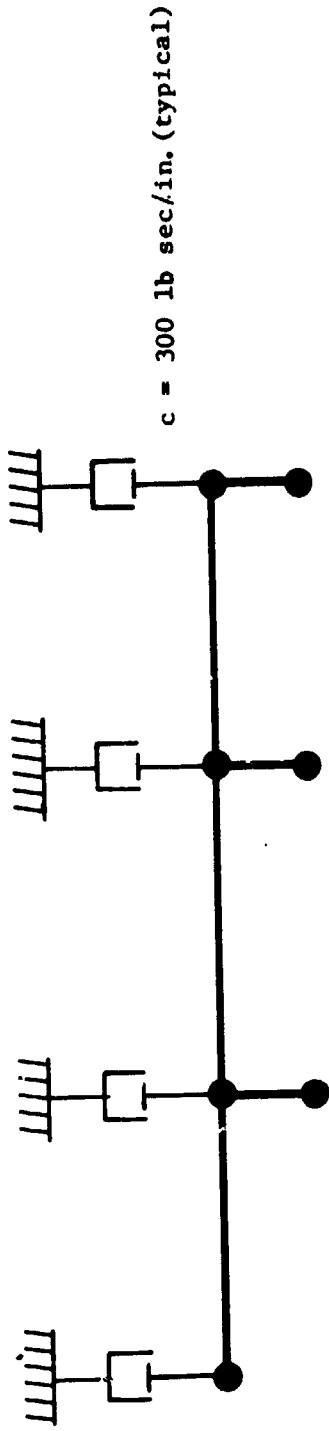
Computations are executed in the following manner.

1. Preset $C_{jj} = 0$, all j .
2. Read T^i and evaluate $C_{jj} = C_{jj} + T_j^{iT} c^i T_j^i$ for all j .
3. Read ρ^i and evaluate $c^i = \phi_R^{iT} \rho^i \phi_R^i$.
4. Read ϕ_R^i .

The procedure is recycled until all (both) of the substructures are taken into account. Matrices ϕ_R^i and T^i were furnished by GAC.

Several different sets of ρ^i damping matrices were assumed, the simplest corresponding to externally-grounded lateral dashpots, as shown in Figure 3. Although this damping distribution gave diagonal ρ^i matrices, the corresponding c^i matrices were not diagonal. In order to specify internal damping, the damping matrices must involve rotational as well as translational coordinates since coupled modes may involve rigid body rotations of the two substructures. Such damping matrices may be derived in the same way as the stiffness matrices. Although this form of damping is more representative, it is not deemed essential for evaluation of coupling procedures, and time constraints were prohibitive. Therefore, only external damping was assumed. This permitted all rotational displacements to be deleted from the substructure modal matrices ϕ_R^i , thereby reducing somewhat the computational effort.

The nominally chosen distribution of damping is illustrated by Figure 3 where dashpots are shown connecting each substructure to ground. The dashpot constants were assigned identical values of 300 lb-sec/in. Tabulated results from the damping synthesis involving Cases one through four are given in Tables one through four, respectively. Damping constants C_{jj} are given for seven elastic modes in each case.



ORBITER

BOOSTER

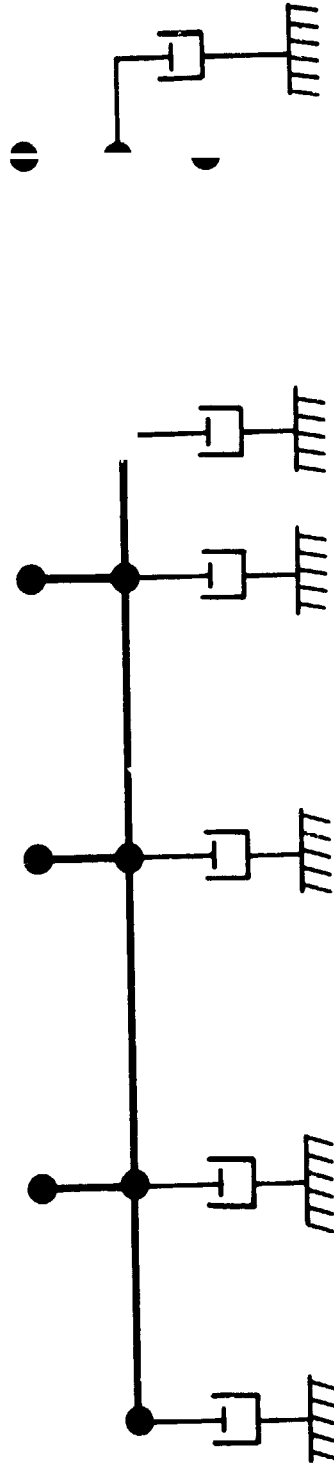


Figure 3. Nonproportional Damping Model for Orbiter and Tank

Table 1 - Damping Constants C_{jj} by Modal Synthesis for Case 1

a. No Mass Loading in Free-Free Modes

<u>Mode No.</u>	<u>10 d.o.f.</u>	<u>16 d.o.f.</u>	<u>30 d.o.f.</u>
1	5.489 E-3	6.549 E-4	6.667 E-3
2	6.603 E-4	6.604 E-3	7.820 E-3
3	3.583 E-4	1.487 E-3	2.631 E-3
4	3.743 E-4	6.661 E-5	1.539 E-3
5	1.320 E-4	1.630 E-6	2.283 E-6
6	6.856 E-6	4.934 E-8	4.029 E-4
7	2.002 E-4	2.560 E-4	6.147 E-4

b. Mass-Loaded Junction Points in Free-Free Modes

1	4.295 E-3	6.565 E-3	6.840 E-3
2	9.309 E-3	7.831 E-3	7.644 E-3
3	1.336 E-3	2.627 E-3	2.630 E-3
4	1.578 E-4	1.530 E-3	1.540 E-3
5	5.942 E-5	1.073 E-6	2.279 E-6
6	2.851 E-6	6.628 E-5	4.029 E-4
7	1.878 E-7	1.169 E-3	6.095 E-4

Table 2 - Damping Constants C_{jj} By Modal Synthesis for Case 2

a. No Mass Loading in Free-Free Modes

1	7.494 E-3	9.424 E-4	6.666 E-3
2	2.692 E-3	9.753 E-3	7.822 E-3
3	2.054 E-4	1.264 E-3	2.630 E-3
4	1.267 E-3	1.187 E-3	1.539 E-3
5	1.958 E-4	8.159 E-7	2.286 E-6
6	7.017 E-5	2.176 E-4	4.029 E-4
7	1.097 E-5	8.608 E-4	6.100 E-4

b. Mass-Loaded Junction Points in Free-Free Modes

<u>Mode No.</u>	<u>10 d.o.f.</u>	<u>16 d.o.f.</u>	<u>30 d.o.f.</u>
1	6.087 E-3	6.843 E-3	6.843 E-3
2	8.096 E-3	7.641 E-3	7.640 E-3
3	1.175 E-3	2.632 E-3	2.630 E-3
4	1.276 E-4	1.542 E-3	1.539 E-3
5	1.149 E-4	1.302 E-6	2.284 E-6
6	4.475 E-6	2.814 E-4	4.029 E-4
7	2.365 E-7	1.167 E-3	6.103 E-4

Table 3 - Damping Constants C_{jj} By Modal Synthesis for Case 3

1	8.943 E-3	6.075 E-4	6.663 E-3
2	2.033 E-4	9.526 E-3	7.592 E-3
3	1.284 E-6	7.237 E-4	1.668 E-3
4	1.181 E-4	6.847 E-4	1.489 E-3
5	1.354 E-7	5.744 E-7	1.890 E-6
6	2.052 E-7	3.135 E-5	3.955 E-4
7	3.188 E-10	8.699 E-5	1.618 E-4

Table 4 - Damping Constants C_{jj} By Modal Synthesis for Case 4

1	9.321 E-3	9.035 E-5	6.843 E-3
2	3.347 E-4	9.613 E-3	7.640 E-3
3	5.630 E-6	7.560 E 4	2.630 E-3
4	1.141 E-3	1.107 E-3	1.539 E-3
5	1.378 E-6	7.544 E-7	2.283 E-6
6	2.198 E-6	2.127 E-4	4.029 E-4
7	4.490 E-11	8.973 E-4	6.033 E-4

It may be observed from these results that all but Cases 1b and 2b yield very poor results for all modes. In Case 1b, none of the modal damping constants have converged in the 10-d.o.f. approximation, while four of the 13 elastic mode damping constants appear to have converged reasonably well in the 16-d.o.f. approximation. Case 2b, based on fixed-interface orbiter modes, is the better of the two. Reasonably good approximations are indicated for the first two elastic modes in the 10-d.o.f. case, while excellent approximations are given for the first four elastic modes in the 16-d.o.f. approximation.

Although the use of fixed-interface substructure modes produces the best results from the standpoint of modal convergence, damping associated with the boundary modes is difficult to assess. In previous examples, both ρ^{BB} and ρ^{BI} have been null. For comparison, Case 2b was evaluated with lateral dampers connecting the orbiter attachment points to ground. Submatrix ρ^{BI} remains null in this case, but ρ^{BB} does not. Damping constants $C_{j,j}$ for the first four elastic modes of the 30-d.o.f. solution are compared in Table 5 to those obtained previously for $\rho^{BB} = 0$. Considering $\rho^{BB} \neq 0$ to provide the reference solution, one observes that having to neglect ρ^{BB} (and ρ^{BI}) destroys some of the advantage offered by the use of fixed-interface modes as far as damping calculations are concerned. Intuitively, this effect should diminish, however, as the ratio of internal coordinates to boundary coordinates increases.

In all of these examples so far, full modal damping matrices c^1 have been utilized. To show what happens when off-diagonal terms of c^1 are neglected, Case 1b was evaluated on this basis. Results corresponding to the 30-d.o.f. solution are presented in Table 6 for comparison to the previous case. In this case, all of the off-diagonal terms were neglected, not just those of c^{1NN} . Had only those of c^{1NN} been neglected, the comparison illustrated in Table 6 might have been closer.

The damping in Mode No. 5 is quite small, presumably because this is a longitudinal mode whereas the others are primarily lateral and no longitudinal dashpots have been included up to this point. The addition of one longitudinal dashpot (300 lb sec/in) to the forward ends of both Orbiter and Tank produced the results shown in Table 7. Although damping in the 5th mode is shown to increase appreciably on a percentage basis, it remains small compared to the other modes. This may be explained by the fact that there are only two longitudinal dashpots compared to ten in the lateral direction, and the likelihood that the modal mass is larger in this mode due to essentially rigid body motion of the Orbiter and Tank in opposing directions.

Table 5 - Effect of Neglecting ρ^{BB} in Modal Damping Computations

<u>Mode No.</u>	<u>Case 2b</u>	
	<u>Damping Constant, C_{jj}</u>	
	<u>$\rho^{BB} = 0$</u>	<u>$\rho^{BB} \neq 0$</u>
1	6.843 E-3	7.165 E-3
2	7.640 E-3	7.857 E-3
3	2.630 E-3	2.707 E-3
4	1.539 E-3	2.050 E-3

Table 6 - Effect of Neglecting Off-Diagonal Terms of the Modal Damping Matrix in Synthesis of C_{ij}

	<u>Case 1B</u>	
	<u>Damping Constant, C_{jj}</u>	
	<u>Off-Diagonal Terms Neglected</u>	<u>Reference</u>
1	5.782 E-3	6.840 E-3
2	3.930 E-3	7.644 E-3
3	1.577 E-3	2.630 E-3
4	1.395 E-3	1.540 E-3
5	4.755 E-6	2.279 E-6
6	2.006 E-4	4.029 E-4
7	3.834 E-4	6.095 E-4

Table 7 - Effect on C_{jj} of Adding Longitudinal Dampers to Orbiter and Tank 30-d.o.f.

	<u>Case 1b</u>	
	<u>Damping Constant, C_{jj}</u>	
	<u>Longitudinal Dampers Added</u>	<u>Reference</u>
1	8.352 E-3	6.840 E-3
2	8.599 E-3	7.644 E-3
3	2.707 E-3	2.630 E-3
4	2.053 E-3	1.540 E-3
5	8.278 E-6	2.279 E-6
6	5.416 E-4	4.029 E-4
7	7.622 E-4	6.095 E-4

8.2 Approximation of the Modal Damping Matrix

This section is included to demonstrate the validity of the perturbation results presented in Section 6. The modal damping matrix of the spring-mass system shown in Figure 4 is sought. In this case, the free vibration of the system is of concern so that the input $g(t)$ shown in the figure may be ignored. The equations of motion are of the form

$$\mu \ddot{x} + \rho \dot{x} + \kappa x = 0$$

where

$$\mu = \begin{bmatrix} 1 & & & \\ & 1 & & \\ & & .5 & \\ & & & .3 \end{bmatrix}$$

$$\rho = \begin{bmatrix} .04 & -.02 & 0 & 0 \\ & .03 & -.01 & 0 \\ \text{Sym} & & .02 & -.01 \\ & & & .01 \end{bmatrix}$$

$$\kappa = \begin{bmatrix} 2 & -1 & 0 & 0 \\ & 2 & -1 & 0 \\ \text{Sym} & & 2 & -1 \\ & & & 1 \end{bmatrix}$$

The eigenvalue problem given by (23) was solved to obtain λ and ϕ as defined by (24) and (25), respectively. Numerical values are given in Table 8. The modal damping matrix c (which is identical to ξ in this case) was approximated using (28a) and (29),

$$c_{jj} = \xi_{jj} = -2\sigma_j \quad (28a)$$

$$c_{jk} = \xi_{jk} = \omega_j \delta \phi_{I_j}^T \mu \phi_{R_k} + \omega_k \phi_{R_j}^T \mu \delta \phi_{I_k} : j \neq k \quad (29)$$

REPRODUCIBILITY OF THE
ORIGINAL PAGE IS POOR

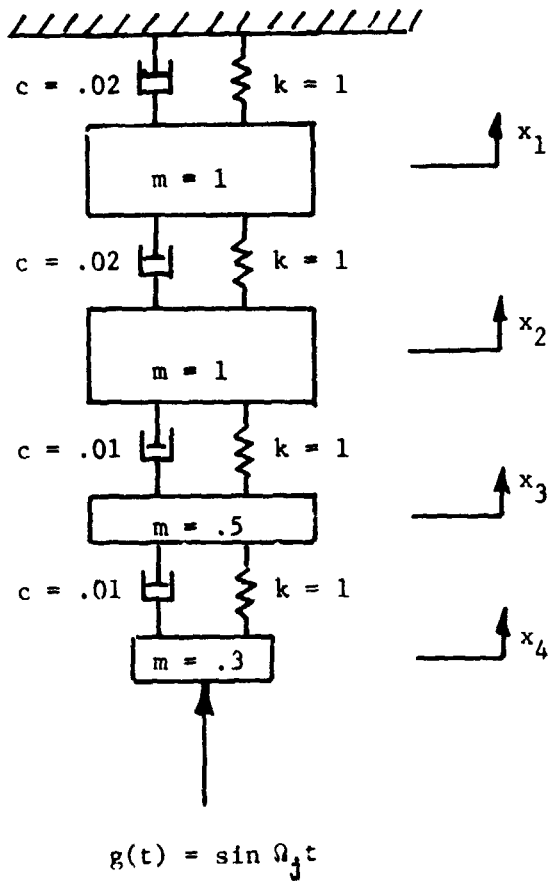


Figure 4. Four-Degree of Freedom Lumped Parameter Model

and also computed directly by (17b),

$$c = \phi_R^T \rho \phi_R \quad (17b)$$

assuming that $\phi_R = \phi_R + \delta\phi_R$ to first-order approximation. The results are compared in Table 9 where they are shown to be in good agreement.

Table 8 - Eigenvalues and Eigenvectors for a 4-d.o.f. System

(a) Eigenvalues

<u>Mode No.</u>	<u>Real (σ_j)</u>	<u>Imag. (ω_j)</u>
1	-2.083 E-3	4.681 E-1
2	-1.062 E-2	1.236
3	-2.579 E-2	1.745
4	-3.317 E-2	2.557

(b) Eigenvectors

Real ($\phi_R + \delta\phi_R \approx \phi_R$)

<u>Coordinate Number</u>	<u>Mode 1</u>	<u>Mode 2</u>	<u>Mode 3</u>	<u>Mode 4</u>
1	3.503 E-1	-6.833 E-1	6.382 E-1	-5.430 E-2
2	6.238 E-1	-3.233 E-1	-6.675 E-1	2.467 E-1
3	7.606 E-1	5.306 E-1	6.001 E-2	-1.066
4	8.142 E-1	9.793 E-1	6.960 E-1	1.108

Imaginary ($\delta\phi_I$)

1	-4.570 E-4	6.809 E-3	1.451 E-2	-2.476 E-3
2	-7.785 E-4	-4.638 E-3	-4.778 E-3	2.286 E-3
3	-2.258 E-4	-2.167 E-3	-7.698 E-3	7.952 E-4
4	0.	0.	0.	0.

Table 9 - Comparison of Modal Damping MatricesApproximate Solution

$$c = \begin{bmatrix} 4.166 \text{ E-3} & -1.408 \text{ E-3} & -1.336 \text{ E-3} & 6.331 \text{ E-4} \\ & 2.124 \text{ E-2} & -9.062 \text{ E-3} & 1.455 \text{ E-3} \\ & & 5.158 \text{ E-2} & -4.277 \text{ E-3} \\ \text{Symmetric} & & & 6.634 \text{ E-2} \end{bmatrix}$$

Reference Solution

$$c = \begin{bmatrix} 4.166 \text{ E-3} & -1.409 \text{ E-3} & -1.336 \text{ E-3} & 6.332 \text{ E-4} \\ & 2.124 \text{ E-3} & -9.060 \text{ E-3} & 1.454 \text{ E-3} \\ & & 5.158 \text{ E-2} & -4.279 \text{ E-3} \\ \text{Symmetric} & & & 6.635 \text{ E-2} \end{bmatrix}$$

8.3 Identification of the Damped Modes

To demonstrate the use of resonant response data to identify damped modes, the four degree of freedom structure illustrated in Figure 4 is again considered. Assuming sinusoidal excitation of the structure as shown, the acceleration frequency response was computed for each of the four masses including both amplitude and phase angle or, equivalently, real and imaginary components of acceleration relative to the forcing function. Numerical values are given in Table 10. The total acceleration amplitudes are plotted as functions of frequency in Figures 5a-d. This frequency response was then normalized so that, initially, the largest element of each column had the complex value (1,0). The real parts of the vectors were used to compute modal mass, and both real and imaginary parts of each vector were divided by the square root of its respective modal mass. The results are shown in Table 11. The normalized modal mass matrix is given in Table 12, where the largest off-diagonal element is noted to be 1.37 E-2.

Resonant frequencies were defined to be those frequencies at which the quadrature response of the largest displacement in a mode reached its peak value. Damping values were obtained from the real parts of the complex eigenvalues. They would be determined experimentally under practical circumstances. Given the force input, the Modal Separation Procedure (MODSEP) was initiated. After each iteration, the magnitude of the normalized incremental changes in both real and imaginary parts of the complex modes were determined from

$$\Delta^k(\phi_{R_j}) = \frac{|\phi_{R_j}^k - \phi_{R_j}^{k-1}|}{|\phi_{R_j}^{k-1}|}$$

$$\Delta^k(\delta\phi_{I_j}) = \frac{|\delta\phi_{I_j}^k - \delta\phi_{I_j}^{k-1}|}{|\delta\phi_{I_j}^{k-1}|}$$

where the superscript is used to denote the number of iteration. These results are listed in Table 13. For practical purposes, convergence is seen to be achieved in only one iteration. The improved modes, real and imaginary parts, are listed in Table 14. The agreement is seen to be good to one or two percent

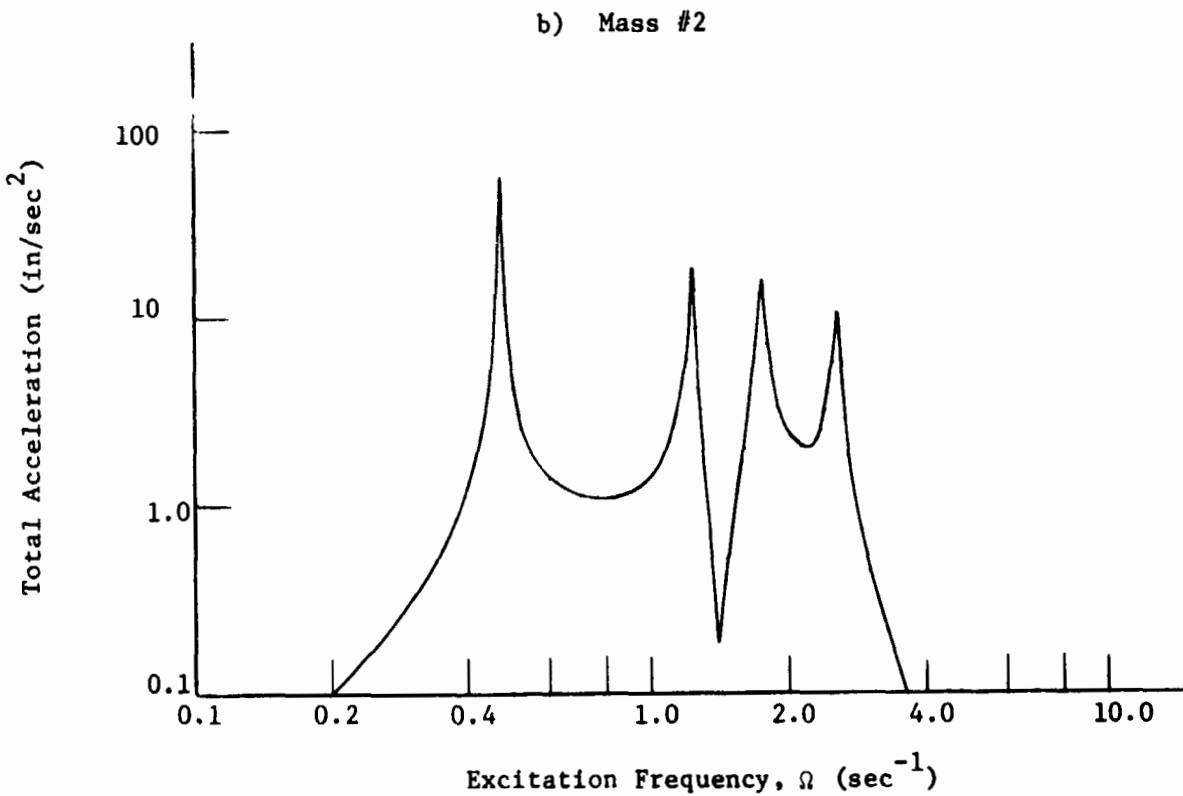
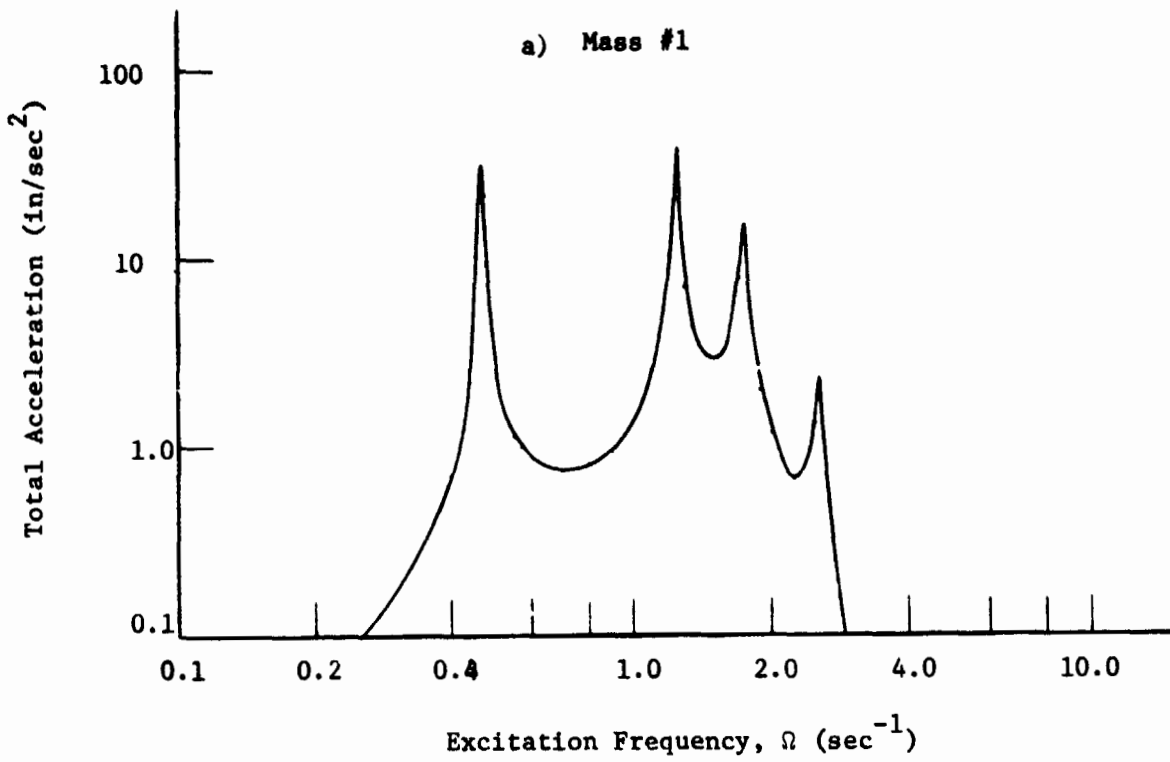


Figure 5. Acceleration Response of the Four d.o.f. Model

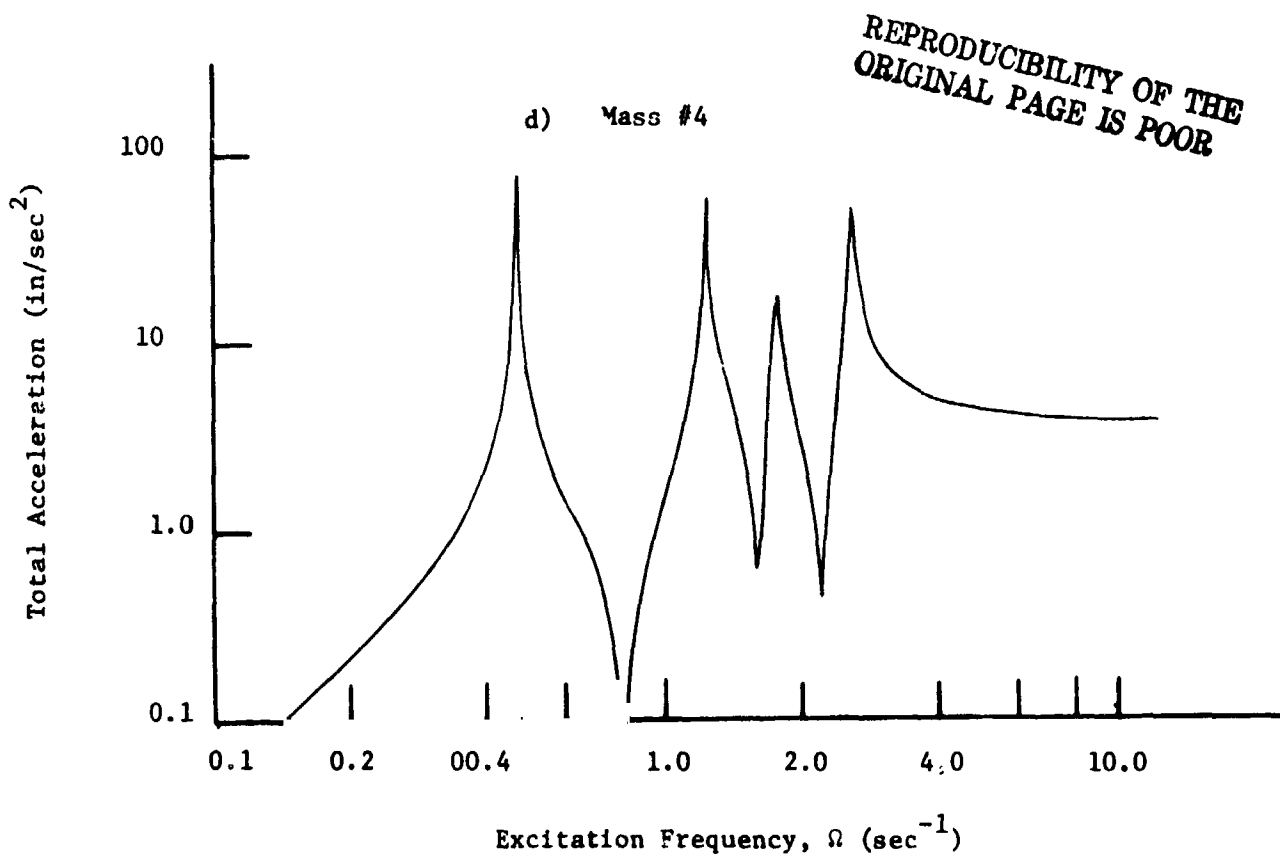
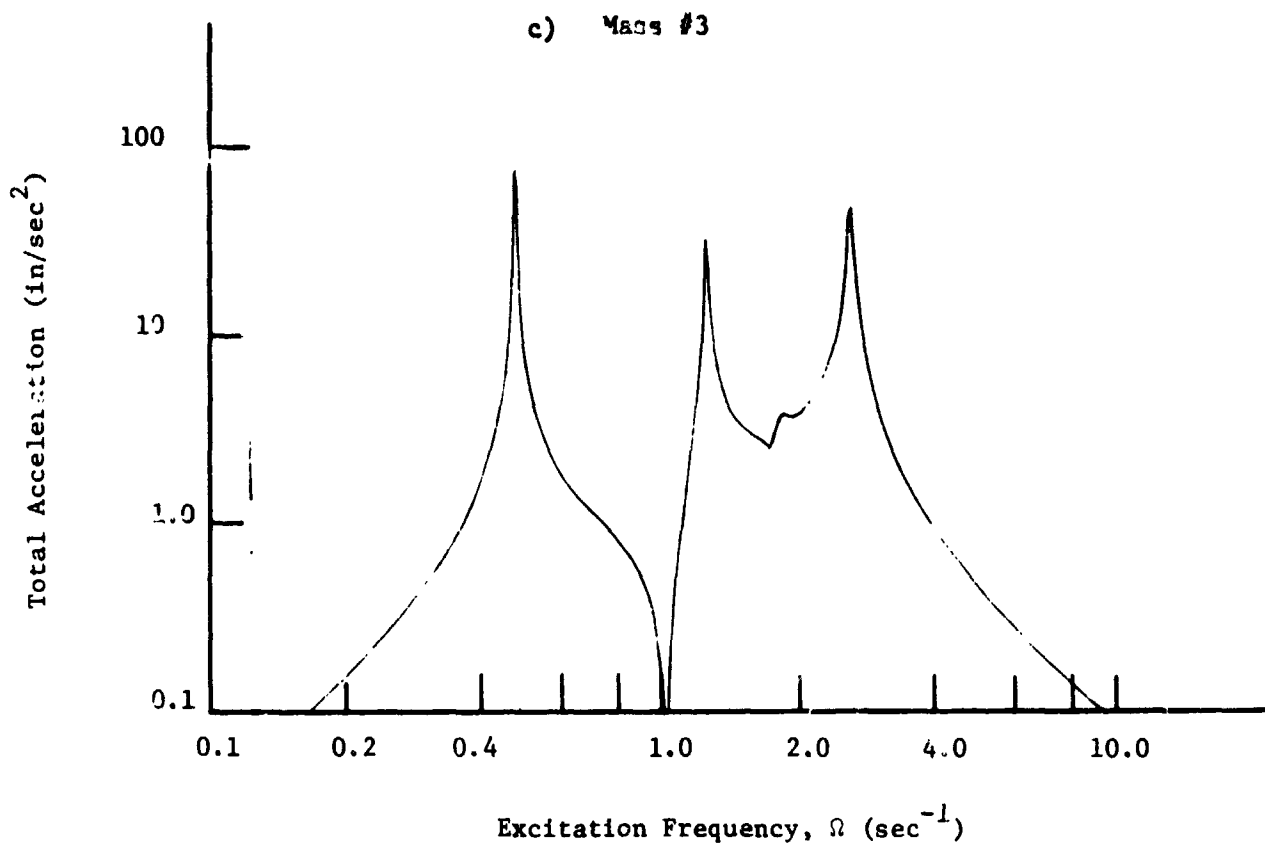


Figure 5. (Cont'd)

Table 10 - Complex Resonant Acceleration Response

<u>Coincident (Real Part)</u>				
<u>Mass No.</u>	<u>Mode 1</u>	<u>Mode 2</u>	<u>Mode 3</u>	<u>Mode 4</u>
1	.1572	-.3917	-1.0092	.3397
2	.2142	1.2831	-.5414	-.7711
3	.0487	1.0940	2.9473	1.0749
4	-.1578	-.2156	1.9115	3.2120

<u>Quadrature (Imaginary Part)</u>				
<u>Mass No.</u>	<u>Mode 1</u>	<u>Mode 2</u>	<u>Mode 3</u>	<u>Mode 4</u>
1	32.0465	-38.9270	15.0036	-2.2961
2	57.0674	-18.4483	-15.7395	10.5035
3	69.5931	30.2452	1.4041	-45.5123
4	74.4808	55.8524	16.4846	47.3419

Table 11 - Normalized Resonant Acceleration Response

<u>Real Part</u>				
<u>Mass No.</u>	<u>Mode 1</u>	<u>Mode 2</u>	<u>Mode 3</u>	<u>Mode 4</u>
1	3.5029E-1	-6.8291E-1	6.3100E-1	-5.3202E-2
2	6.2378E-1	-3.2374E-1	-6.6981E-1	2.4462E-1
3	7.6070E-1	5.3055E-1	7.4002E-2	-1.0635
4	8.1413E-1	9.7990E-1	7.0813E-1	1.1134

<u>Imaginary Part</u>				
<u>Mass No.</u>	<u>Mode 1</u>	<u>Mode 2</u>	<u>Mode 3</u>	<u>Mode 4</u>
1	-2.4612E-3	9.5097E-3	1.1652E-1	-1.1599E-2
2	-3.6637E-3	-2.1261E-2	-5.4412E-2	3.4729E-2
3	-2.1450E-3	-2.1242E-2	-1.1802E-1	-9.7437E-2
4	0.	0.	0.	0.

Table 12 - Initial Modal Mass Matrix

$$\phi_R^T \mu \phi_R = \begin{bmatrix} 1.0 & -3.8313E-5 & 4.3135E-3 & 1.3142E-3 \\ & 1.0 & 1.3730E-2 & 2.2449E-3 \\ & & 1.0 & -2.8946E-4 \\ \text{Symmetric} & & & 1.0 \end{bmatrix}$$

Table 13 - Normalized Change in Modal Vector Length

<u>Iteration 1</u>		
<u>Mode No.</u>	<u>Real Part</u>	<u>Imaginary Part</u>
1	3.1019E-5	8.1573E-1
2	6.8161E-4	8.0687E-1
3	1.6637E-2	9.0720E-1
4	3.9757E-3	9.8476E-1
<u>Iteration 2</u>		
1	1.2322E-5	3.2084E-4
2	6.9856E-5	4.0783E-4
3	4.9095E-4	2.3828E-3
4	9.0579E-5	3.3180E-3
<u>Iteration 3</u>		
1	2.6201E-8	5.4733E-7
2	4.2167E-7	2.3002E-6
3	2.9780E-6	4.7326E-6
4	6.6202E-7	9.7453E-6

Table 14 - Improved Modal Vectors

Mode/Mass	Real Parts		Imaginary Parts		
	MODSEP	Reference	MODSEP	Reference	
1	1	3.5032E-1	3.5027E-1	-4.5713E-4	-4.5704E-4
	2	6.2380E-1	6.2380E-1	-7.7822E-4	-7.7854E-4
	3	7.6069E-1	7.6065E-1	-2.2671E-4	-2.2582E-4
	4	8.1409E-1	8.1418E-1	0.	0.
2	1	-6.8342E-1	-6.8334E-1	6.8140E-3	6.8086E-3
	2	-3.2321E-1	-3.2328E-1	-4.6422E-3	-4.6355E-3
	3	5.3066E-1	5.3063E-1	-2.1807E-3	-2.1667E-3
	4	9.7923E-1	9.7934E-1	0.	0.
3	1	6.3763E-1	6.3822E-1	1.4370E-2	1.4513E-2
	2	-6.6783E-1	-6.6749E-1	-4.6619E-3	-4.7784E-3
	3	6.0753E-2	6.0011E-2	-7.6738E-3	-7.6975E-3
	4	6.9664E-1	6.9598E-1	0.	0.
4	1	-5.4558E-2	-5.4308E-2	-2.4867E-3	-2.4760E-3
	2	2.4751E-1	2.4667E-1	2.2613E-3	2.2857E-3
	3	-1.0657	-1.0659	-6.2719E-4	-7.9520E-4
	4	1.1079	1.1076	0.	0.

Table 15 - Final Modal Mass Matrix

$$\phi_R^T \mu \phi_R = \begin{bmatrix} 1.0 & -4.6318E-5 & 2.7321E-5 & 4.2270E-4 \\ & 1.0 & 8.4953E-4 & 2.2443E-4 \\ & & 1.0 & -4.1186E-4 \\ \text{Symmetric} & & & 1.0 \end{bmatrix}$$

except for element (4,3) which is about 20% off. (The probable source of error will be discussed momentarily.) The final modal mass matrix is shown in Table 15. The largest off-diagonal element now is 8.49 E-4 , down a factor of sixty-two from its initial value of 1.37 E-2 . The full modal damping matrix given in Table 16 was found to be in good agreement with the reference values except for fourth row elements which deviate by as much as 18.3%. This is a direct result of the 20% deviation in the imaginary part of the third element of mode 4.

In the foregoing example, all four modes were used. The first three and first two were used in subsequent work to assess the effect of modal truncation on ξ . These results are shown in Table 17. The effect of modal truncation is shown to be small in this case.

While this example problem seems to demonstrate the theoretical validity of the procedure formulated in Part A, it also points up a potential problem. The 20% error in the fourth mode, which was noted earlier, does not appear to be the result of a trivial input error or an error in the formulation of the method. Similar results were obtained for other examples; however, it was found that these errors could be reduced by identifying resonant frequencies more accurately.

The source of the error is believed to be attributable to the fact that large changes in phase accompany very small changes in frequency near resonance. In the present example, resonant excitation frequencies were specified to five significant figures. Even so, changes in the fifth significant figure resulted in changes on the order of 100% in some of the coincident response values because of the small amount of damping (around 1%). The problem is compounded by the fact that as damping becomes smaller, phase angles become smaller at the same time their derivatives with respect to frequency become larger, so that the sensitivity factor is of the form $(d\theta/d\omega)/\theta$. Hence, precise frequency determination is very important.

In the present investigation, the resonant frequencies Ω_j were assumed equal to the natural undamped frequencies ω_{o_j} on a one-to-one basis. In practical applications, particularly when modes are not well separated, it may be necessary to analytically determine modal frequencies ω_{o_j} slightly different from the corresponding excitation frequencies Ω_j . Sweeping across ω_{o_j} would allow one to compute the rate of change of quadrature response with respect to frequency. The frequency at which this function is a minimum may be used to determine ω_{o_j} , as suggested by Kennedy and Pancu in Reference [9]. While this approach seems to merit consideration, alternative procedures might also be sought. A need for further investigation of this problem is clearly indicated.

Table 16 - Comparison of Modal Damping Matrices

<u>Col/Row</u>	<u>MODSEP</u>	<u>Eq. (32)</u>	<u>Eq. (33)</u>
1 1	4.1663E-3	4.1663E-3	4.1662E-3
2	-1.4179E-3	-1.4085E-3	-1.4087E-3
3	-1.2800E-3	-1.3356E-3	-1.3360E-3
4	7.4791E-4	6.3308E-4	6.3325E-3
2 2	2.1240E-2	2.1240E-2	2.1237E-2
3	-8.9431E-3	-9.0619E-3	-9.0595E-3
4	1.6128E-3	1.4548E-3	1.4544E-3
3 3	5.1583E-2	5.1583E-2	5.1581E-2
4	-4.2064E-3	-4.2773E-3	-4.2791E-3
4 4	6.6356E-2	6.6356E-2	6.6346E-2

Table 17 - Effect of Truncation on Computation of the Modal Damping Matrix

<u>Col/Row</u>	<u>2 Modes</u>	<u>3 Modes</u>	<u>4 Modes</u>
1 1	4.1663E-3	4.1663E-3	4.1663E-3
2	-1.4132E-3	-1.4179E-3	-1.4179E-3
3		-1.3630E-3	-1.2800E-3
4			7.4791E-4
2 2	2.1240E-2	2.1240E-2	2.1240E-2
3		-8.8476E-3	-8.9431E-3
4			1.6128E-3
3 3		5.1583E-2	5.1583E-2
4			-4.2064E-3
4 4			6.6356E-2

8.4 Conclusions

There are several important conclusions to be drawn from the numerical examples presented in this section. The convergence of system damping values obtained by modal synthesis is governed by convergence of the system eigenvectors. Since this topic is to be discussed more fully in Reference [7], it will not be elaborated upon here. From the standpoint of damping synthesis, the coupling procedures which avoid the use of fixed-boundary modes are preferable. The possible advantage of better convergence that fixed-boundary mode formulations offer is outweighed by the difficulty of determining both the static and dynamic modes experimentally, and by the difficulty of relating experimental damping properties to such a coordinate system. Of the modal coupling procedures which do not rely on fixed-boundary modes, the one utilizing mass loading at interface boundaries may be more desirable than the one utilizing just the free-free modes. Provided that appropriate means are available to determine what the mass loading should be, this procedure tends to converge faster with no apparent disadvantage relative to identification of damping properties. In fact, the dissipative energy characteristics should be brought out better for the same reasons that the strain energy characteristics are.

A four-degree of freedom lumped mass model was used to illustrate the accuracy attainable by the approximate method for generating modal damping matrices given the damped modes. For damping values on the order of 1%, it was found that the approximation yielded comparable results. When the damped modes were not given, it was shown that they could be derived from resonant response information by an iterative procedure which converged rapidly in that case.

A significant problem was, however, indicated. As the modal separation procedure is presently used, it is assumed that excitation is applied to the structure precisely at its resonant frequencies. It is unlikely that this will be realizable in practical situations where modes are closely spaced in frequency. In this case, it may only be possible to excite the structure near a resonant frequency. In this case, more information will be required to identify modal frequencies to the degree of precision required by this procedure. This is an area which demands further investigation.

9. Experimental Verification

The chief purpose of this study is to apply the matrix method for damping synthesis to a real structural system and compare predicted values of system modal damping with those obtained by direct measurement. In the recent past, LaRC has conducted vibration tests on a 1/15th-scale dynamic model of a Shuttle vehicle. The model consists of an Orbiter and a Booster which can be coupled by special spring assemblies. Each of these components is constructed of thin-walled tapered aluminum tubing. Propellant tanks are mass simulated by strapping lead ballast to each component at appropriate locations.

Two basic modifications were made for this investigation. Previously, the coupling configuration included only two spring assemblies, making the interface forces between the Orbiter and Booster statically determinant. For these tests, a third spring assembly was added between the original two, creating redundant load paths. Also, pin connections were added to the spring assemblies, eliminating the requirement for slope continuity at the connection points.

Since earlier tests were concerned mainly with the undamped characteristics of the structure, the inherently small amount of damping in the system (less than 0.5%) did not pose a problem. In this study, however, it was estimated that modal damping on the order of several percent would be required in order to extract meaningful data with the available analog test and data reduction equipment. Thus it was decided to attach three externally grounded dampers to the Orbiter. For comparative purposes, no damping was added to the Booster. It was felt that this lopsided distribution of damping would represent a worst case in some respects and help to elucidate significant trends in the data.

9.1 Description of Tests

Schematic drawings of the 1/15th-scale model Orbiter and Booster substructures are shown in Figure 6. The coordinates defined in this figure correspond to the accelerometer locations used during vibration tests. The spring assemblies were included as part of the Booster substructure. Interface points between the Orbiter and Booster are defined to coincide with pinned connections between the two. A lumped mass distribution was defined for the system taking into account the physical distribution of mass and requirements for accelerometer placement. Distributions for both the Orbiter and the Booster are given in Table 13.

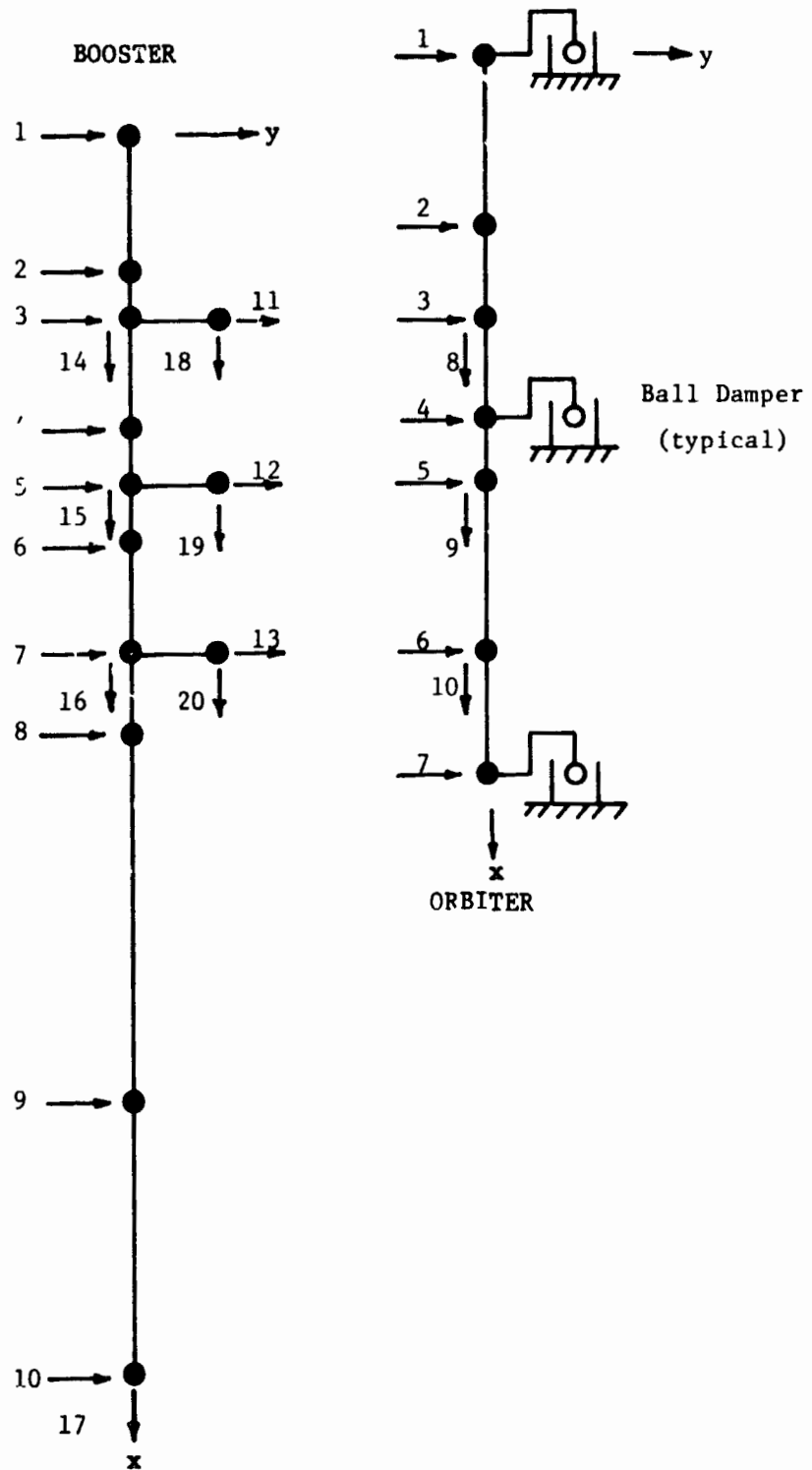


Figure 6. 1/15th-Scale Dynamic Model of Orbiter and Booster Substructures

Table 18 - Mass Distribution for the 1/15-Scale Dynamic Model of a Shuttle Vehicle

ORBITER			
<u>Coordinate Number</u>	<u>Station x</u>	<u>Station y</u>	<u>Weight lbs</u>
1	-0.50	0	6.40
2	18.6	0	62.85
3	28.0	0	4.80
4	39.6	0	1.53
5	46.5	0	9.34
6	65.2	0	3.87
7	77.75	0	1.33
8	28.0	0	74.55
9	46.5	0	10.38
10	65.2	0	5.20
BOOSTER			
1	0.0	0	1.20
2	15.0	0	83.04
3	20.3	0	11.35
4	32.0	0	48.25
5	38.7	0	6.87
6	45.3	0	48.75
7	57.5	0	8.83
8	66.0	0	21.4
9	105.6	0	32.1
10	134.9	0	17.89
11	20.3	9.1	2.2 (15.32)*
12	38.7	9.1	2.2 (14.08)*
13	57.5	9.1	2.2 (16.64)*
14	20.3	0	95.59
15	38.7	0	103.87
16	57.5	0	30.23
17	134.9	0	49.99
18	20.3	9.1	2.5 (15.62)*
19	38.7	9.1	2.5 (14.38)*
20	57.5	9.1	2.5 (16.94)*

*with mass loading

Discrete dampers were connected to the Orbiter at the locations indicated in Figure 6. These dampers were identical, each consisting of a wooden ball attached to the Orbiter and placed in a glass jar fixed to ground. The jars were filled with Dow Corning damping fluid having a viscosity of 20K centistokes. The balls were immersed in the fluid. Relative motion between a ball and jar was permitted in both vertical (in and out of the jar) and horizontal directions. The damping characteristics of a typical ball damper were evaluated by rigidly attaching the ball to a shaker, with force and acceleration transducers between them in series. The vertical and horizontal test setups are shown in Figures 7a and b respectively. Sinusoidal excitation was provided at peak amplitudes ranging from 0.1 g to 2 g, over selected frequencies from 25 to 500 Hz. Based on the assumption of linear viscous damping (damping force proportional to velocity), values of the proportionality "constant" c were determined from the peak exciting force amplitude F , the peak acceleration amplitude a , their relative phase angle θ , and the frequency of excitation ω .

$$c = \frac{\omega F \sin\theta}{a} \quad (39)$$

Tabulated results received from LaRC are presented in Table 19. Damping in both horizontal and vertical directions was found to be linear with respect to amplitude. Only averages for the four amplitudes are shown. These values are plotted against frequency in Figure 8. They vary considerably over the frequency range. Another method for determining c is discussed in Section 9.3, where a comparison with these results is made.

Substructure vibration tests were run separately for the Orbiter and the Booster. The Orbiter was suspended horizontally in the Orbiter/Booster plane and free-free modes were excited in the pitch (lateral in-plane) direction by a shaker located at its tail. Each of the dampers, one at the nose, one at midspan, and one at the tail, are shown in Figures 9a-c, respectively. Booster vibration tests were made with the Booster suspended vertically. Free-free modes were excited by placing an exciter at the tail of the Booster. Two sets of modes were obtained, one without mass loading and one with. No external dampers were used on the Booster.

Finally, the Orbiter and Booster were connected and suspended vertically. Two sets of modes were obtained by exciting the structure in the pitch direction at the Booster tail, then in the axial direction at the Booster tail. Three externally grounded dampers were attached to the Orbiter as in the substructure tests.

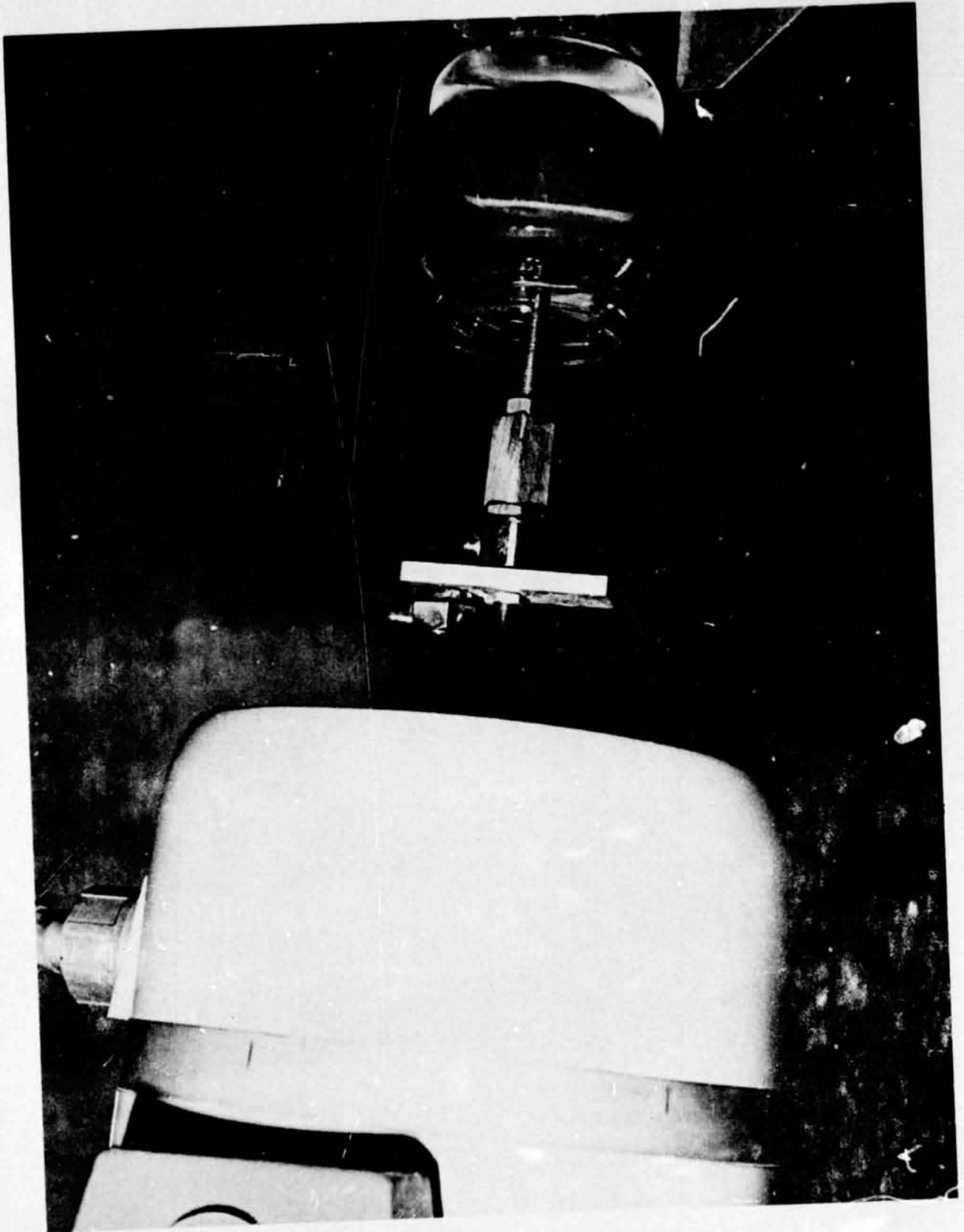


Figure 7-a. Ball Damper Test Configuration, Vertical Motion

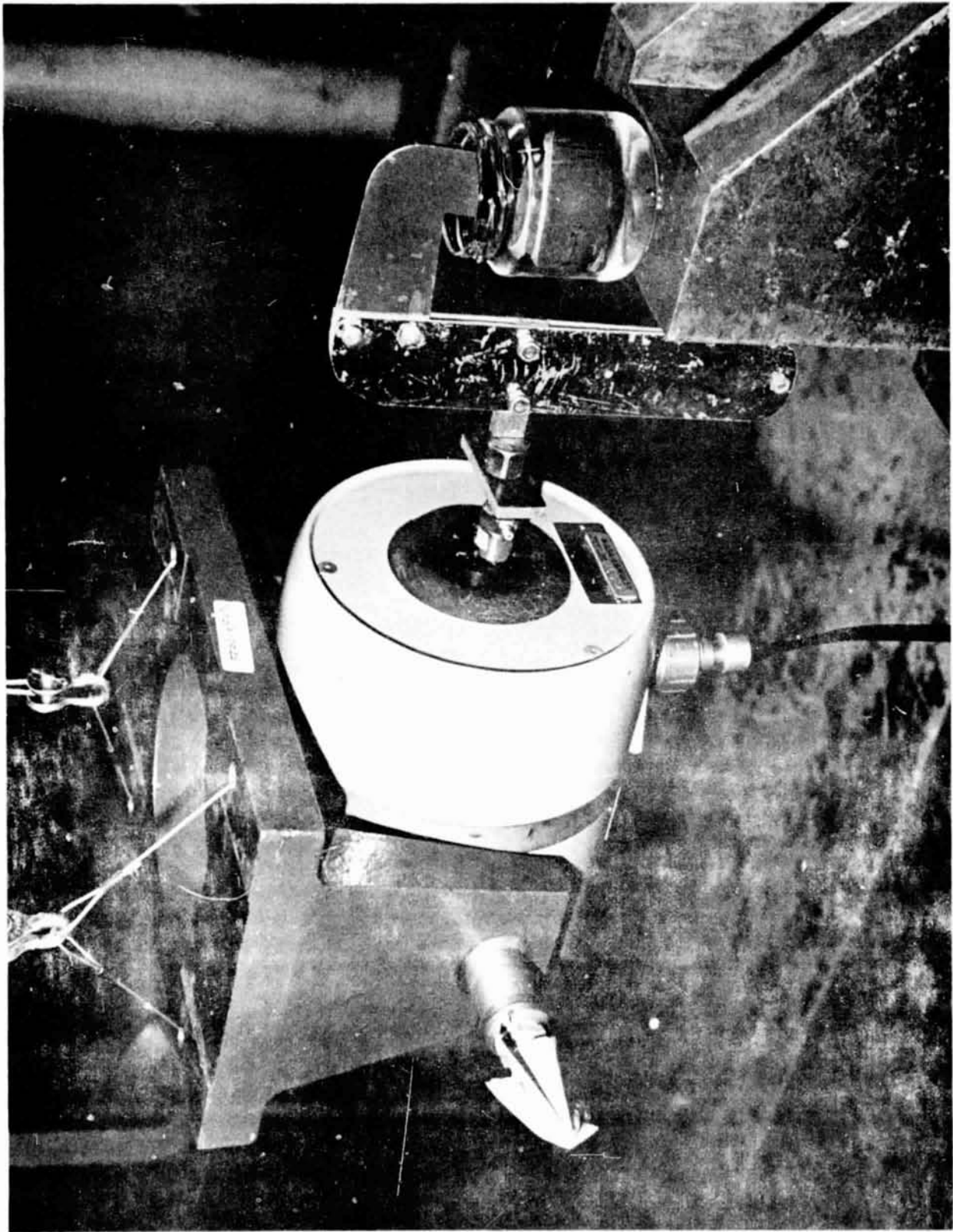


Figure 7-b. Ball Damper Test Configuration, Horizontal Motion

Table 19 - Ball Damper Characteristics

<u>Frequency</u> <u>(Hz.)</u>	<u>c_v</u> <u>(lb sec/in)</u>	<u>c_H</u> <u>(lb sec/in)</u>
25	.711	.544
30	.686	.530
40	.665	.502
50	.629	.471
70	.584	.425
100	.521	.380
150	.458	.365
200	.431	.340
300	.377	.342
400	.325	.392
500	.378	.435

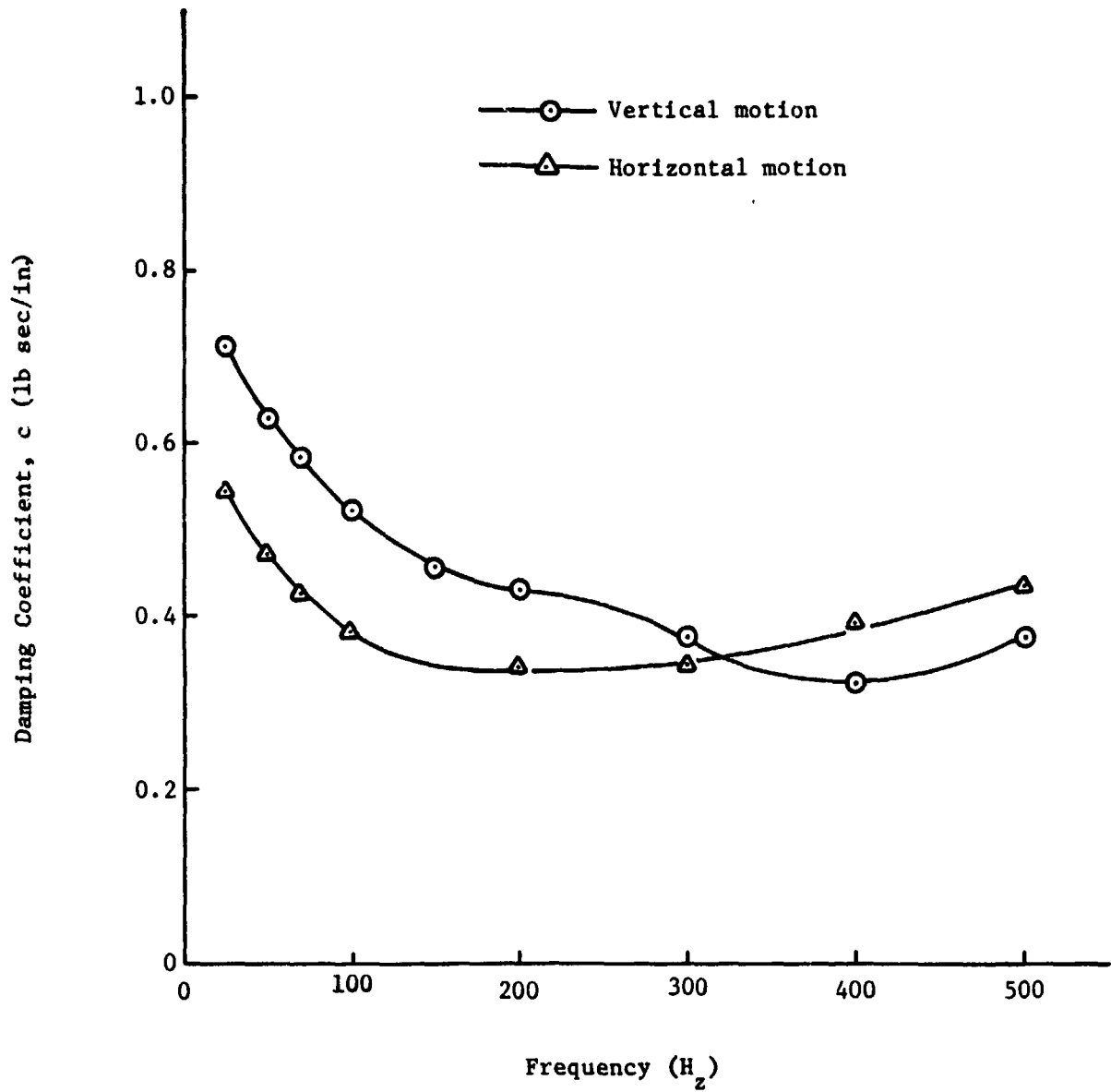


Figure 8. Ball Damper Characteristics
Determined from Measurements of Damping Force and Velocity

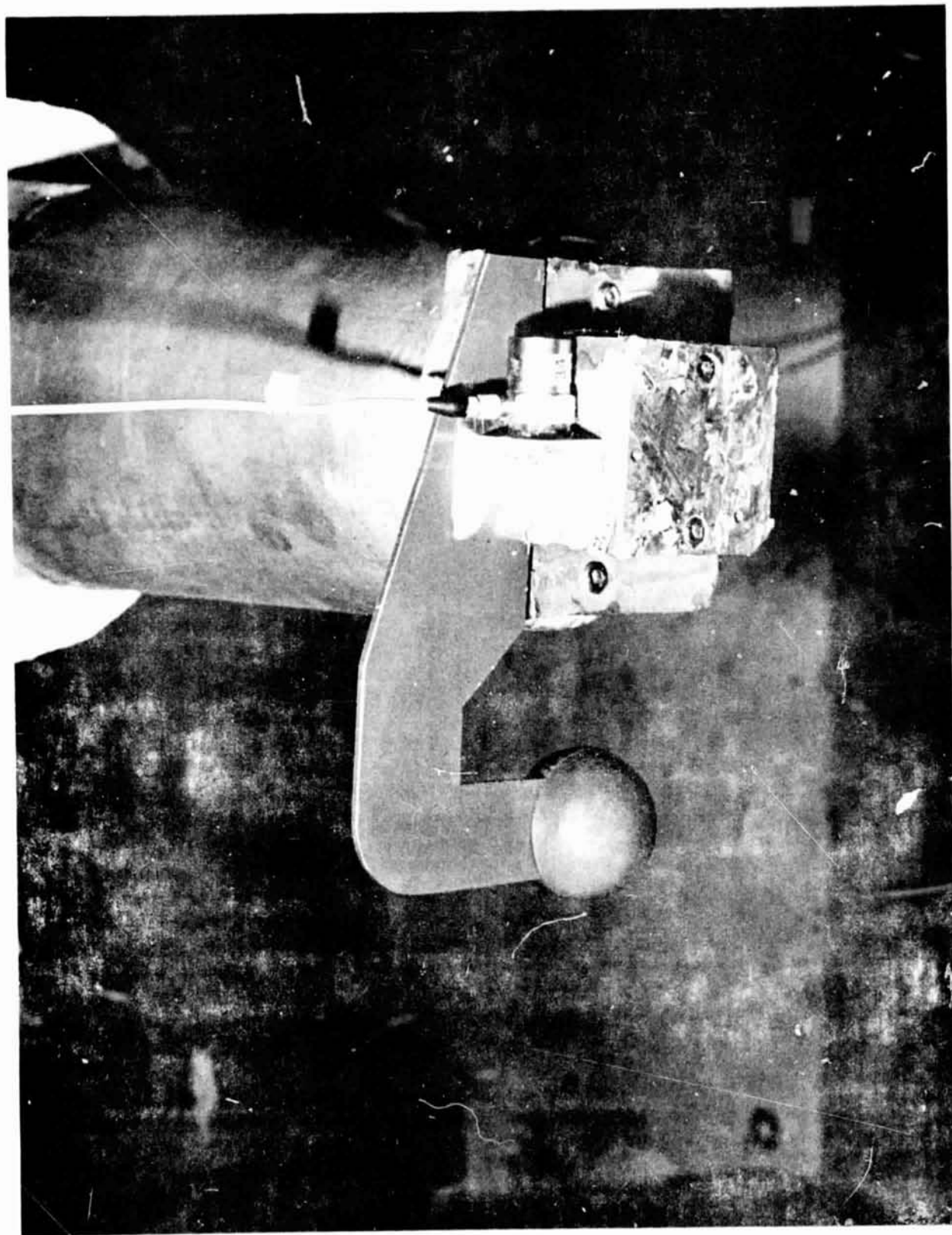


Figure 9-a. Ball Damper Installation for Orbiter Test, Nose Damper.

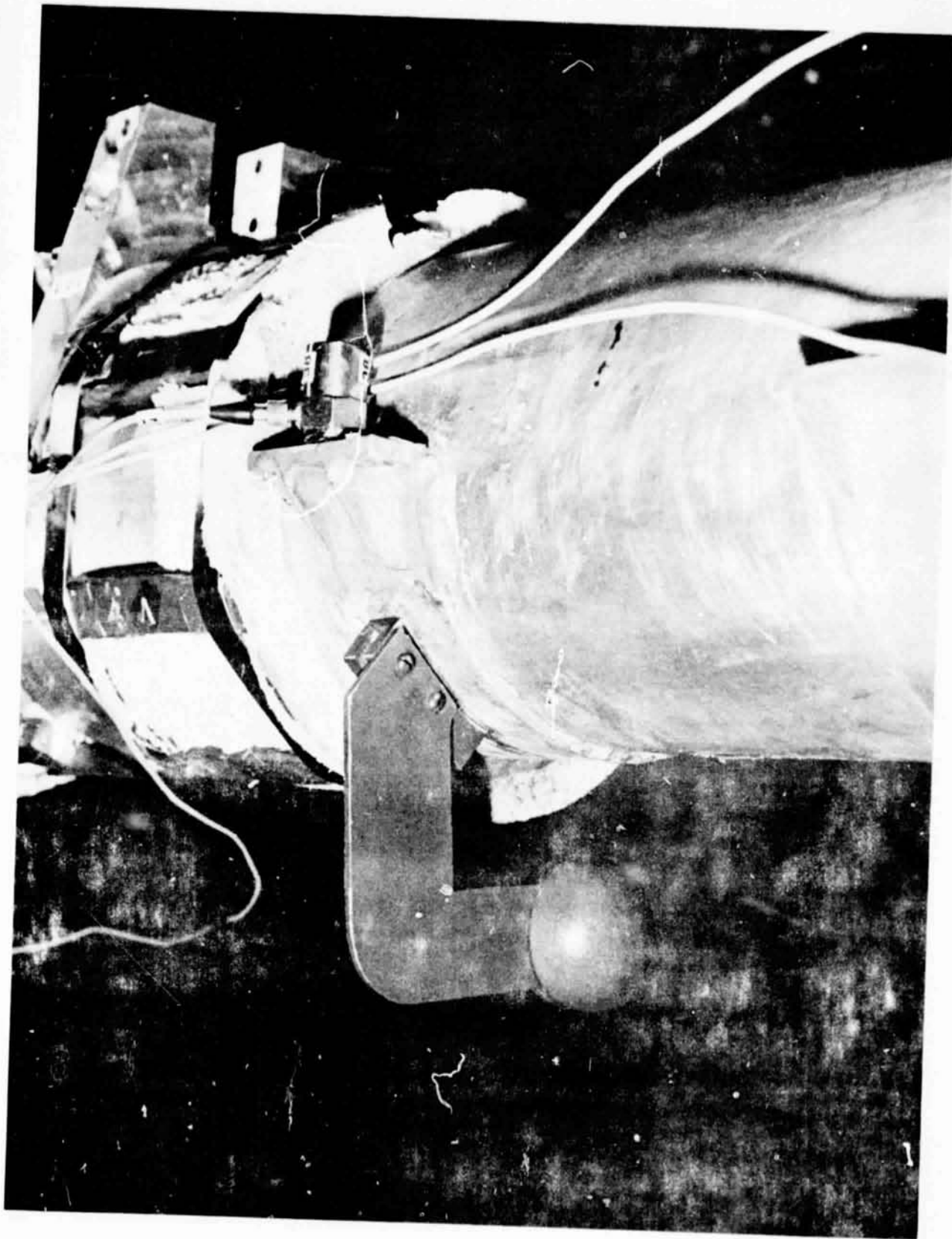


Figure 9-b. Ball Damper Installation for Orbiter Test, Midspan Damper

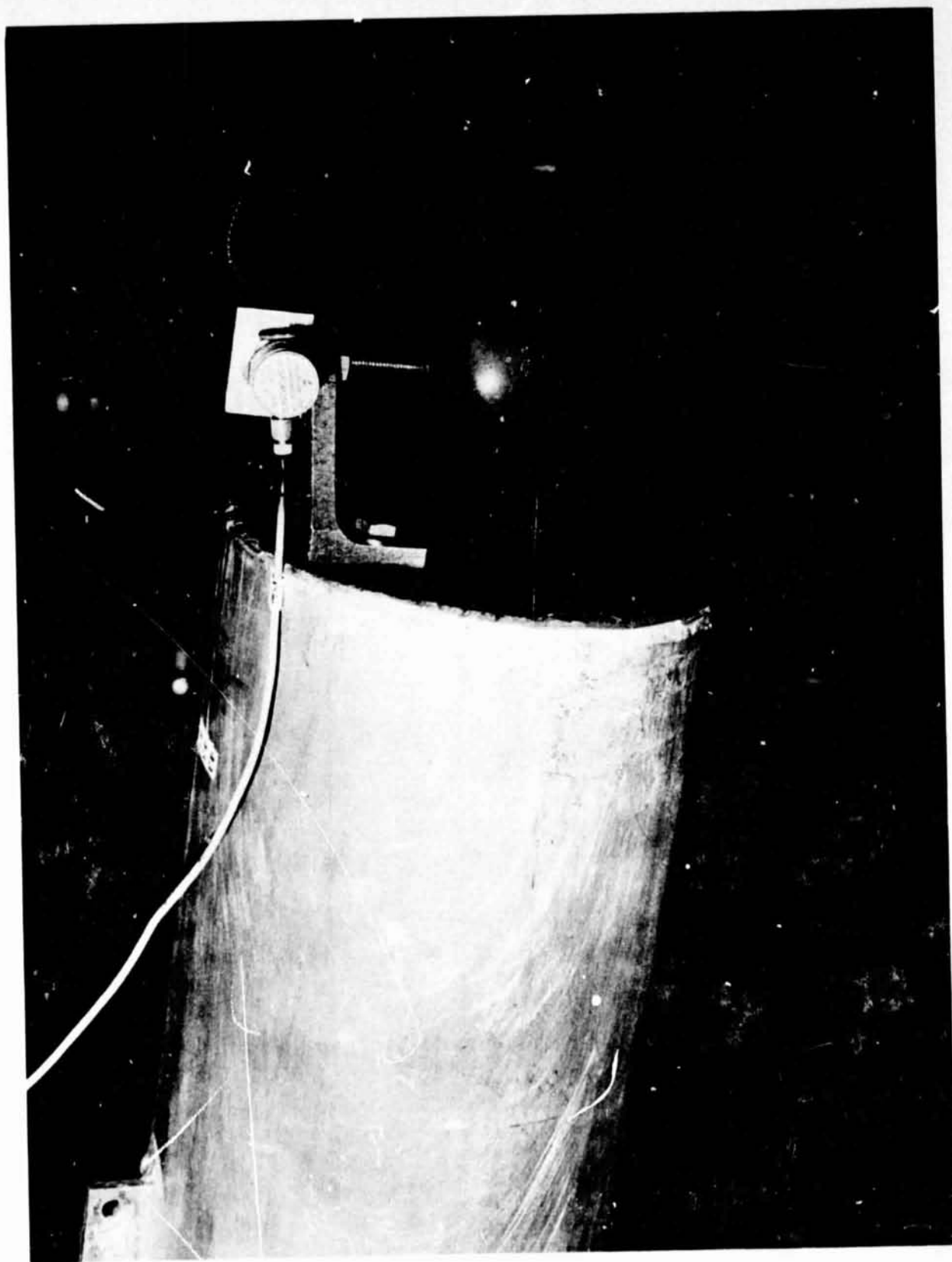


Figure 9-c. Ball Damper Installation for Orbiter Test, Tail Damper

This time, however, the Orbiter was vertical. In order to introduce damping in the longitudinal direction and accommodate the new orientation of the Orbiter with respect to the jars, different mounting brackets were used for the balls. They are shown for the nose, midspan, and tail of the Orbiter in Figures 10a-c. These brackets are stiff in both the pitch and axial directions.

9.2 Summary of Test Results

For each of the component and system tests defined in Section 9.1, the input force and acceleration response data were recorded on magnetic tape. The tapes were shipped to TRW for data reduction using the Spectral Dynamics Model SD109B Co/Quad Analyzer. Acceleration response at each station was separated into components in phase (Coincident) and 90° out of phase (Quadrature) with the forcing function. These reduced data were recorded in digital form on punched cards. A duplicate copy was given to GAC.

In addition, measurements of modal damping were made at LaRC. Three methods were used based on (a) half-power-point bandwidth, (b) log decrement, and (c) Kennedy-Pancu [9] methods. All the modes obtained from component and system tests are listed in Table 20. Along with the measured frequency of each mode are included the damping values obtained in each case. Since most of the damping in the system came from the external dampers on the Orbiter, the damping properties of the Booster were not considered particularly significant. Therefore, modal damping for the mass-loaded Booster modes was measured for only a selected number of modes.

9.3 Orbiter Damping Matrix

Evaluation of the Orbiter damping matrix is considered first for several reasons. The Orbiter is by far the simpler of the two components. Only the first three bending modes were found below 500 Hz. The frequency of the first axial mode (although not shown) was determined to be above 500 Hz. From Table 20, it is noted that the frequency separation between modes is nearly an octave in each case. Modal damping calculations made by the three methods are

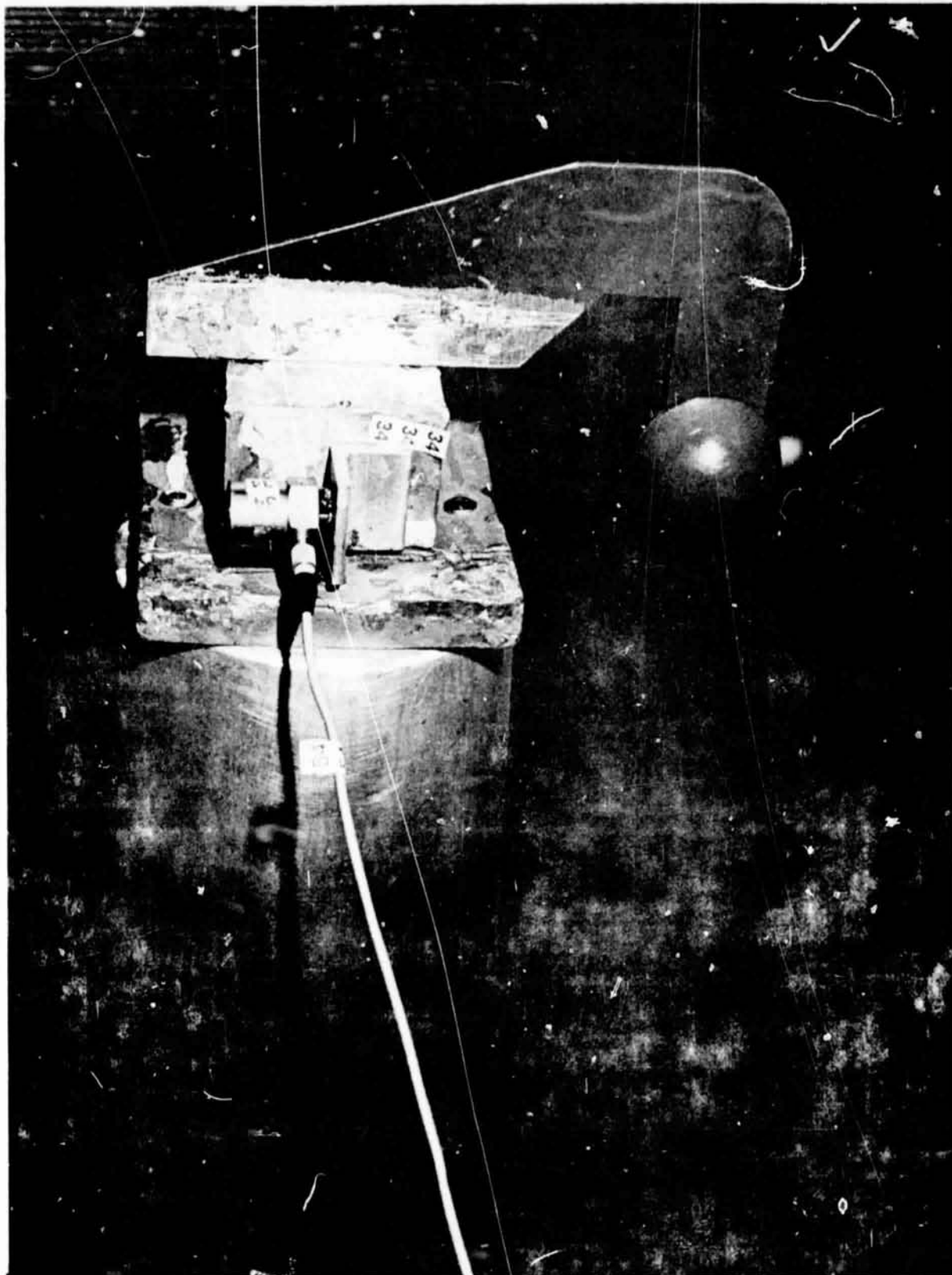


Figure 10-a. Ball Damper Installation for Coupled Orbiter/Booster Test,
Orbiter Nose Damper

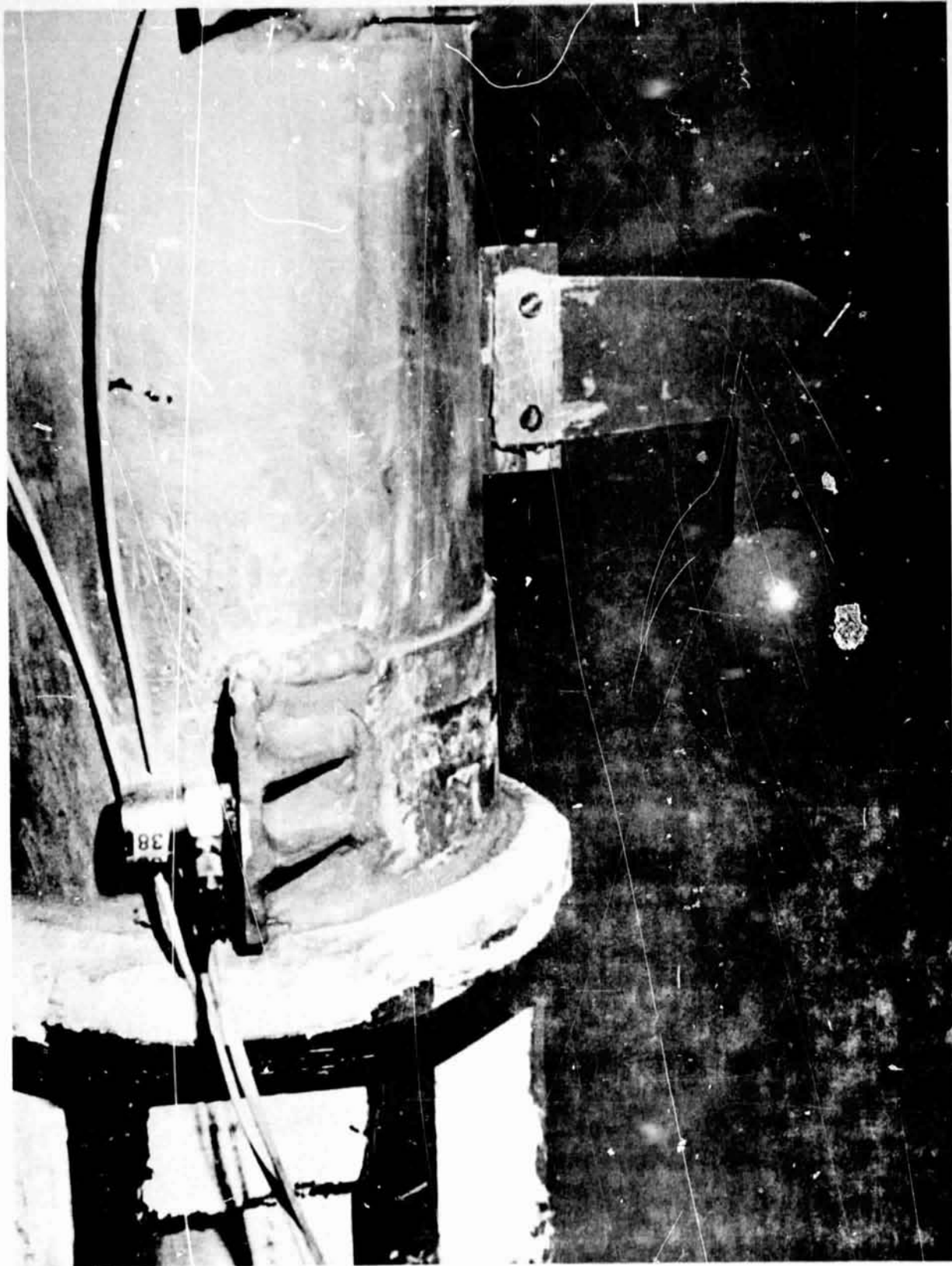


Figure 10-b. Ball Damper Installation for Coupled Orbiter/Booster Test,
Orbiter Midspan Damper

REPRODUCIBILITY OF THE
ORIGINAL PAGE IS POOR

18058-6001-RU-00
Page 61

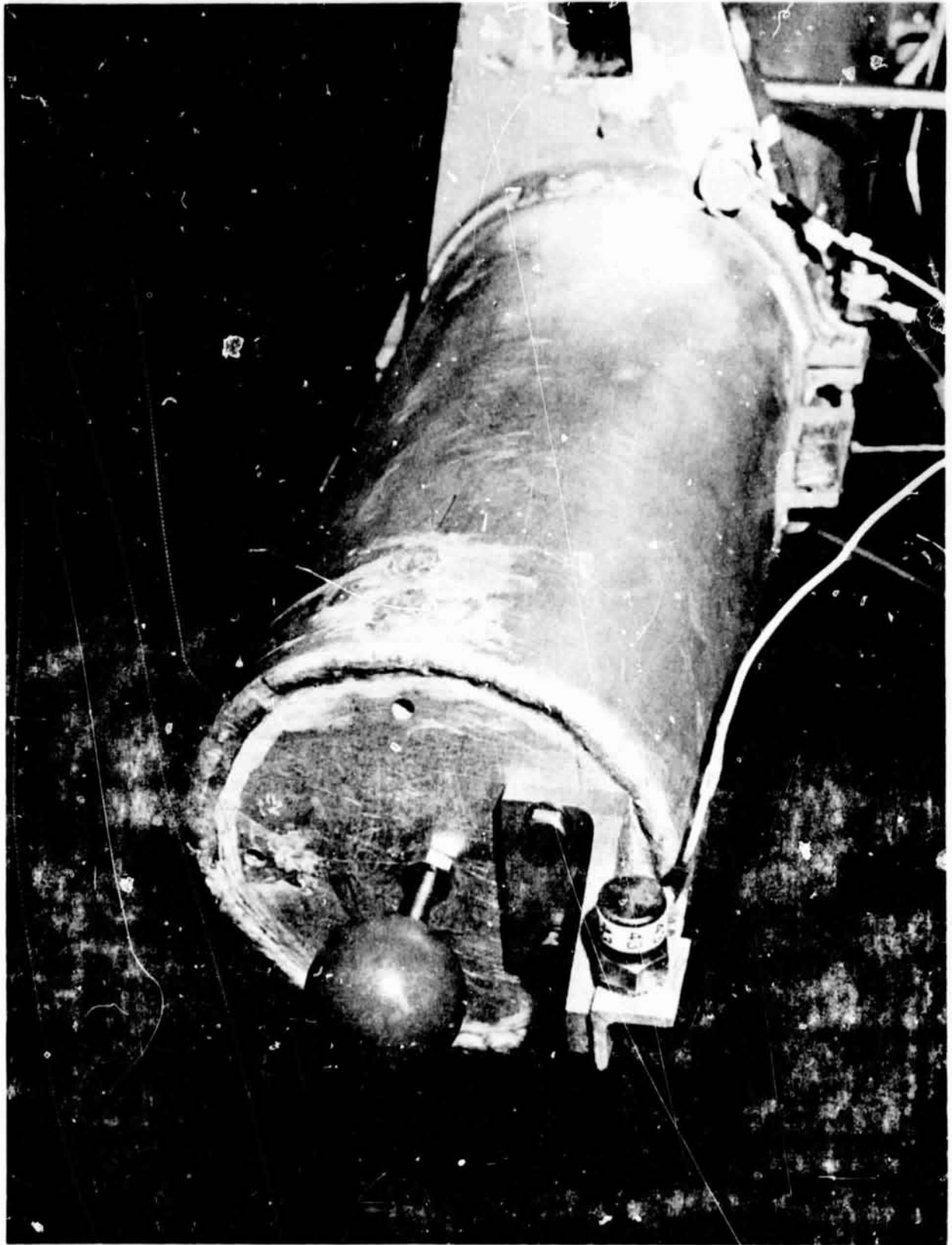


Figure 10-c. Ball Damper Installation for Coupled Orbiter/Booster Test,
Orbiter Tail Damper

Table 20 - Experimental Modal Frequencies and Damping Values

LATERAL (PITCH) EXCITATION OF ORBITER AT STA. 74

Mode Description	Frequency (Hz.)	Force (lbs)	Percent Critical Damping*		
			(a)	(b)	(c)
1st bending	101.40	0.78	3.43	3.33	3.78
2nd bending	219.78	0.58	2.00	1.90	2.32
3rd bending	414.93	0.50	0.75	0.78	0.87

LONGITUDINAL (AXIAL) EXCITATION OF BOOSTER AT STA. 136

Spring axial	145.56	0.94	----	----	----
Spring axial	151.51	0.59	----	----	----
Spring axial	162.60	0.49	----	----	----
1st longitudinal	259.74	0.59	.231	----	.281

LATERAL (PITCH) EXCITATION OF BOOSTER AT STA. 134

1st bending	37.93	0.45	----	.290	.281
2nd bending	101.62	0.49	.197	.179	.181
spring axial	145.56	0.49	.210	.198	.200
spring axial	151.05	0.51	.132	.163	.142
spring axial	162.86	0.49	.144	.144	.152
3rd bending	183.90	0.50	----	(.300)**	----
spring pitch	211.12	0.50	----	(.200)**	----
spring pitch	220.75	0.51	----	(.200)**	----
spring pitch	224.71	0.51	----	.204	----
4th bending	284.09	0.50	----	.597	----
5th bending	369.00	1.00	----	----	----

*(a) Half-power-point bandwidth; (b) log decrement; (c) Kennedy-Pancu

**Data unavailable. Values in parentheses were assumed for analysis

Table 20 (Cont'd)

LATERAL EXCITATION OF ORBITER/BOOSTER ASSEMBLY AT BOOSTER STA. 134

Mode Number	Frequency (Hz.)	Force (lbs)	Percent Critical Damping		
			(a)	(b)	(c)
1	26.01	1.01	2.77	2.85	3.01
2	38.73	----	0.96	0.94	0.62
3	57.57	0.99	0.76	.49 - .96	0.64
4	92.25	1.00	1.67	1.37	1.08
5	108.22	0.70	0.30	0.256	0.221
6	125.31	1.00	3.15	3.36	3.47
7	185.18	0.97	0.282	0.366	0.289
8	281.69	1.41	0.425	0.412	0.378

LONGITUDINAL EXCITATION OF ORBITER/BOOSTER ASSEMBLY AT BOOSTER STA. 135

1	57.43	2.01	---	----	0.563
2	108.3	----	----	----	----
3	185.52	1.50	----	----	----
4	256.41	0.99	----	----	0.307

LATERAL EXCITATION OF BOOSTER WITH MASS LOADING AT STA. 134

1	34.05	0.50	----	0.42	----
2	52.77	1.00	----	----	----
3	71.27	0.99	----	----	----
4	76.39	1.00	----	----	----
5	81.49	1.00	----	0.33	----
6	109.76	0.70	----	0.44	----
7	182.81	0.50	----	0.32	----
8	186.56	0.98	----	----	----
9	187.61	0.99	----	----	----
10	198.41	0.98	----	----	----
11	202.83	1.48	----	----	----
12	279.32	1.40	----	0.48	----

LONGITUDINAL EXCITATION OF BOOSTER WITH MASS LOADING AT STA. 134

1	53.44	1.51	----	----	----
2	65.35	1.46	----	----	----
3	257.06	1.00	----	----	----

in very good agreement. Of course, most of the damping was placed in the Orbiter specifically to enhance the chances of achieving conclusive results. A major part of the effort was therefore devoted to evaluating the damped characteristics of the Orbiter and interpreting the results.

This study was not without its share of problems. Certain unexpected difficulties did arise which caused part of the schedule to be compressed in time. Unfortunately, when some of the Orbiter test data appeared to be in error, it was not possible to repeat any tests on the damped configuration, but only on the undamped one. As a result, two sets of data became available, neither of which could be considered complete or entirely free of possible error. This situation required some exercise of judgement in deciding how best to utilize the data.

There was one other complicating factor. Both sets of data led to poor orthogonality between the first and third modes. It was speculated that this might be a result of the lumped mass matrix which was used, in the sense that no rotational mass was assigned to either of the lead weights used to simulate propellant tanks. Modal slopes are significant at these locations, particularly in the third mode. To test the hypothesis, the modes were plotted from available data and slopes were scaled. Additional coordinates corresponding to slope at Stations 18.6 and 46.5 were included, and representative mass moments of inertia were inserted in the mass matrix. This improved the orthogonality considerably. The difficulty was that modal slopes could not be scaled very accurately due to the small number of data points along the Orbiter.

The second set of Orbiter response data corresponding to the undamped configuration yielded better modes than the original data since the momentum balance and orthogonality were both better than in the first set. The decision was made to use these modes in the synthesis even though they lacked the damping information. Comparison of real mode plots between the two sets indicated reasonably good agreement as far as the overall appearance of the mode shapes was concerned. Based on the assumption that the introduction of small amounts of damping should not alter the quadrature response appreciably, the quadrature response obtained in the undamped test was combined with the coincident response from the damped test to complete the second set of data. This was accomplished

by matching accelerometer response at the input locations (Station 74 in each case) and multiplying the coincident response from the damped tests by the ratio of corresponding quadrature elements at each station. The forcing functions assumed for the second set of data were identical to those obtained from the damped tests.

In order to be as objective as possible under the circumstances, damping matrices for the Orbiter were computed for each of four cases:

- Case 1a. Original data--no rotational mass
- Case 1b. Original data--rotational mass included
- Case 2a. New augmented data--no rotational mass
- Case 2b. New augmented data--rotational mass included.

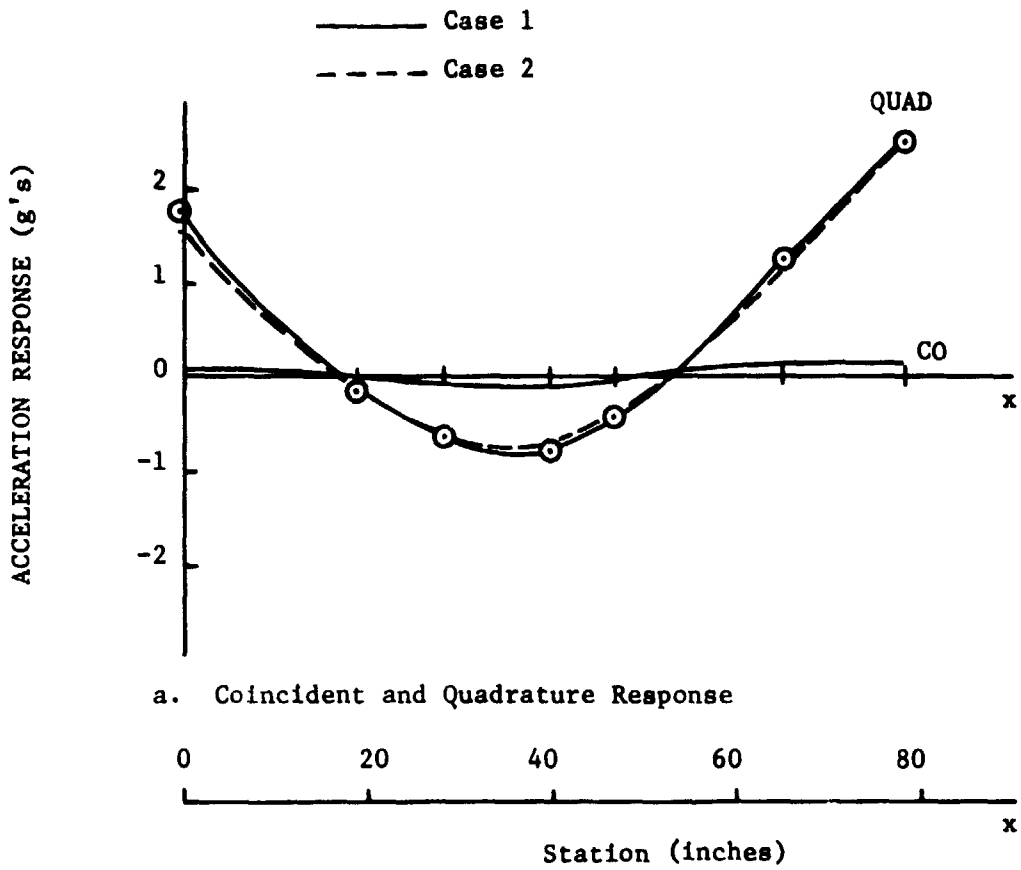
Before introducing any results, it is of interest to first examine the response data which comprise the basis of these computations.

Coincident and Quadrature response at the first three resonant frequencies of the Orbiter are plotted in Figures 11 through 13. The solid lines correspond to the original data, while the dotted lines represent the augmented data. The two are in reasonably good agreement after adjusting the acceleration response at the nose of the Orbiter in the first mode of the original data for an apparent gain error of 10 db. It is observed that the Coincident data tend to display the same general shape as the Quadrature data.

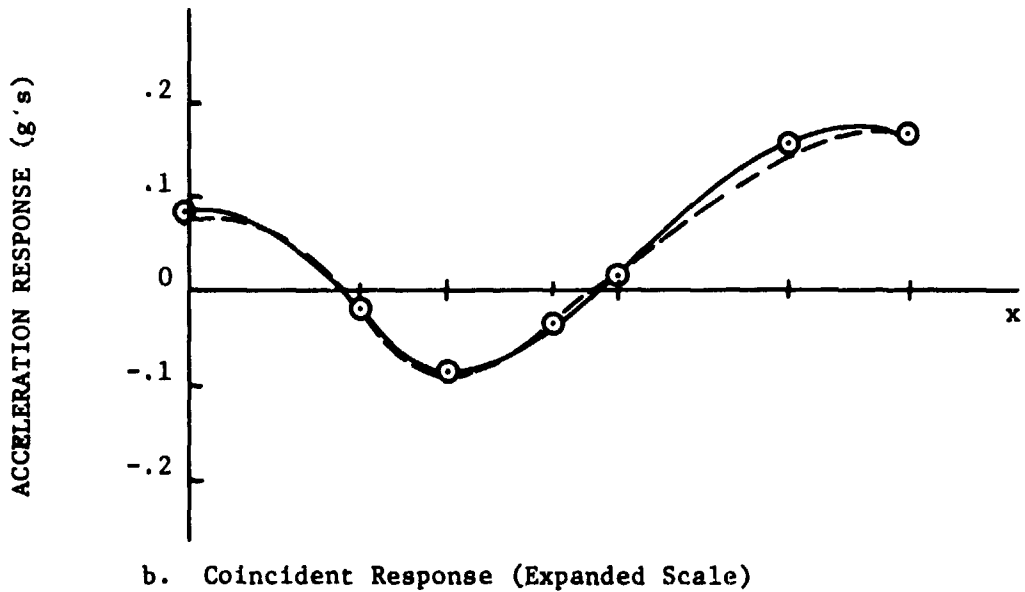
Before modal separation was begun, the rigid-body response was removed from the total response. Forces tending to excite rigid-body response included both the exciter force and the damper forces. The damper characteristics had to be known a priori. While it would have been desirable to avoid this by introducing some form of internal damping instead, no way of doing so was readily available. On the other hand, there is a distinct advantage to using external dampers whose characteristics are known because it provides an alternative way of evaluating the modal damping matrix.

Earlier when the characteristics of the ball dampers were discussed, an alternate method for evaluating these characteristics was mentioned. This method is based on Equation (28a).

$$\phi_{R_j}^T \rho \phi_{R_j} = 2\zeta_j \omega_j \quad (28a)$$

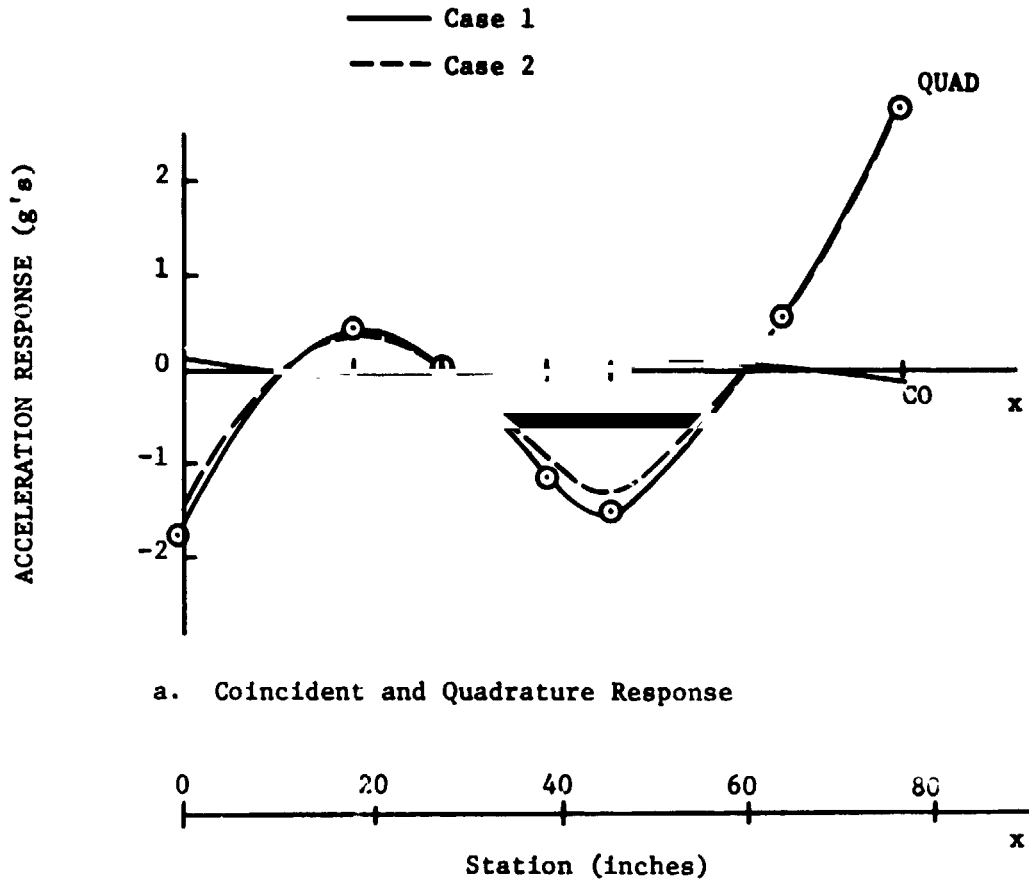


a. Coincident and Quadrature Response

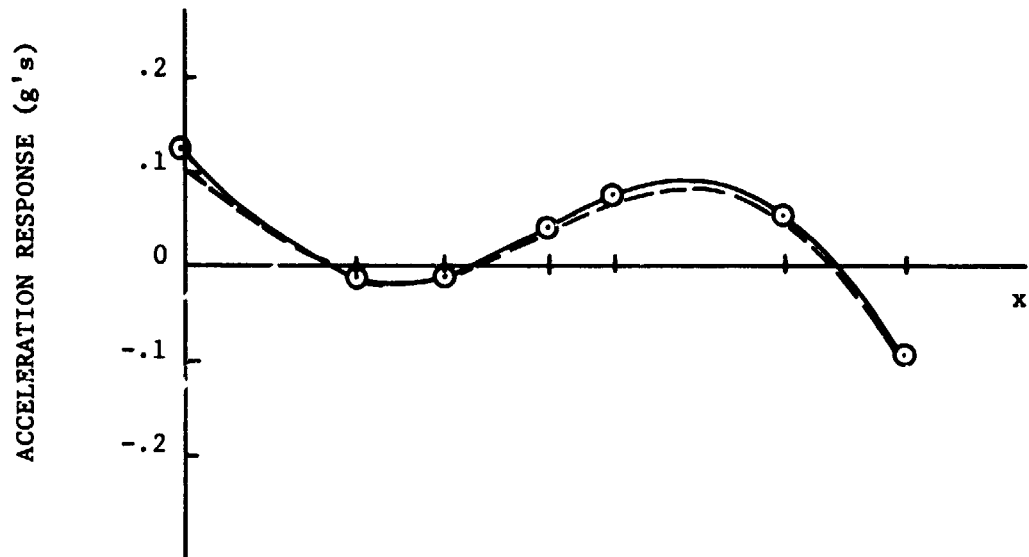


b. Coincident Response (Expanded Scale)

Figure 11. Orbiter Acceleration Response at First Resonant Frequency

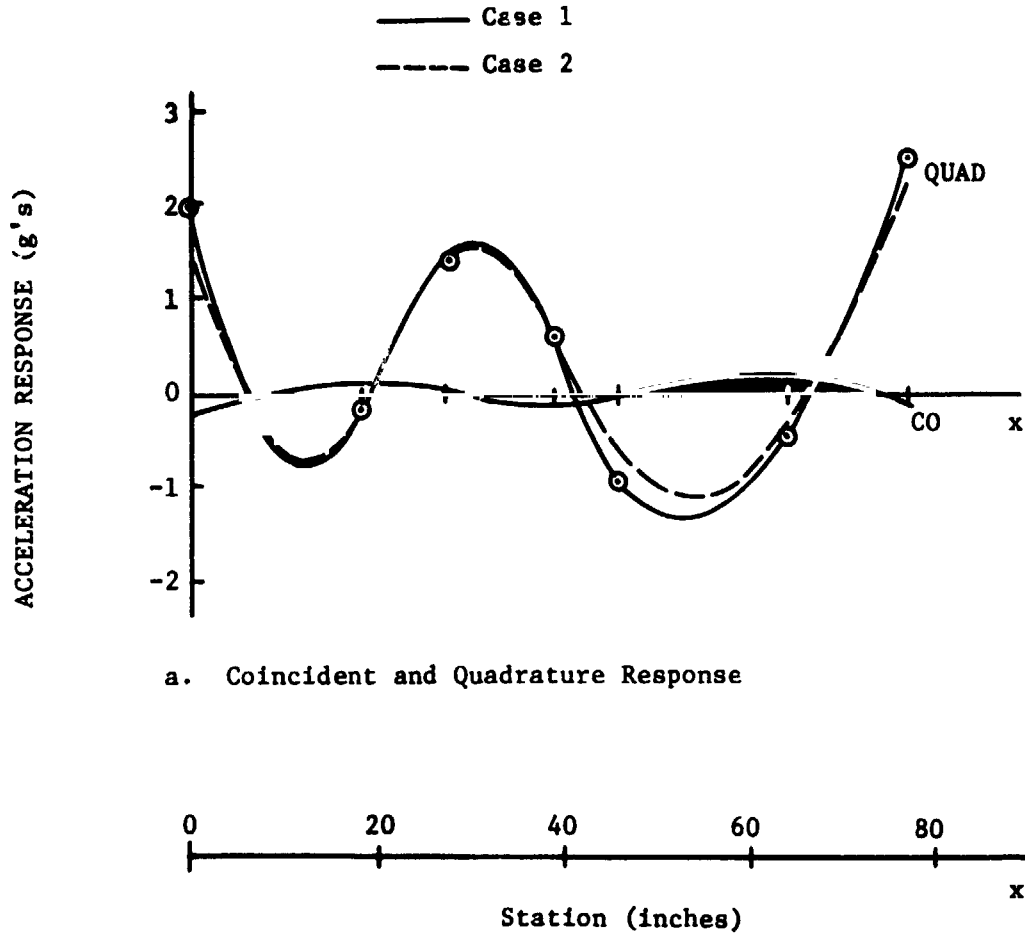


a. Coincident and Quadrature Response

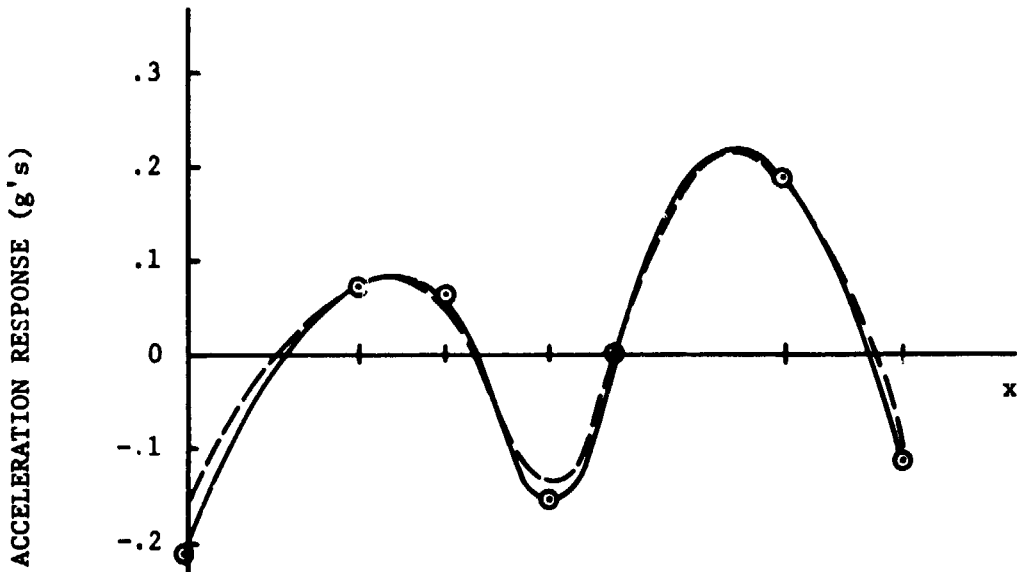


b. Coincident Response (Expanded Scale)

Figure 12. Orbiter Acceleration Response at Second Resonant Frequency



a. Coincident and Quadrature Response



b. Coincident Response (Expanded Scale)

Figure 13. Orbiter Acceleration Response at Third Resonant Frequency

Assuming that internal damping in the Orbiter is small compared to the external damping, that the three ball dampers are identical, and that they introduce damping forces proportional to velocity by the constant c , (28a) suggests that

$$c = \frac{2\zeta_j \omega_{o_j}}{\sum_{k=1,4,7} \phi_{R_{kj}}^2} \quad (40)$$

where the three dampers are located at coordinates 1, 4, and 7. Having measured values of ζ_j , ω_{o_j} , and $\phi_{R_{kj}}$, values of c were computed for each of the three modes (Case 2b). They were not in very good agreement with those values of c presented in Figure 8 except for the first mode at about 100 Hz. Instead of c tending to decrease with increasing frequency (as in Figure 8), it increased as shown in Figure 14. This presented somewhat of a dilemma as to what values should be used.

It was learned that θ in (39) varied from 39.8° down to 8.9° in going from 100 Hz to 400 Hz in the case of horizontal motion, and from 71° down to 14.3° in the case of vertical. The damping force on the ball was of the same order as the driving force and the inertial force. The "virtual mass" of the fluid is an uncertain factor, and could vary with frequency. On the other hand, the damping forces exerted on the Orbiter at resonance are much smaller than inertial forces, and fluid mass should have no significant effect in this case. It is therefore believed that values of c obtained from (40) are more reliable than those obtained from (39). Unfortunately, there was no clear cut way of checking values of c for vertical motion since, in the system tests, horizontal and vertical motion occur together.

In evaluating the modal damping matrix of the Orbiter, an average value of $c = 0.68$ was assumed for the damper constant in each of the four cases. For comparison, a value of $c = 0.36$ was also used in Case 2b.

The task of computing reference values for the modal damping matrix by

$$\xi = \phi_R^T \rho \phi_R$$

is not altogether straightforward either because of the variability with frequency of the damper "constants". However, from the form of (29), it is observed that in each of the two terms on the right-hand side, the frequency is associated with

the imaginary part of the mode $\delta\phi_{I_j}$, which must be related to ζ_j . Other things being equal, the term having the larger of the two frequencies should dominate. In evaluating $\xi = \phi_R^T \rho \phi_R$, it is therefore justified at least to some extent to replace the nonzero elements of the diagonal matrix ρ by unity, and compute a matrix ξ' . Then each element ξ'_{jk} can be multiplied by the value of c corresponding to $\omega_{\sigma_k} > \omega_{\sigma_j}$. This sort of frequency scaling will cause the diagonal elements of the reference matrix to be identical to the diagonal elements of the other matrices, and will cause the off-diagonal elements to be proportioned accordingly. The reference modal damping matrix determined in this manner is presented for comparison to matrices computed from the damped modes in Cases 1a, 1b, 2a, and 2b in Table 21. Also included is Case 2b, computed on the basis that $c = 0.36$, instead of $c = 0.68$. This case is labeled Case 3.

Several things are apparent in Table 21. Most noticeably, the off-diagonal elements in the third column are more sensitive to differences among cases. This is to be expected because of the importance of rotational mass in the third mode. The final modal mass matrices obtained in Cases 1a, 1b, 2a, and 2b are:

Modal Mass Matrices

<u>Case 1a</u>	<u>Case 2a</u>
$\begin{bmatrix} 1.0 & - .097 & .623 \\ & 1.0 & - .123 \\ & & 1.0 \end{bmatrix}$	$\begin{bmatrix} 1.0 & - .010 & .543 \\ & 1.0 & - .093 \\ & & 1.0 \end{bmatrix}$
<u>Case 1b</u>	<u>Case 2b</u>
$\begin{bmatrix} 1.0 & - .103 & .308 \\ & 1.0 & - .071 \\ & & 1.0 \end{bmatrix}$	$\begin{bmatrix} 1.0 & - .019 & .167 \\ & 1.0 & - .043 \\ & & 1.0 \end{bmatrix}$

Table 21 - Comparison of Orbiter Modal Damping Matrices

<p><u>Case 1a</u></p> $\begin{bmatrix} 42.4 & 37.0 & 5.77 \\ & 52.5 & 16.1 \\ & & 40.7 \end{bmatrix}$	<p><u>Reference</u></p> $\begin{bmatrix} 42.4 & 30.0 & 46.8 \\ & 52.5 & 18.9 \\ & & 40.7 \end{bmatrix}$
<p><u>Case 1b</u></p> $\begin{bmatrix} 42.4 & 42.0 & 80.5 \\ & 52.5 & -13.2 \\ & & 40.7 \end{bmatrix}$	
<p><u>Case 2a</u></p> $\begin{bmatrix} 42.4 & 34.4 & 35.6 \\ & 52.5 & 41.6 \\ & & 40.7 \end{bmatrix}$	
<p><u>Case 2b</u></p> $\begin{bmatrix} 42.4 & 37.2 & 128.2 \\ & 52.5 & 8.25 \\ & & 40.7 \end{bmatrix}$	<p><u>Case 3</u></p> $\begin{bmatrix} 42.4 & 39.8 & 123.1 \\ & 52.5 & 11.5 \\ & & 40.7 \end{bmatrix}$

Case 2b is shown to represent the best of them. Significant improvements in orthogonality are seen to be offered by inclusion of rotational mass and by the second set of data over the first. It may also be noted that ξ_{12} is relatively stable and differs from the reference value by the least amount. A computation was also made using Case 2b, but only two of the three modes. In this case, $\xi_{12} = 39.0$, which is still in the right ballpark.

It is of interest to look at the imaginary parts $\delta\phi_{I_j}$ of the damped modal vectors ϕ . They are plotted in Figure 15. They do not resemble the real parts of the modes as closely as the Coincident response resembled the Quadrature, partly because of the way in which they are normalized. Ten data points were available to plot these curves. Eight of them are accounted for by the circled dots. The other two come from slopes obtained at Stations 18.6 and 46.5. Without these, it would have been difficult to plot $\delta\phi_{I_j}$ for the third mode. Each of the vectors $\delta\phi_{I_j}$ was normalized so as to cause the phase angle to be zero for the largest element in the mode. This element happened to correspond to the tail in every case. It is possible that this type of normalization could obscure some otherwise meaningful characteristics of the vectors. Other forms of normalization were not explored, however.

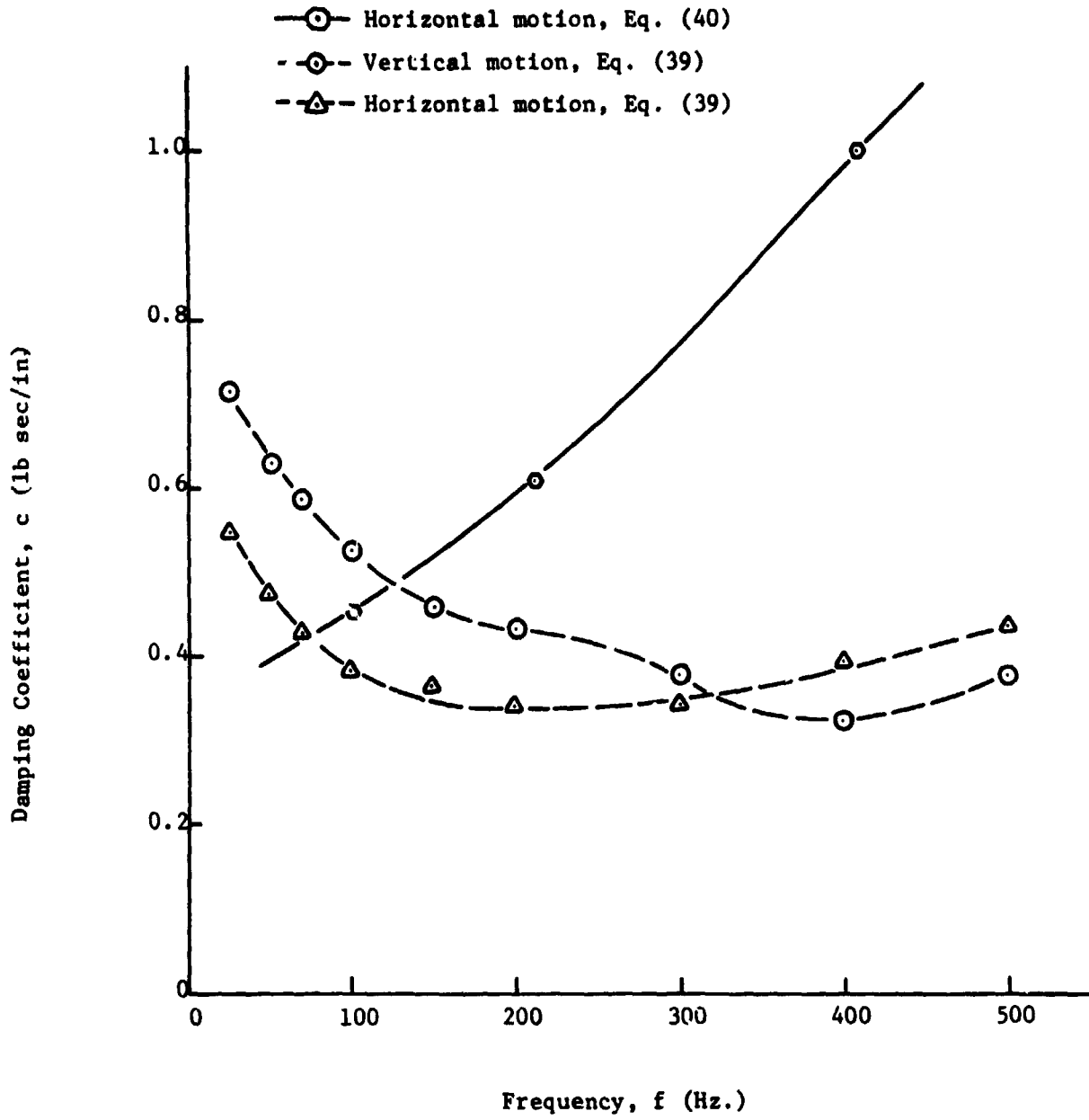


Figure 14 - Comparison of Ball Damper Characteristics
Obtained by Different Methods

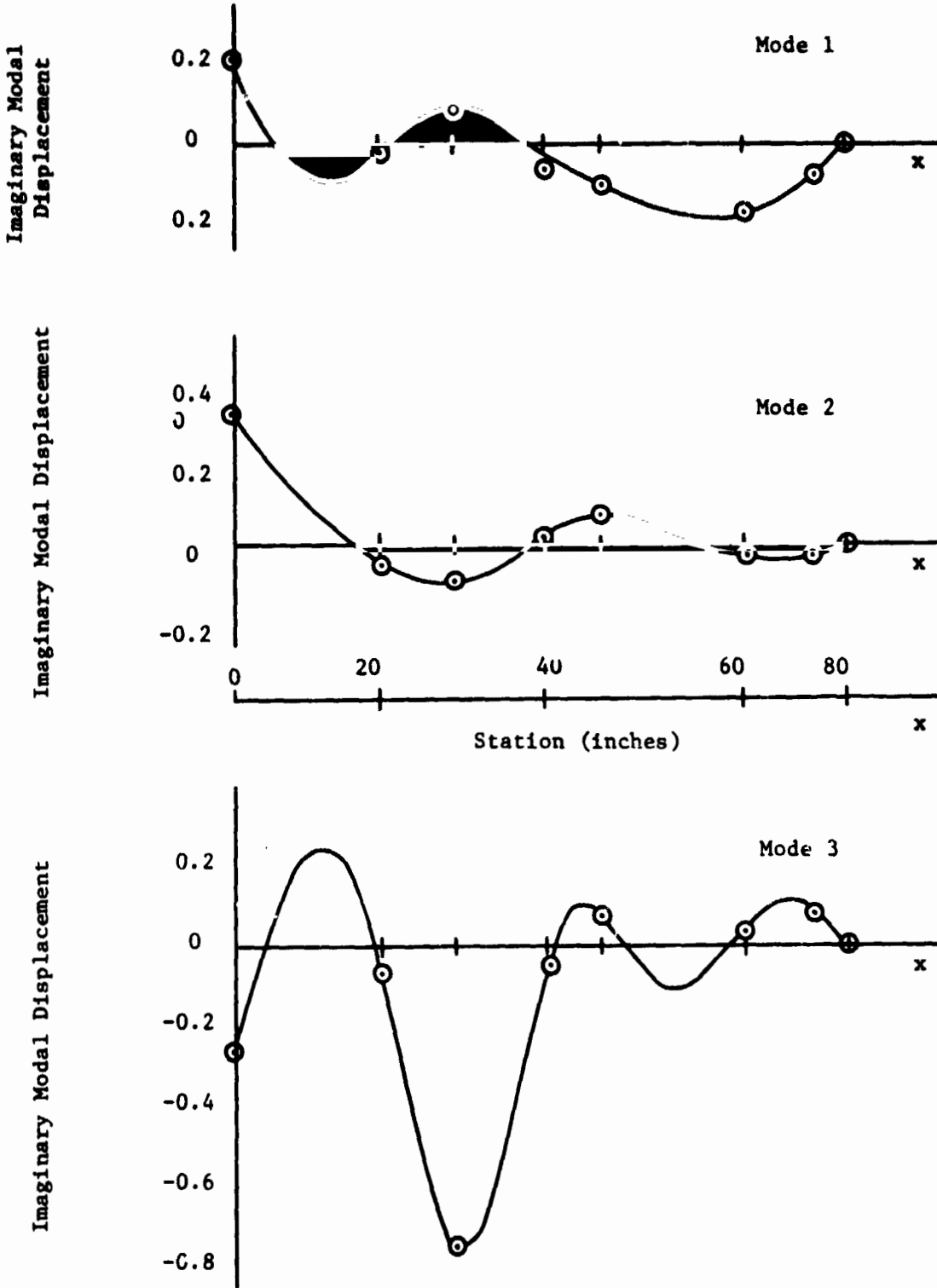


Figure 15 - Imaginary Parts of Damped Orbiter Bending Modes

9.4 Booster Damping Matrix

Since the amount of damping in the Booster is very small, there was not much hope of computing a meaningful modal damping matrix aside from the diagonal terms. Nevertheless, an attempt was made to see how the modal separation program would work. Resonant response for the first nine Booster frequencies with no mass loading was entered. The iterative procedure failed to converge. This result was not unexpected. In the first place, the damping is so small that the accuracy of the coincident response measurements is in question, and secondly, the frequency separation among spring modes in particular violates the criteria for convergence derived in the Appendix. It was noted, however, that after just one iteration, the orthogonality of the modal mass matrix was improved significantly, in particular, with respect to the seventh mode, which is the lowest frequency spring mode in the pitch direction. The original seventh column of the modal mass matrix is shown in Table 22 for comparison to the same column after one iteration of MOLSEP.

Table 22 - Improvement of Orthogonality Among Booster Modes
 (Column 7 of Modal Mass Matrix)

<u>Row No.</u>	<u>Original</u>	<u>Improved</u>
1	- .116	- .319
2	.055	.134
3	- .094	- .019
4	- .010	.053
5	.055	.055
6	- .419	- .065
7	1.000	1.000
8	.428	.194
9	- .809	.039

The overall change is seen to be for the better even though some of the elements did become larger. This kind of improvement was not realized for the Orbiter because the poor orthogonality there was caused by an incomplete description of the third mode, and not by having more than one mode contributing to the resonant response.

The effort to compute a damping matrix was pursued further, however, by introducing fewer modes in the separation algorithm. A case involving only the first two bending modes was tried first. This eliminated the frequency separation problem. Convergence was achieved in a single iteration. Then the first axial spring mode at 145.56 Hz was included in a three-mode case. This time, convergence (to approximately two significant figures in $\delta\phi_I$) was achieved in four iterations. The second axial spring mode at 151.51 Hz was added to make a four-mode case. Computations diverged.

In the Appendix, a convergence criterion is derived in terms of a scaled impedance matrix $\tilde{Z}(i\Omega_j)$ associated with each resonant excitation frequency Ω_j . In the case of proportional damping and in the case of diagonal modal damping in general, \tilde{Z} is a diagonal matrix whose largest element \tilde{Z}_{jj} is unity. The other diagonal elements diminish in size as they become further displaced from the unit element. In the case of nonproportional damping in general, \tilde{Z} is a fully-populated matrix whose elements tend to diminish in magnitude as they become further displaced from the unit element in any direction. A criterion for convergence is that each element $\tilde{Z}_{kl} = e_k^T \tilde{Z}(i\Omega_j) e_l$ (e_k denoting the kth column of the identity matrix I) of each resonant impedance matrix $\tilde{Z}(i\Omega_j)$ satisfy

$$\tilde{Z}_{kl} = \left| \frac{\epsilon_{kl}}{\epsilon_{ll}} \right| \sqrt{\frac{2\zeta_l}{(\beta^2 - 1)}} \ll 1$$

where $\beta = \omega / \omega_{cl} > 1$. Some typical values for Booster calculations are given in Table 23.

Table 23 - Convergence Indicators for Booster Damping Matrix Calculations

Number of Modes	k,l	β^2	$\zeta_k \times 10^2$	$\sqrt{2\zeta_l / (\beta^2 - 1)}$	$ \epsilon_{kl} / \epsilon_{ll} $	$ \tilde{Z}_{kl} $
2	2,1	7.18	.290	.0306	.583	.0178
3	3,2	2.06	.179	.0581	4.64	.270
4	4,3	1.08	.198	...	*	*
5	5,4	1.165	.183	...	*	*
6	6,5	1.278	.144	...	*	*

*Values unknown because iteration failed to converge

The modal damping matrix computed in the three-mode case was found to be

$$\xi = \begin{bmatrix} 1.382 & .805 & -10.58 \\ & 2.285 & 6.195 \\ \text{Sym.} & & 3.622 \end{bmatrix}$$

The (3,2) elements of ξ are seen to be quite large. This may be due to an insufficient number of response measurements, as the results of some of the Orbiter calculations suggested. It is not particularly easy to believe that an axial spring mode could couple so strongly with the bending modes. What appears to be happening is that the modal mass of the spring mode is so small that the elements of $\delta\phi_{I_3}$ are large compared to corresponding elements of $\delta\phi_{I_2}$ or $\delta\phi_{I_1}$, for example, since the modes are normalized to give unit modal mass. Errors would tend to be amplified in this case.

It is clear from Table 21 that the two-mode case should have converged rapidly since the upper bound B on $\tilde{Z}_{k\ell}$ was much smaller than unity. It is interesting also to note that in the three-mode case, convergence was achieved even though B = .270. This is not too surprising since other off-diagonal elements of the \tilde{Z} matrices are much smaller. In the cases involving four or more modes, convergence was not achieved at all, so that values of $\xi_{k\ell}$ are unknown.

It is of interest to examine the response measurements and the first two damped modes computed for the Booster. Response measurements are plotted in Figures 16 and 17, while the corresponding damped modes are plotted in Figures 18 and 19. Again, apparent errors were found in the original response data so that tests were rerun for some of the modes (including the first). Data from the second test are plotted with circles, while data obtained originally are plotted with triangles. Ten-db gain errors were apparent at Stations 20.3 and 45.3 in the first mode of the original data.

Several things are observed in Figure 16. Coincident data from the first test follow the shape of the Quadrature data and are greater in magnitude than coincident data from the second test, which also exhibit more scatter. Different procedures for data reduction were used in each case. In the first case, data were recorded simultaneously on tape over a 20-second time interval and reduced

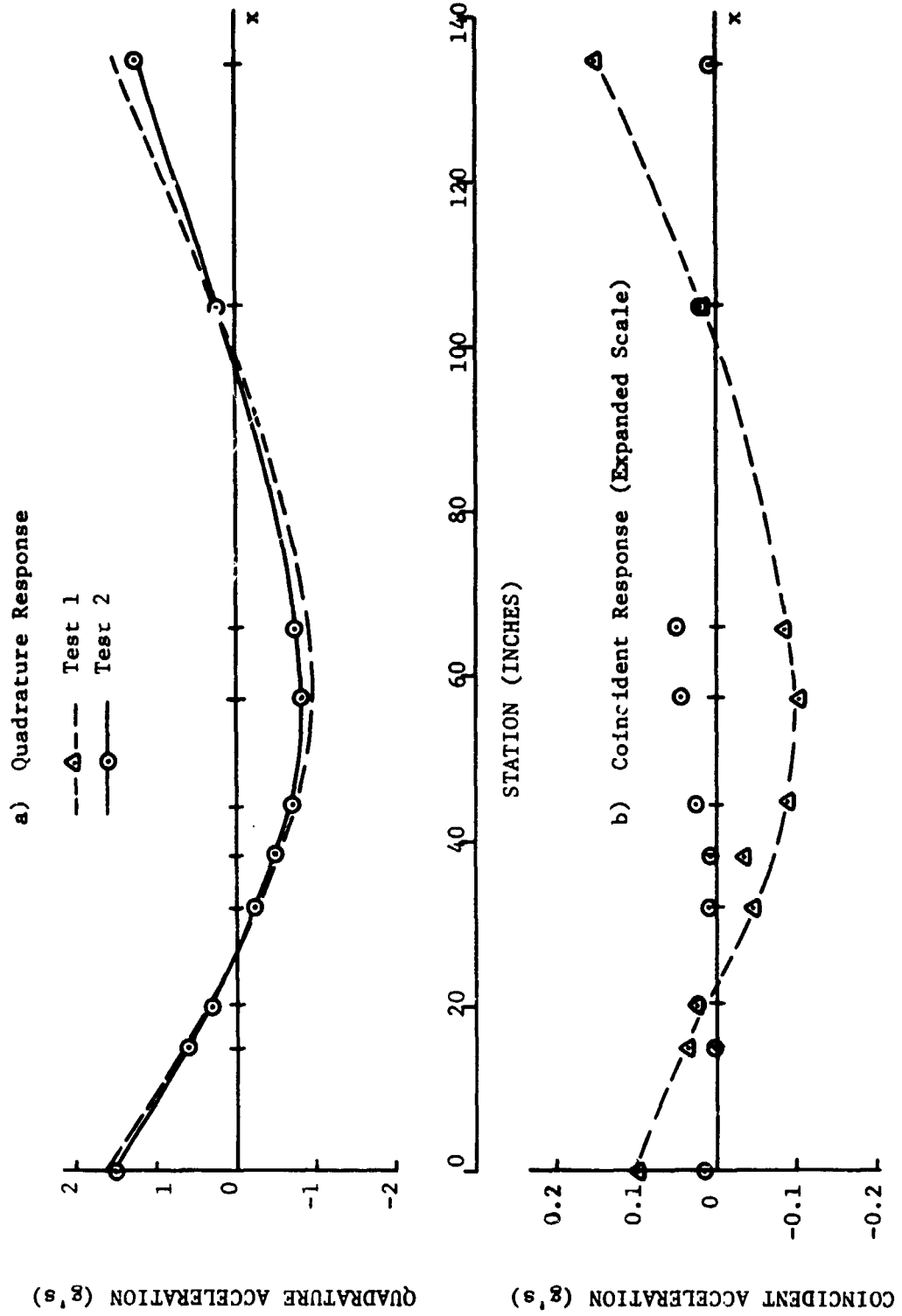


Figure 16. Booster Acceleration Response at First Resonant Frequency

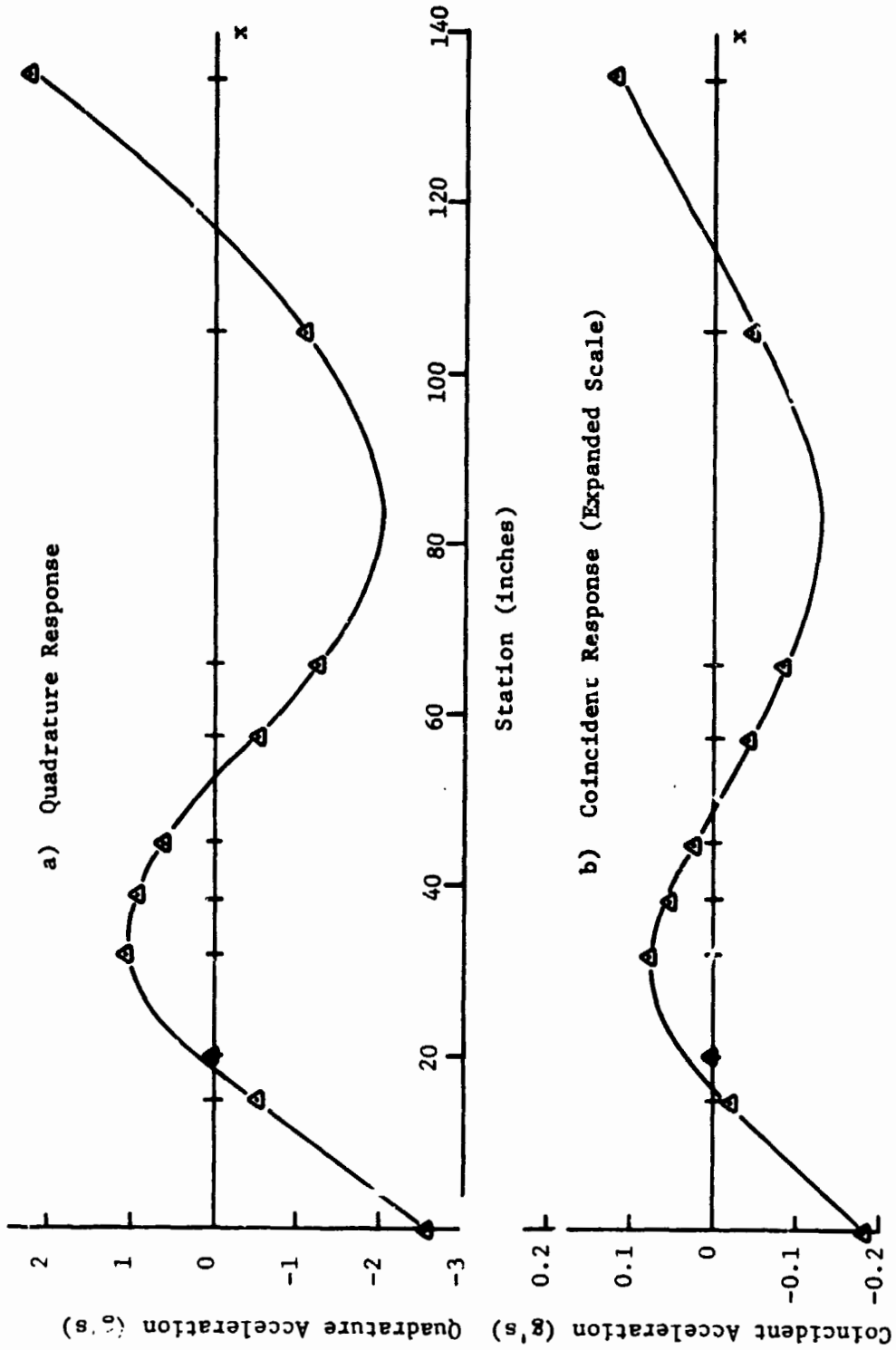


Figure 17. Booster Acceleration Response at Second Resonant Frequency

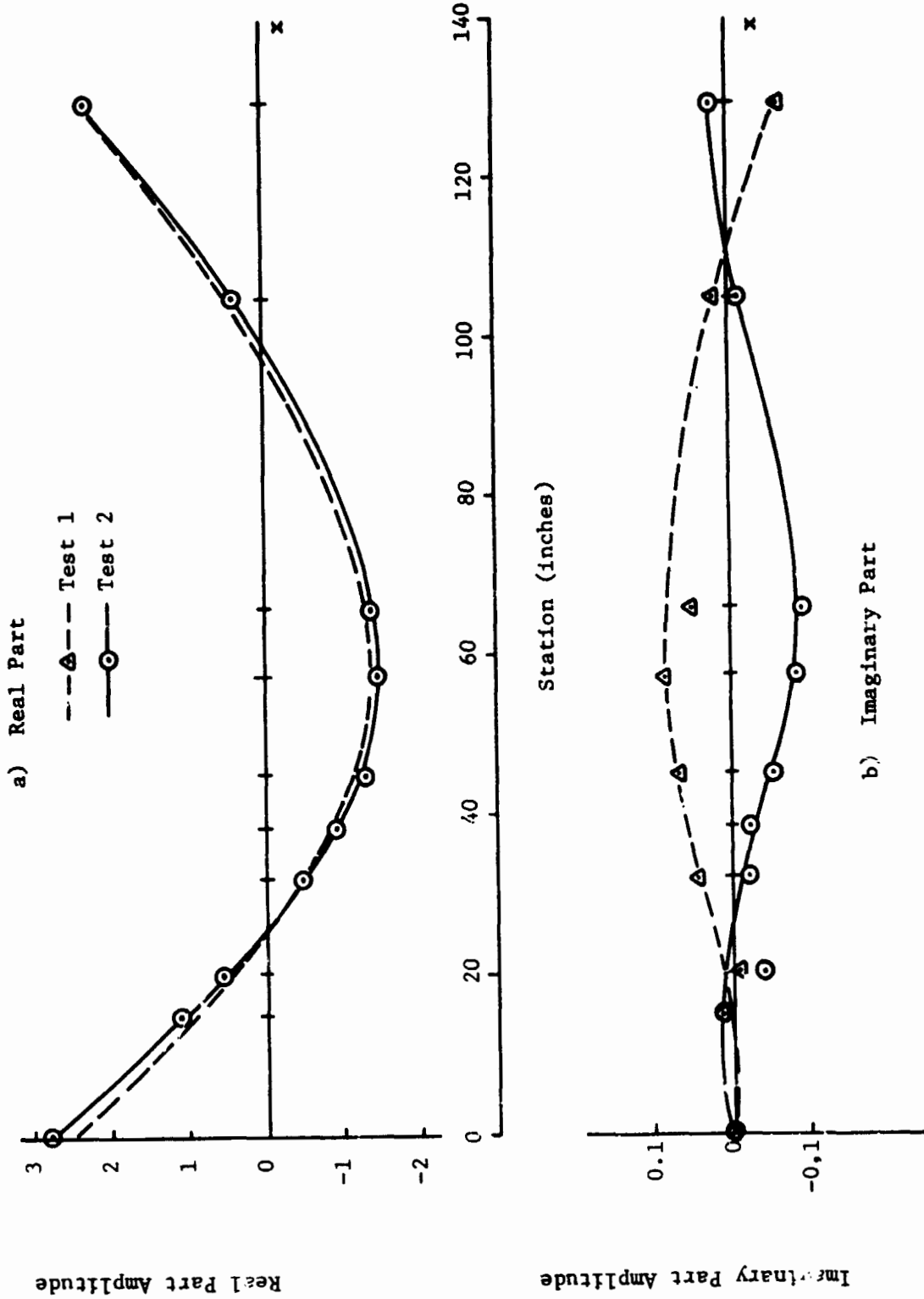


Figure 18. First Damped Bending Mode of the Booster

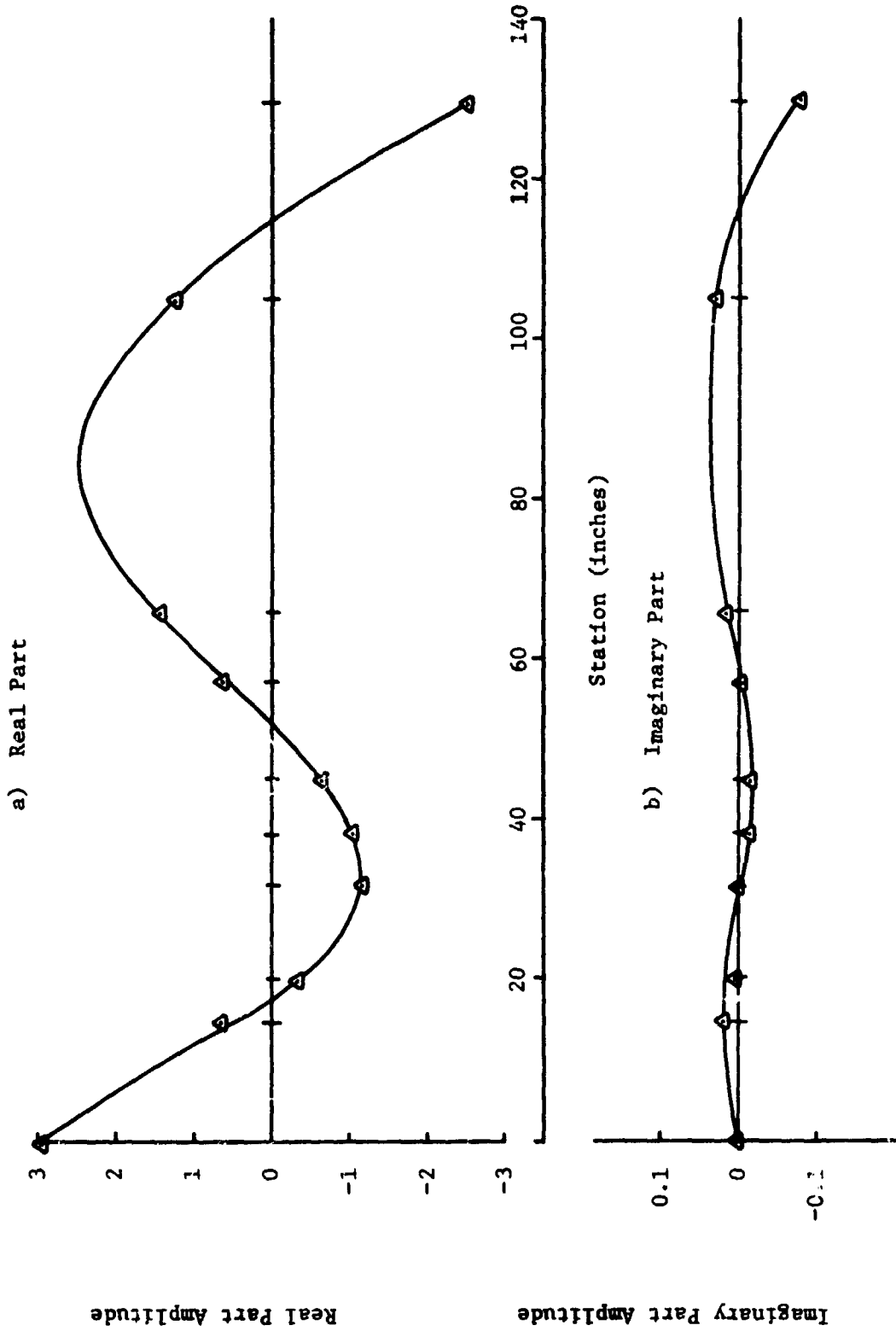


Figure 19. Second Damped Bending Mode of the Booster

using the Co/Quad Analyzer. Data from the second test were recorded manually in real time over approximately a five-minute time interval. Amplitude and phase information were taken, phase angles being read from a phase meter. No phase lock system was used in either case although preliminary tests indicated no significant phase shifts over a typical 20-second interval. Over a five-minute period, however, the possibility of significant phase shifts is acknowledged. Phase drifting could explain the scatter as well as all of the positive Coincident data points.

Another notable characteristic is that the imaginary parts of the modes are considerably greater in magnitude than they should be if only damping information were reflected (see Section 6). Yet, $\xi_{12} < \xi_{11} = 2\omega_1 \zeta_1$. A plausible explanation for this is that the mode was probably not tuned perfectly, causing some of the resonant quadrature response to "spill" over into the coincident. This would tend to account for the fact that the Coincident and Quadrature shape characteristics are so similar, at least in the first test. This explanation would also admit the possibility that computations of ξ_{12} might not be altered appreciably if phase shifts were proportional to the real part of the mode. This is,

$$\phi_{R_2}^T \mu (\epsilon \phi_{R_1} + \delta \phi_{I_1}) = \phi_{R_2}^T \mu \delta \phi_{I_1}$$

(where ϵ is a small proportionality constant) because of the supposed orthogonality of ϕ_{R_2} and ϕ_{R_1} .

The damped mode characteristics shown in Figure 18 are interesting, too. Aside from the sign difference in the imaginary part of the mode, results from the two tests bear a fairly close resemblance. For the sake of comparison, the modal matrix obtained with the substitution of Test 2 data for the first resonance into Test 1 data is

$$\xi = \begin{bmatrix} 1.385 & .052 & -8.382 \\ & 2.285 & 2.286 \\ \text{Sym.} & & 3.622 \end{bmatrix}$$

Because of the dependency of damper characteristics on frequency, it was hard to decide which values to choose for c_H and c_V . To be consistent with earlier computations of the modal damping matrix, a value of $c_H = 0.68$ was used. Figure 14 indicates that while no corresponding values of c_V are available from Orbiter damping tests, separate tests performed on a typical damper indicate that $c_V > c_H$. It was therefore assumed that $c_V = 0.900$.

The selection of these values might be disputed on the grounds that according to Figure 14, $c_H = 0.68$ corresponds to a frequency of approximately 250 Hz, while the system modes range from about 26 to 200 Hz. At 100 Hz, $c_H = 0.45$. Maintaining the same ratio between c_H and c_V would indicate a corresponding value of $c_V = 0.62$. Computations were made using both sets of values, and are shown in Table 24 for comparison to measured values. The agreement is seen to be quite good, especially for the case where $c_H = 0.68$ and $c_V = 0.90$.

Table 24. A Comparison of Predicted and Measured System Damping

System Mode	$c_H = .45$ $c_V = .62$	$c_H = .68$ $c_V = .90$	$c_H = .68^*$ $c_V = .90$	Reference (Experimental)
1	2.24	3.23	3.21	2.77 -3.01
2	.768	1.03	1.02	.62 - .96
3	.485	.658	.660	.49 - .96
4	.835	.765	.855	1.08 -1.67
5	.262	.311	.331	.221- .30
6	2.42	2.98	3.10	3.15 -3.47
7	.193	.197	.219	.282- .366

Another set of computations using these values for c_H and c_V , only this time a diagonal c^{2NN} sub-matrix was assumed for the the Orbiter by setting the off-diagonal element to zero. These results are also shown in Table 24, Interestingly enough, deleting the off-diagonal element made little difference. The reason is obvious when one looks at the modes of the coupled system. There is so much frequency separation between the Orbiter modes that for all practical purposes, they combine only one at a time in the synthesis of system modes.

*The off-diagonal element of the Orbiter modal damping matrix was neglected in this case.

This conclusion is somewhat disappointing in the respect that a comparison of the predicted modal damping constants of the system to those measured directly does not establish the importance of including the off-diagonal terms. In fact, the overall effect of neglecting the off-diagonal term seemed to make things a little better rather than worse, especially for the fourth mode. One must be cautioned against drawing this conclusion too readily, however, because the modal damping predicted in the fourth system mode was significantly in error to begin with. The reason for the error is indicated by a comparison of the predicted and experimental modes (Reference [7]). The experimental mode exhibited a large displacement of the Orbiter tail, whereas the predicted mode indicated practically no displacement. The predicted frequency was 98.26 Hz, whereas the experimental frequency was only 92.25 Hz. The system mode did contain a large amount of the first Orbiter bending mode whose frequency is 101.41 Hz.

9.6 Conclusions

Application of a matrix method for damping synthesis to real structures has produced encouraging results. The predicted values of system modal damping agreed very well with measured values, for the most part. Resonant response was successfully used to evaluate the coupling term between the first two Orbiter modes. Coupling terms involving the third mode were also computed, but not enough response measurements were available to fully describe that mode. Consequently, large amounts of uncertainty were introduced in those terms.

Damping calculations were made with the Booster test data also, even though damping levels were very small. Notable in this case is the improvement in orthogonality among the Booster modes which resulted from the modal separation effort. While computations involving more than the first three modes failed to converge, the results were at least in agreement with the convergence criteria derived in the Appendix. Computations involving only two or three modes did converge, but there was no way of verifying the results. The damped modes contained no obvious discrepancies, and the imaginary parts indicated reasonably smooth curves.

The synthesis of Orbiter and Booster damping matrices to predict System damping yielded results which agreed very well with direct measurement. Part of the success must be attributed to the use of external damping, however, so that the results are not as conclusive as they might be had a different model been chosen.

PART C. APPLICATION AND FUTURE DEVELOPMENT

10. Current Applicability

Parts A and B document the development of a new method for damping synthesis based on the use of substructure damping matrices. The method depends on the ability to determine the damped modes of isolated substructures. These modes are complex, and embody phase as well as amplitude information. While the use of complex modes in the dynamic analysis of linear systems is not uncommon, it does represent a departure from the mainstream of structural dynamics analysis and testing. As a consequence, two major obstacles arise: conceptual difficulty related to the physical interpretation of complex modal vectors and practical problems which have not previously been encountered because there has not been a need to acquire complex modal data. This section is included to help overcome these obstacles by providing a condensation of concepts and findings which are particularly relevant to practical application.

The combined use of amplitude and phase information to evaluate dynamics characteristics is certainly not new. Classical analysis of feedback control systems has frequently employed the Nyquist diagram which is a polar plot of output/input amplitude versus phase angle. Kennedy and Pancu [9] used the same representation of data for structural vibration analysis. The primary difference between these techniques and the present use of complex modes is that the former is used to completely characterize a system between discrete points over a continuous frequency spectrum, whereas the latter is used to characterize the entire system in terms of a discrete frequency spectrum. Most current text books on structural dynamics describe two alternative methods for response analysis: the Frequency Response Method and the Normal Mode Method. The present work draws upon both approaches and, in a sense, bridges the gap between them. The amplitude and phase response of a structure to sinusoidal excitation determine its frequency response. This, in turn, is used to evaluate the damped modes. Because structural damping tends to be small, the damped modes are related to the classical (and hypothetical) undamped modes in a simple manner; i.e., to first-order approximation, the real part of a damped mode is equal to the undamped mode while the magnitude of the imaginary part is small compared to that of the real part. Through a linear perturbation of the undamped equation of motion, the damped modes are used to determine a full modal damping matrix for the structure or substructure.

From the perturbation equations developed in Section 6, it is evident that the magnitude of modal phase angles one might expect to find would be on the order of ζ , the critical damping ratio. Thus, for a structure having 1% damping in a given mode, modal phase angles on the order of .01 radian, or $.6^\circ$, could be expected. In order to determine such phase angles experimentally, measurement errors must be relatively small. This matter is discussed more fully in Section 11.

It has been pointed out that phase angles associated with the resonant response of a structure to sinusoidal excitation are likely to be much larger than ζ . This may be due to the presence of off-resonant mode contribution in the total response as well as small differences between excitation and modal frequencies. The effect of the latter is to "spill" some of the real part of the mode over onto the imaginary axis; this should be of little consequence however, because of modal orthogonality with respect to the mass matrix, as pointed out in Section 9.4. Off-resonant mode response must, of course, be separated from resonant mode response in order to determine the damped modes. The iterative procedure developed to do this appears to work satisfactorily except when modes become too closely spaced, in which case, the iterative computations may fail to converge. Quantitative criteria for convergence are derived in the Appendix, and indicate that for damping on the order of 1%, modal separation should be at least 20% to achieve convergence. The larger the amount of damping, the more frequency separation is required. Damping on the order of 5% will require a frequency separation of about 50%, in general. These conditions assume a ratio of unity between the respective off-diagonal and diagonal terms of the modal damping matrix; which is to say, the two modes in close proximity to each other are strongly coupled by damping. As this ratio becomes smaller, the requirement for frequency separation is reduced according to the square root of this ratio.

Another requirement discovered in the course of this investigation is that the excitation frequency at each resonance must be maintained at the resonant frequency to perhaps five significant figures when damping is on the order of 1%. Resonance may be defined as the frequency at which the quadrature response peaks for that part of the structure undergoing the largest amplitude of response.

A sufficient number of response measurements will be required to fully describe each mode of interest. Interpolation may be used where appropriate. If poor orthogonality of the "undamped" modes is evident even after modal separation, either a poor mass matrix or an incomplete description of the motion (not enough response points) or both may be suspected, assuming that the modes were properly tuned during test. Poor orthogonality in this case will imply errors in damping matrix computations since the same quantities are involved.

Some comments are in order with regard to choosing a physical model for the experimental support of an effort such as this. In retrospect, it has become clear that the use of external damping has led to certain practical difficulties. In the first place, it was hard to determine the characteristics of the ball dampers used in this study. Different methods employed to evaluate their damping "constants" led to different conclusions, thus introducing considerable uncertainty. Since this information was needed to remove rigid-body response from the total resonant response and to account for the coupling between rigid and flexure modes, the uncertainty had a significant influence on damping computations. Furthermore, since the lower system modes contained large amounts of Orbiter rigid-body motion, the influence of rigid-body damping upon predictions of overall system damping was strong. In this respect, the 1/15th-Scale Dynamics Model of Shuttle was not well suited to the objectives of a damping study. Although attempts were made to increase the level of damping by adding internal damping, no method was found to provide enough damping because of the large stiffness and mass of the lead-weighted tubular structure. In the future, this problem can be avoided by the use of lighter weight, more flexible structures for which damping tape and the like are capable of providing sufficient damping. Flat beam type as well as hinged structures are possibilities for consideration.

Of course, in the case where the design of a test specimen is dictated by other requirements, it may be necessary to "work" with only a small amount of internal damping. Improvements in phase measurement accuracy will undoubtedly be required. Data acquisition is discussed in the following section.

11. Data Acquisition

At the outset of this study, an investigation was made to determine the degree of accuracy to which phase angle data could be measured with available analog equipment [10]. Phase errors are introduced by the transducers and conditioning equipment, by the recording and playback equipment, and by the analog data reduction equipment. An effort was made to determine the magnitude of these errors and to minimize them whenever possible.

Tests were conducted at LaRC to determine the variability of phase angles measured by different piezoelectric accelerometers. The accelerometers were mounted on a rigid mass attached to a shaker. Relative phase angles between pairs of them were recorded versus frequency for all 30 accelerometers used in this series of tests. These data fell within a $\pm 0.1^\circ$ bandwidth over a frequency range of 30-500 Hz.

To assess the magnitude of phase error which could be introduced by recording and play-back tape systems, LaRC recorded sinusoidal signals on tape and shipped them to TRW for playback and analysis [11]. Static phase shifts tending to increase with frequency were observed (as much as 10° at 450 Hz). These were presumably caused by imperfect alignment of the record and reproduce heads. The need for phase calibration of each channel had been anticipated in advance, and a special calibration device was built. At tape speeds of 15 ips, dynamic phase variations of $\pm 1^\circ$ were observed at 450 Hz. These can be caused by tape stretching and low frequency flutter. It was decided to increase the tape speed to 60 ips to minimize flutter and operate in the tape synchronization mode to compensate for tape deformation. In this manner, dynamic phase variations were reduced to $\pm 0.1^\circ$ (over a 20-second time period).

The third possible source of error is the analog data reduction equipment which included a Spectral Dynamics 1012B Dual Channel Tracking Filter and a Spectral Dynamics SD109B Co/Quad Analyzer. While amplitude errors were assessed, phase angle error data and/or specifications were unavailable. Precautions were taken, however, to have the system carefully tuned for optimum performance during this task.

C - 2

If the phase error introduced by the Co/Quad Analyzer is also assumed to be on the order of $\pm 0.1^\circ$, the cumulative error would be about $\pm 0.2^\circ$, or .0035 radians. In order to get meaningful damping measurements, the amount of damping should therefore be greater than one percent. This was the reason for adding external damping to the Orbiter.

In summary, phase errors must be held to a minimum. A phase-lock system is recommended to prevent the excitation frequency from drifting and introducing phase shifts. For 1% damping, the overall phase error should be held to $\pm 0.2^\circ$. This allows for approximately $\pm 0.1^\circ$ errors in the instrumentation, tape handling, and Co/Quad reduction, respectively. All data should be recorded simultaneously on tape for a period of 20 to 30 seconds at a tape speed of 60 ips to minimize effects of low frequency flutter. Tape playback should operate in the synchronization mode to compensate for tape deformation. Every channel of data should be phase calibrated to compensate for head misalignment.

With regard to improving measurement accuracy, a digital system offers potential advantages over an analog system. By digitizing the data in real time, the analog tape problems are eliminated completely since records would be stored in digital form. The Co/Quad analysis could then be accomplished by digital filtering and Fast Fourier Transform methods, rather than having to use a tracking filter and the Co/Quad Analyzer. The only problem remaining would be one of improving the instrumentation and/or conditioning equipment. This problem has not been considered yet.

12. Comparison with Energy Method

Two methods for damping synthesis have now been proposed. They are distinguished by the form in which substructure damping properties are described. In the matrix method they are described by a modal damping matrix, and in the energy method, by total dissipative energy. In the matrix method, the spatial distribution of damping throughout the structure is represented; in the energy method, a kind of average distribution is represented in the sense that total dissipation energy is a summation over the structure. Herein is believed to be the basic difference between the two methods.

As might be expected, it is more difficult to determine the modal damping matrix of a structure than total dissipative energy. More data are required and measurement accuracy is more of a problem because of the need to measure small phase angles. In general, it will cost more to get the better resolution offered by the matrix method.

In an attempt to compensate somewhat for the lack of resolution in the energy method, Kana and Huzar have proposed the use of engineering judgement to categorize structural modes so as to form more than one energy curve for a given substructure. More judgement would then be required to decide which curve to use when trying to establish damping energy on the basis of some given kinetic energy. An advantage of the matrix method is that it can be fully automated with no human interaction required.

Regarding the question of linearity, it is recognized that the matrix method presupposes linearity in the equations of motion. This type of linearity was also assumed by Kana and Huzar. Although they claim this is not a fundamental requirement, their report does not indicate how nonlinear problems might be handled.

One final consideration is that of uncertainty in the predicted values of system damping. Even when making direct measurements, it is not uncommon to experience errors on the order of 50%. While the energy method is attractive from the standpoint that energy data are believed to be fairly reliable, it will be difficult if at all possible to assess errors introduced by ignoring the distribution of damping. The matrix method is more amenable to a rigorous statistical evaluation of error because the information used in computations relates directly to measured quantities such as frequency, response and mass distribution; it does not involve human judgement.

13. Final Conclusions

A matrix method for damping synthesis has been developed. Its theoretical basis relies on a linear perturbation of the undamped equation of motion for lightly-damped structures. Verification has been accomplished using both analytical models, which satisfy the inherent assumptions of linear viscous damping, and experimental data from tests of real structures. The results are encouraging in that the nonproportional damping characteristics of real structures have been determined for the first time, making it possible to synthesize the damping matrix of a structural system from those of its component parts.

The present study has encompassed a number of separate investigations, related to damping synthesis. The following major conclusions have been drawn from this study:

1. Modal damping in structural systems can be determined to first order approximation by operating on the substructure modal damping matrices with the same linear transformations used to couple and diagonalize the mass and stiffness matrices. Solution of the complex eigenproblem is not required so that the procedure will be easy to incorporate in existing structural dynamics computer programs such as NASTRAN.
2. Coupling procedures involving fixed-interface, free-interface and mass-loaded-interface substructure modes were investigated for their suitability to damping synthesis. The two major considerations included the practical ability to determine an adequate description of damping at the substructure level, and the convergence of synthesized values of system level damping. Convergence of system damping depends directly on the convergence of system eigenvectors. While the fixed-interface mode method is superior from the standpoint of convergence, it requires the use of static modes which are difficult to determine experimentally and contain no damping information. The free-interface mode method avoids the use of static modes but converges poorly in general. The use of mass-loaded interface modes appears to yield a favorable compromise between the other two methods, offering reasonably good convergence without the use of static modes. Provided that a way of

2. (Cont'd)
determining and applying appropriate mass distribution to the interface boundaries can be found, this method appears to hold the most promise.
3. The basic feasibility of determining substructure modal damping matrices from resonant response data has been established. The damping may be nonproportional, leading to a fully-populated modal damping matrix. Resonant response data are used to compute the damped modes which are also complex. These in turn are used to evaluate the off-diagonal terms of the modal damping matrix. The off-diagonal terms must in general be included in the synthesis. It is only when the modes of a given substructure participate one at a time in the system modes that the off-diagonal terms (while perhaps comparable in magnitude to the diagonal terms) may be neglected. Although this was evidently the case in the present application to a real structural system, it will seldom be true of more realistic structures.
4. The isolation of damped structural modes from total structural response to sinusoidal excitation requires an iterative computational procedure wherein the damped modes and the modal damping matrix are alternately computed. Criteria for the convergence of this procedure have been derived and appear to be in agreement with experience to date. (See Section 9.4 for example.)
5. A significant improvement in the orthogonality of the "undamped modes" (real parts of the damped modes) may be achieved as a by-product of the damping matrix computations. This will be true whenever poor orthogonality of the "raw modal data" (quadrature component of resonant response) is caused by the presence of off-resonant mode contributions in the resonant response. Improvements will not be realized whenever the poor orthogonality is due to having a poor mass matrix or to an inadequate description of the modes.
6. Predictions of structural system damping based on experimentally determined substructure damping matrices have been verified by direct measurement.

7. Further development will be required to enable the separation of closely-spaced modes from the total response at resonance. This is a problem even when the imaginary parts of the modes are of no concern; but it is more of a problem when the complex damped modes are being sought because the requirements on frequency separation are more stringent.
8. It may be necessary in applying this method to define modal frequencies independently of resonant excitation frequencies because of the difficulty in exciting a structure precisely (five or six-digit accuracy) at a modal frequency. In this case, additional information will be required to help identify the modal frequencies.
9. Phase errors introduced by the transducer and analog tape systems have each been held to $\pm 0.1^\circ$. If phase errors in the Co/Quad data reduction are held to a comparable level (and it appears that they are), the total measurement error in the analog system should be on the order of $\pm 0.2^\circ$. This degree of accuracy should permit the measurement of nonproportional damping in systems with damping levels as small as 1% to within approximately 30% accuracy. The use of digital data acquisition systems should further reduce measurement errors in the latter two stages significantly. The basic limitation would then lie with the transducers and conditioning equipment.

14. Recommendations for Future Work

While the basic methodology for damping synthesis by the matrix method has been developed and demonstrated, there are certain limitations to its current applicability, as already discussed. The following recommendations are made for further refinement:

1. Investigate methods for separating closely-spaced modes.
2. Investigate methods for more accurately identifying modal frequencies.
3. Implement the use of digital data acquisition and reduction.
4. Design and test a physical model without external damping, where the substructures' resonant frequencies are more closely spaced. Compare predicted and measured values of system damping.
5. Develop a systematic procedure for estimating the uncertainty in predicted values of system damping. This should be based on an appropriate statistical characterization of all input data.

Acknowledgements

The present study was sponsored by the NASA Langley Research Center, and was performed under subcontract to the Grumman Aerospace Corporation, Contract Number 0-16232-c. The cooperation of Murray Bernstein and Stephen Goldenberg of GAC, and Robert Fralich, NASA Technical Monitor, is gratefully acknowledged. Test data were provided by Sumner Leadbetter and Robert Herr of LaRC. Their cooperation throughout the study, particularly during the final phase which required some additional testing, is greatly appreciated.

Data reduction at TRW was performed by C. P. Wright, of the Environmental Test Department, who deserves much credit for achieving the high level of accuracy required in this study. His cooperation and assistance are acknowledged with thanks.

REFERENCES

1. Lazan, B. J., Damping of Materials and Members in Structural Mechanics, Pergamon Press, New York, 1968.
2. Lazan, B. J. and Goodman, L. E., "Material and Interface Damping", Chapter 36 of Handbook of Shock and Vibration Control, Harris, C. and Crede, C., Editors, McGraw-Hill Book Co., Inc., New York, 1961.
3. Chang, C., "Nonlinear Dynamic Analysis of Structures", HREC-1435-1 and HREC-1435-2, Lockheed Missiles and Space Company, Huntsville, Alabama, 1970.
4. Collins, J. D., Hart, G. C., Hurty, W. C. and Kennedy, B., "Review and Development of Modal Synthesis Techniques", Technical Report No. 1073-1, J. H. Wiggins Co., Palos Verdes Estates, California, May, 1972.
5. Kana, D. D. and Huzar, S., "Synthesis of Shuttle Vehicle Damping Using Substructure Test Results", Southwest Research Institute, Interim Report, Project No. 02-3131, June, 1972.
6. Hasselman, T. K., "A Method for Constructing a Full Modal Damping Matrix from Experimental Measurements", Vol. 10, No. 4, AIAA Journal, April, 1972.
7. Goldenberg, S., "Study of Modal Coupling Procedures for the Shuttle", Grumman Aerospace Corporation, NASA CR-112252, 1972.
8. Stahle, C. V., Jr., "Phase Separation Technique for Ground Vibration Testing", Aerospace Engineering, July, 1962.
9. Kennedy, C. C., and Pancu, C.D.P., "Use of Vectors in Vibration Measurement and Analysis", Journal of the Aeronautical Sciences, Vol. 14, No. 11, November, 1947.
10. Wright, C. P., "Co/Quad Analysis of Langley Research Center Modal Data", TRW Systems, Report No. 8222-25-398, 28 March 1972.

References (Cont'd)

11. Wright, C. P., "Analysis of Langley Research Center Phase Calibration Tapes", TRW Systems, Report No. 8222.25-408, 14 June 1972.
12. Gantmacher, F. R., The Theory of Matrices , Vol. I, Chelsea Publishing Co., New York, N. Y., 1959.
13. Wilkinson, J. H., The Algebraic Eigenvalue Problem, Clarendon Press, Oxford, 1965.

APPENDIX
CONVERGENCE OF THE MODAL SEPARATION PROCEDURE

The identification of damped modes depends on being able to implement an iterative procedure for removing the off-resonant mode response from the total response of a structure at resonance. In order for the process to converge, certain conditions should be satisfied. While an exhaustive investigation of this matter has not been attempted, some relationships have been derived which may be interpreted as criteria for convergence. They are not claimed to constitute sufficient conditions or even necessary conditions in a strict sense. They are plausible, however, and seem to be consistent with experience.

In deriving these relationships, it will again be convenient (and will avoid confusion) to consider the response vector x to represent flexible-body motion only. Thus, when discussing the total response of a free-free structure excited by forces which do not add vectorially to zero, it will be assumed that rigid-body response has been removed.

In the present study, vibration tests were conducted on "free-free" structures which were externally damped. Strictly speaking, they are no longer free-free in this case. Coupling between the rigid-body modes and flexible-body modes is introduced by the dampers. Thus the matrix c^{iNB} , which appears in Equation (19b) of Section 6, has nonzero elements. This need not complicate the study of convergence. Although forces arising from this term may be included in the generalized forces which excite flexible modes, it is simpler, and does not sacrifice generality to ignore them altogether. Besides, this type of damping is artificial and will presumably not be encountered in most practical applications.

Perturbation Analysis

It is assumed that the n equations of motion for a real structure may be written in the form [Equation (31) of Section 7]

$$\mu \ddot{x}(t) + \rho \dot{x}(t) + \kappa x(t) = f(t). \quad (A1)$$

Consistent with the approach taken in [6], the n second-order differential equations of (A1) may be put in first-order form leading to a $2n$ eigenproblem. The solution of this eigenproblem will result in a set of complex eigenvalues λ and

eigenvectors ϕ , where λ is considered to be a complex diagonal matrix, and ϕ , a complex full matrix. The elements of λ are of the form

$$\lambda_j = \sigma_j + i\omega_j$$

where σ_j is the modal decay rate for mode j , and ω_j is the damped natural frequency of that mode. The j th complex eigenvector may be expressed in the form

$$\phi_j = \phi_{Rj} + \delta\phi_{Rj} + i\delta\phi_{Ij} \quad (A3)$$

where ϕ_{Rj} is defined to be the classical undamped mode. The equations of motion may be transformed according to

$$x = \phi_R q \quad (A4)$$

where ϕ_R is a real matrix whose columns are ϕ_{Rj} . Then, (A1) becomes

$$I\ddot{q} + \xi\dot{q} + \omega_0^2 q = \phi_R^T f(t) \quad (A5)$$

where it is assumed that ϕ_R has been normalized so as to result in $\phi_R^T \mu \phi_R = I$ and $\phi_R^T \kappa \phi_R = \omega_0^2$. Here I denotes an identity matrix while ω_0^2 denotes a real diagonal matrix whose elements correspond to the undamped frequencies squared of the various modes. The matrix $\xi = \phi_R^T \rho \phi_R$ is a full modal damping matrix, i.e., non-diagonal in general. It will be assumed that $f(t)$ is of the form

$$f(t) = P_{x_j} g_j(t) \quad (A6)$$

where P_{x_j} is a vector characterizing the spacial distribution of the forcing function $f(t)$, used to excite the j th mode, and $g(t)$ is the corresponding scalar function of time. Then, (A5) may be written

$$I\ddot{q} + \xi\dot{q} + \omega_0^2 q = P_{q_j} g_j(t) \quad (A7)$$

where $P_{q_j} = \phi_R^T P_{x_j}$.

It will be convenient to represent ξ as the sum of two matrices

$$\xi = \xi_d + \xi_n \quad (\text{A8})$$

where ξ_d is a diagonal matrix containing the diagonal elements of ξ , and ξ_n is a matrix with a null diagonal containing all the off-diagonal elements of ξ .

Thus, ξ_d may be considered to be the diagonal damping matrix of the system. Equation (A7) then becomes

$$I\ddot{q} + (\xi_d + \xi_n) \dot{q} + \omega_o^2 q = P_{q_j} g_j(t) \quad (\text{A9})$$

The Laplace transformation of (A9) leads to

$$[(i\Omega)^2 I + (i\Omega)(\xi_d + \xi_n) + \omega_o^2] H_{q_j}(i\Omega) = P_{q_j} \quad (\text{A10})$$

where H_{q_j} is the frequency response vector in the q coordinate system. Further defining a complex impedance matrix $Z(i\Omega)$ by

$$Z(i\Omega) = Z_d(i\Omega) + Z_n(i\Omega), \quad (\text{A11a})$$

$$Z_d(i\Omega) = [(\omega_o^2 - \Omega^2) + (i\Omega) \xi_d], \quad (\text{A11b})$$

$$Z_n(i\Omega) = (i\Omega) \xi_n, \quad (\text{A11c})$$

one may express (A10) in the form

$$[Z_d(i\Omega) + Z_n(i\Omega)] H_{q_j}(i\Omega) = P_{q_j} \quad (\text{A12})$$

Since $Z_d(i\Omega)$ is a diagonal matrix, a scaling transformation

$$q = Z_d^{-1/2}(i\Omega) \gamma$$

may be made leading from (A12) to

$$[I + \tilde{Z}_n] H_{\gamma_j} = P_{\gamma_j}, \quad (\text{A13})$$

where $\tilde{Z}_n = Z_d^{-1/2} Z_n Z_d^{-1/2}$, $H_{\gamma_j} = Z_d^{1/2} H_{q_j}$ and $P_{\gamma_j} = Z_d^{-1/2} P_{q_j}$. Then

$$H_{\gamma_j} = [I + \tilde{Z}_n]^{-1} P_{\gamma_j}. \quad (\text{A14})$$

Examination of \tilde{Z}_n reveals that its diagonal elements will be zero, and that its off-diagonal elements will be much less than unity in magnitude whenever $\Omega = \Omega_j = \omega_{0j}$ for any frequency ω_{0j} , provided that adequate separation exists among the various resonant frequencies of the structure. For these discrete frequencies, (A14) becomes

$$H_{\gamma_j}(i\Omega_j) = [I + \tilde{Z}_n(i\Omega_j)]^{-1} P_{\gamma_j}(i\Omega_j) \quad (\text{A15})$$

The matrix $[I + \tilde{Z}_n(i\Omega_j)]^{-1}$ has the series representation

$$[I + \tilde{Z}_n(i\Omega_j)]^{-1} = \sum_{k=0}^{\infty} [-\tilde{Z}_n(i\Omega_j)]^k \quad (\text{A16})$$

provided that the eigenvalues of $Z_n(i\Omega_j)$ are less than unity in magnitude [10]. In practice, this condition may be established on the basis of Gershgorin's disk theorem [11] which states that all the eigenvalues of the complex matrix G lie in at least one of the disks of radius $r_j = \sum_{k \neq j} |G_{jk}|$ centered at G_{jj} . It is clear that on the basis of (A16), (A15) may be expressed in the manner

$$H_{\gamma_j}(i\Omega_j) = [I - \tilde{Z}_n(i\Omega_j)] P_{\gamma_j}(i\Omega_j) \quad (\text{A17})$$

to first-order approximation. Consistent with this formulation, it is useful to also expand $H_{\gamma_j}(i\Omega_j)$ and $P_{\gamma_j}(i\Omega_j)$ in power series about some nominal values

$H_{\gamma_{0j}}(i\Omega_j)$ and $P_{\gamma_{0j}}(i\Omega_j)$, retaining only the first two terms in each case. Equation

(A17) then becomes

$$\left[H_{\gamma_{0j}}(i\Omega_j) + \delta H_{\gamma_j}(i\Omega_j) \right] = \left[I - \tilde{Z}_n(i\Omega_j) \right] \left[P_{\gamma_{0j}}(i\Omega_j) + \delta P_{\gamma_j}(i\Omega_j) \right] \quad (\text{A18})$$

Treating $H_{\gamma_{o_j}}$, I , and $P_{\gamma_{o_j}}$ as zeroth-order terms and δH_{γ_j} , \tilde{Z}_n , and δP_{γ_j} as first-order terms, one may equate terms of the same order resulting in

$$H_{\gamma_{o_j}}(i\Omega_j) = P_{\gamma_{o_j}}(i\Omega_j)$$

$$\delta H_{\gamma_j}(i\Omega_j) = \delta P_{\gamma_j}(i\Omega_j) - \tilde{Z}_n(i\Omega_j) P_{\gamma_{o_j}}(i\Omega_j)$$

Transformation from the γ back to the q coordinate system, with the notational convention $Z(i\Omega_j) = Z_j$, gives

$$H_{q_{o_j}} = Z_{d_j}^{-1} P_{q_{o_j}} \quad (A19a)$$

$$\delta H_{q_j} = Z_{d_j}^{-1} \delta P_{q_j} - Z_{d_j}^{-1} Z_{n_j} Z_{d_j}^{-1} P_{q_{o_j}} \quad (A19b)$$

In order to define $P_{q_{o_j}}$, it is required that some initial approximation of the undamped modes be available. The quadrature acceleration response provides this information. The normalized acceleration response $H_{\ddot{x}_j}$ corresponding to the total response of the structure when excited by a sinusoidal force at frequency Ω_j is therefore considered to be the sum of two components

$$H_{\ddot{x}_j} = \frac{1}{g_0} \left[CO(\ddot{x}_j) + i QUAD(\ddot{x}_j) \right]$$

where

$$g(t) = g_0 \sin \Omega_j t$$

$$x_j = x_0 \sin(\Omega_j t + \theta_j)$$

$$CO(\ddot{x}_j) = -\Omega_j^2 x_0 \cos \theta_j$$

$$QUAD(\ddot{x}_j) = -\Omega_j^2 x_0 \sin \theta_j$$

Initially, then, ϕ_{R_j} may be assigned the values

$$\hat{\phi}_{R_j} = QUAD(H_{\ddot{x}_j}) / [QUAD(H_{\ddot{x}_j})^T + QUAD(H_{\ddot{x}_j})]^{1/2} \quad (A20)$$

Then, P_{q_0j} is defined to be

$$P_{q_0j} = \hat{\phi}_R^T P_{x_j}$$

Since $Z_d(i\Omega_j)$ has been defined in (A11b), $H_{q_0j}(i\Omega_j)$ is also now defined.

The vector P_{q_j} has been used in (A7) to represent the total generalized force vector in the q coordinate system. With P_{x_j} considered to be known, $P_{q_j} = \phi_R^T P_{x_j}$ is determined by ϕ_R . Then

$$\delta P_{q_j} = (\phi_R - \hat{\phi}_R)^T P_{x_j}$$

The interpretation of δP_{q_j} as a first-order term in (A18) is valid as long as

$$\frac{|Z_d^{-1/2}(\phi_R - \hat{\phi}_R)^T P_{x_j}|}{|Z_d^{-1/2} \phi_R^T P_{x_j}|} \ll 1 \quad (\text{A21})$$

An alternative form for Equation (35) of Section 7 applied to the first iteration of this procedure, is

$$\phi_R = \hat{\phi}(H_{q_0} D)^{-1} \quad (\text{A22})$$

where $\hat{\phi} = H_x D$ and D is a complex diagonal matrix having elements

$$D_{jj} = (e_j^T H_{q_0} e_j)^{-1} \quad (\text{A23})$$

The vector e_j corresponds to the j th column of the identity matrix. The matrix D acts as a normalizing matrix such that when $\hat{\phi}_j$ represents response in only the resonant mode, then $\phi_{R_j} = R(\hat{\phi}_j) = \hat{\phi}_{R_j}$ to first-order approximation. From (A22),

$$R(\phi - \hat{\phi}) = R[\hat{\phi}(D^{-1} H_{q_0}^{-1} - I)]. \quad (\text{A24})$$

Since the diagonal elements of the matrix $H_{q_0} D$ are, by definition, unity, one can represent $H_{q_0} D$ as

$$H_{q_0} D = I + \Delta \quad (A25)$$

where Δ is a matrix whose diagonal elements are zero. If the eigenvalues of Δ are less than unity in magnitude, a series representation may be used for $(H_{q_0} D)^{-1}$ as discussed earlier. Furthermore, with adequate frequency separation of the modes, the elements of Δ will be small in magnitude compared to unity. In this case, the approximation

$$(H_{q_0} D)^{-1} = I - \Delta \quad (A26)$$

is valid. Substitution of this result into (A24) leads to

$$R(\phi - \hat{\phi}) = R[\hat{\phi}(I - \Delta - I)] = R(-\hat{\phi}\Delta) \quad (A27)$$

Use of (A22), (A26), and (A27) in (A21) gives

$$\frac{|Z_{d_j}^{-1/2} R(-\hat{\phi}\Delta)^T P_{x_j}|}{|Z_{d_j}^{-1/2} R[\hat{\phi}(I-\Delta)]^T P_{x_j}|} \ll 1 \quad (A28)$$

It is clear that (A28) will be true if the elements of Δ are in fact small compared to unity.

The element Δ_{kj} of Δ is

$$\Delta_{kj} = e_k^T (H_{q_0} D) e_j \quad (A29)$$

From (23), it is found that the j th element of D is

$$\begin{aligned} D_{jj} &= (\mathbf{e}_j^T \mathbf{H}_{q_{o_j}} \mathbf{e}_j)^{-1} = (\mathbf{e}_j^T \mathbf{H}_{q_{o_j}})^{-1} \\ &= [\mathbf{e}_j^T \mathbf{Z}_d^{-1}(i\Omega_j) \hat{\Phi}_R^T \mathbf{P}_{x_j}]^{-1} \\ &= \left[\frac{\hat{\Phi}_{R_j}^T \mathbf{P}_{x_j}}{(\omega_{o_j}^2 - \Omega_j^2) + i\Omega_j(2\zeta_j \omega_{o_j})} \right]^{-1} \end{aligned}$$

When $\Omega_j = \omega_{o_j}$, then

$$D_{jj} = \frac{i(2\zeta_j)\omega_{o_j}^2}{\hat{\Phi}_{R_j}^T \mathbf{P}_{x_j}} \quad (A30)$$

The vector $(\mathbf{H}_{q_c} \mathbf{D})\mathbf{e}_j = D_{jj} \mathbf{H}_{q_{o_j}}$ is found to be

$$D_{jj} \mathbf{H}_{q_{o_j}} = D_{jj} \mathbf{Z}_d^{-1}(i\Omega_j) \hat{\Phi}_R^T \mathbf{P}_{x_j}$$

Because $\mathbf{Z}_d^{-1}(i\Omega_j)$ is a diagonal matrix

$$\mathbf{e}_k^T D_{jj} \mathbf{H}_{q_{o_j}} = \frac{i(2\zeta_j)\omega_{o_j}^2}{\hat{\Phi}_{R_j}^T \mathbf{P}_{x_j}} \frac{\hat{\Phi}_{R_k}^T \mathbf{P}_{x_j}}{[(\omega_{o_k}^2 - \omega_{o_j}^2) + i(2\zeta_k \omega_{o_k} \omega_{o_j})]}$$

for $\Omega_j = \omega_{o_j}$. Then

$$\Delta_{kj} = \frac{i(2\zeta_j) \frac{\omega_{o_j}^2}{\omega_{o_k}^2} \left[\left(1 - \frac{\omega_{o_j}^2}{\omega_{o_k}^2}\right) - i \left(2\zeta_k \frac{\omega_{o_j}}{\omega_{o_k}}\right) \right] \hat{\Phi}_{R_k}^T \mathbf{P}_{x_j}}{\left[\left(1 - \frac{\omega_{o_j}^2}{\omega_{o_k}^2}\right)^2 + \left(2\zeta_k \frac{\omega_{o_j}}{\omega_{o_k}}\right)^2 \right] \hat{\Phi}_{R_j}^T \mathbf{P}_{x_j}} \quad (A31)$$

It is clear from this result that to keep the magnitude of Δ_{kj} small compared to unity, it is required that

$$\frac{2\zeta_j \left(\frac{\omega_{oj}}{\omega_{ok}}\right)^2 \left| \frac{\hat{\phi}_{R_k}^T P_{x_j}}{\hat{\phi}_{R_j}^T P_{x_j}} \right|}{\left[\left(1 - \frac{\omega_{oj}^2}{\omega_{ok}^2}\right)^2 + \left(2\zeta_k \frac{\omega_{oj}}{\omega_{ok}}\right)^2 \right]^{1/2}} \ll 1 \quad (\text{A32a})$$

It is meaningful to denote the quantity

$$\frac{2\zeta_j \frac{\omega_{oj}^2}{\omega_{ok}^2}}{\left[\left(1 - \frac{\omega_{oj}^2}{\omega_{ok}^2}\right)^2 + \left(2\zeta_k \frac{\omega_{oj}}{\omega_{ok}}\right)^2 \right]^{1/2}} = \bar{Q}_{kj} \quad (\text{A32b})$$

where \bar{Q}_{kj} could be interpreted as a normalized dynamic amplification factor for the k th mode being excited at frequency ω_{oj} . Thus, (A32a) may be written in the form

$$\bar{Q}_{kj} \left| \frac{P_{q_{okj}}}{P_{q_{ojj}}} \right| \ll 1 \quad (\text{A32c})$$

where $P_{q_{okj}}$ represents the k th element of the generalized force vector which excites the structure at frequency ω_{oj} . The requirement will be satisfied if

there is adequate frequency separation. Otherwise, it will be necessary to shape the force distribution P_{x_j} so as to achieve

$$\frac{P_{q_{okj}}}{P_{q_{ojj}}} = \frac{\hat{\phi}_{R_k}^T P_{x_j}}{\hat{\phi}_{R_j}^T P_{x_j}} \ll 1 \quad (A33)$$

The justification for ignoring ξ_n in the first iteration depends on being able to write

$$[I + \tilde{Z}_n (i\Omega_j)]^{-1} = [I - \tilde{Z}_n (i\Omega_j)] \quad (A34)$$

It is therefore required that each element $e_k^T \tilde{Z}_n e_j$ of \tilde{Z}_n satisfy the relation

$$|e_k^T \tilde{Z}_n e_j| \ll 1 \quad (A35)$$

From the definition of \tilde{Z}_n which follows Equation (A13),

$$\tilde{Z}_n = Z_d^{-1/2} Z_n Z_d^{-1/2}$$

Then

$$e_k^T \tilde{Z}_n e_j = e_k^T Z_d^{-1/2} Z_n Z_d^{-1/2} e_j = e_k^T Z_d^{-1/2} e_k e_k^T Z_n e_j e_j^T Z_d^{-1/2} e_j \quad (A36)$$

It is recalled that

$$e_j^T Z_d^{-1/2} e_j = [(\omega_{oj}^2 - \Omega^2) + i2\zeta_j \omega_{oj} \Omega]^{-1/2}$$

and that

$$e_k^T Z_n e_j = i\Omega \xi_{n_{kj}} \quad (A37)$$

where $\xi_{n_{kj}}$ is the kj th element of the modal damping matrix ξ for $j \neq k$. The largest

value of $e_k^T \tilde{Z}_n e_j$ is realized whenever Ω equals either ω_{o_k} or ω_{o_j} . Without loss of generality, it may be assumed that $\Omega = \omega_{o_j} < \omega_{o_k}$. Then

$$e_j^T \tilde{Z}_d^{-1/2} e_j = (12\zeta_j \omega_{o_j}^2)^{-1/2} = (12\zeta_j \omega_{o_j}^2)^{-1} (12\zeta_j \omega_{o_j}^2)^{1/2}$$

Furthermore,

$$1 \omega_{o_j} \xi_{n_{kj}} (12\zeta_j \omega_{o_j}^2)^{-1} = \xi_{n_{kj}} / 2\zeta_j \omega_{o_j} \quad (A38)$$

Substitution of (A37) and (A38) into (A36) for $\Omega = \omega_{o_j}$ leads to

$$e_k^T \tilde{Z}_n e_j = \left[\frac{12\zeta_j \omega_{o_j}^2}{(\omega_{o_k}^2 - \omega_{o_j}^2) + 12\zeta_k \omega_{o_j} \omega_{o_k}} \right]^{1/2} \frac{\xi_{n_{kj}}}{2\zeta_j \omega_{o_j}}$$

$$= \left\{ \frac{1(2\zeta_j) \frac{\omega_{o_j}^2}{\omega_{o_k}^2} \left[\left(1 - \frac{\omega_{o_j}^2}{\omega_{o_k}^2} \right) - 1 \left(2\zeta_k \frac{\omega_{o_j}}{\omega_{o_k}} \right) \right]}{\left[\left(1 - \frac{\omega_{o_j}^2}{\omega_{o_k}^2} \right)^2 + \left(2\zeta_k \frac{\omega_{o_j}}{\omega_{o_k}} \right)^2 \right]} \right\}^{1/2} \frac{\xi_{n_{kj}}}{2\zeta_j \omega_{o_j}}$$

$$|e_k^T \tilde{Z}_n e_j| = \left\{ \frac{2\zeta_j \frac{\omega_{o_j}^2}{\omega_{o_k}^2}}{\left[\left(1 - \frac{\omega_{o_j}^2}{\omega_{o_k}^2} \right)^2 + \left(2\zeta_k \frac{\omega_{o_j}}{\omega_{o_k}} \right)^2 \right]^{1/2}} \right\} \left| \frac{\xi_{n_{kj}}}{2\zeta_j \omega_{o_j}} \right| \quad (A39)$$

The use of Equation (28a) from Section 6, and the use of (A32b) in (A39) suggest that (A35) may be written

$$|e_k^T \tilde{z}_n e_j| = (\bar{Q}_{kj})^{1/2} \left| \frac{\xi_{kj}}{\xi_{jj}} \right| \ll 1 \quad (\text{A40})$$

With regard to frequency separation, Equation (A40) is seen to be more restrictive than (A32c) because \bar{Q}_{kj} is, for the most part, expected to be less than unity.

A tentative criterion for frequency separation can easily be derived by writing (A40) in the form

$$(\bar{Q}_{kj})^{1/2} = \bar{B} \ll 1$$

where $\bar{B} = B |\xi_{jj}/\xi_{kj}|$ and $B = |e_k^T \tilde{z}_n e_j|$. Squaring both sides of the equation and defining $\omega_{ok}/\omega_{oj} = \beta > 1$, gives

$$\frac{4\zeta_j^2}{\bar{B}^4} = (\beta^2 - 1)^2 + 4\zeta_k^2 \beta^2$$

$$\beta^4 - 2(1 - 4\zeta_k^2) \beta^2 + \left(1 - \frac{4\zeta_j^2}{\bar{B}^4}\right) = 0$$

For small ζ_k ,

$$\beta^2 \approx 1 + \sqrt{1 - \left(1 - \frac{4\zeta_j^2}{\bar{B}^4}\right)}$$

$$\beta = \sqrt{1 + \frac{2\zeta_j}{\bar{B}^2}} = \sqrt{1 + \frac{2\zeta_j}{B^2} \left(\frac{\xi_{kj}}{\xi_{jj}}\right)^2}$$

If B is interpreted as the largest value permissible for any $|e_k^T \tilde{z}_n e_j|$, all k,j, then for $\omega_{ok}/\omega_{oj} > 1$, it would be required that

$$\frac{\omega_{ok}}{\omega_{oj}} \geq \sqrt{1 + \frac{2\zeta_j}{B^2} \left(\frac{\xi_{kj}}{\xi_{jj}}\right)^2} \quad : \text{ all } j, k \quad (\text{A41})$$

For example, not knowing (ξ_{kj}/ξ_{jj}) ahead of time, one might tentatively assume that $(\xi_{kj}/\xi_{jj}) \leq 1$. Then it would be required that

$$\frac{\omega_{ok}}{\omega_{oj}} \geq \sqrt{1 + \frac{2\zeta_j}{B^2}} \quad : \text{all } j, k$$

For $\zeta = .01$, $B = .2$, the minimum ratio ω_{ok}/ω_{oj} permitted would be

$$\frac{\omega_{ok}}{\omega_{oj}} = \sqrt{1 + \frac{.02}{.04}} = 1.225$$

However, the value of $B = .2$ was selected somewhat arbitrarily, and will, in fact, depend upon both the size and distribution of the scaled impedance matrix \tilde{Z} . The larger the dimension of \tilde{Z} (i.e., the larger the number of modes considered), the lower one would expect the upper bound B to be. Another way to look at (A41) is to express $|e_k^T \tilde{Z}_n e_j|$ as a function of (ξ_{kj}/ξ_{jj}) , B and ζ_j .

$$|e_k^T \tilde{Z}_n e_j| = \left| \frac{\xi_{kj}}{\xi_{jj}} \right| \sqrt{\frac{2\zeta_j}{(B^2 - 1)}} \quad (\text{A42})$$

Thus, the largest absolute value of any element of the scaled impedance is seen to be

$$|e_k^T \tilde{Z}_n e_j|_{\max} = \left[\left| \frac{\xi_{kj}}{\xi_{jj}} \right| \sqrt{\frac{2\zeta_j}{(B^2 - 1)}} \right]_{\max}$$

The question of how small $|e_k^T \tilde{Z}_n e_j|_{\max}$ must be in order to ensure convergence has not been investigated. This condition appears to be fairly restrictive for many conceivable applications. However, it could turn out that modes which are closely spaced in the frequency spectrum have very weak coupling in the damping matrix. If two modes are orthogonal mainly because they represent local motion in different parts of the same structure, one would expect corresponding values of ξ_{kj} to be small. Another example is given by a beam which has weak coupling between in-plane and out-of-plane vibration, but nearly the same frequency in each case. The implications here suggest a need for further investigation.

So far in this treatment, it has been assumed that the values of ξ are deterministic. In practice, this will not be the case since there will always be some element of uncertainty. A statistical treatment of the problem has not yet been attempted. One would expect that the implication of randomness in ξ might have an impact on the problem of convergence. If so, the requirements involving exciter placement, frequency separation, amount of damping, and measurement accuracy will be interrelated. A systematic accounting of randomness may be of value at some future time, after other refinements have been made, and more experience with the method is acquired.